



## A new look at the environmental conditions favorable to secondary ice production.

Alexei Korolev<sup>1</sup>, Ivan Heckman<sup>1</sup>, Mengistu Wolde<sup>2</sup>, Andrew S. Ackerman<sup>3</sup>, Ann M. Fridlind<sup>3</sup>,  
Luis Ladino<sup>1,4</sup>, Paul Lawson<sup>5</sup>, Jason Milbrandt<sup>1</sup>, Earle Williams<sup>6</sup>

<sup>1</sup>Environment and Climate Change Canada, Toronto, ON, Canada

<sup>2</sup>National Research Council, Ottawa, ON, Canada

<sup>3</sup>NASA Goddard Institute for Space Studies, New York, NY, USA,

<sup>4</sup>Centro de Ciencias de la Atmósfera, Universidad Nacional Autónoma de México, México City, México,

<sup>5</sup>Stratton Park Engineering Company, Boulder, CO, USA

<sup>6</sup>Massachusetts Institute of Technology, Boston, MA, USA

Correspondence to: A. Korolev ([alexei.korolev@canada.ca](mailto:alexei.korolev@canada.ca))

**Abstract.** This study attempts identification of mechanisms of secondary ice production (SIP) based on the observation of small faceted ice crystals (hexagonal plates or columns) with characteristic sizes smaller than 100  $\mu\text{m}$ . Due to their young age, such small ice crystals can be used as tracers for identifying the conditions for SIP. Observations reported here were conducted in oceanic tropical mesoscale convective systems (MCS) and mid-latitude frontal clouds in the temperature range from 0°C to -15°C heavily seeded by aged ice particles. It was found that both in MCSs and frontal clouds, SIP was observed right above the melting layer and extended to the higher altitudes with colder temperatures. It is proposed that the initiation of SIP above the melting layer is related to the circulation of liquid drops through the melting layer. Liquid drops formed via melting ice particles are advected by the convective updrafts above the melting layer, where they impact with aged ice, freeze and shatter. The ice splinters generated by shattering initiate the chain reaction of SIP. The size of the splinters generated during SIP were estimated as 10  $\mu\text{m}$  or less. In most SIP cases, small secondary ice particles spatially correlated with liquid phase, vertical updrafts and aged rimed ice particles. However, in many cases neither graupel nor liquid drops were observed in the SIP regions, and therefore, the conditions for an active Hallett-Mossop process were not met. A principal conclusion of this work is that the freezing drop shattering mechanism is alone among established SIP mechanisms in plausibly accounting for the measured ice concentrations in the observed conditions. No other SIP mechanisms could be confidently identified from the airborne in-situ observations.

### 1. Introduction

Secondary ice production (SIP) has long been acknowledged as a fundamental cloud microphysical process (e.g., Pruppacher and Klett, 1997; Khain and Pinsky, 2019). Along with the other leading processes in cold clouds, such as primary ice formation via activation of ice nucleating particles (INPs), vapor growth and sublimation, including the special case of the Wegener-Bergeron-Findeisen (WBF) process operating between liquid and ice saturation, ice particle aggregation, and riming and sedimentation, SIP is likely to commonly play a critical role in the formation of size distributions and habits of ice particles (e.g., Ackerman et al. 2015; Ladino et al. 2017). Through the modulation of ice particle concentration, SIP can thereby impact precipitation formation, rate of glaciation of mixed phase clouds, longevity of ice clouds, cloud electrification and radiative properties of clouds. On the global scale, SIP may



significantly impact the hydrological cycle and climate in general. However, the commonality and precise mechanisms of SIP have remained persistently poorly established. Better establishing knowledge of mechanisms of SIP is of great importance for developing a parameterization of the ice initiation processes in weather prediction and climate models.

Even though SIP was observed in cloud chambers in early laboratory experiments (e.g. Findeisen, 1940; Findeisen and Findeisen, 1943; Brewer and Palmer, 1949; Malkina and Zak, 1952; Puzanov and Accuratov, 1952; Schafaer, 1952; Bigg, 1957), the geophysical significance of SIP was recognized only after the beginning of regular airborne studies of cloud microstructure in different geographical regions (e.g. Koenig 1963, 1965; Hobbs, 1969; Mossop, 1970, 1985; Mossop et al. 1972; Ono, 1972; Hallett et al. 1978; Hobbs and Rangno 1985, 1990; Beard 1992; and many others). A systematically observed difference of up to five orders of magnitude between concentrations of INP and measured ice concentration urged provision of an explanation of the physical processes underlying this discrepancy. One of the explanations suggested an enhancement of the concentration of ice particles via a mechanism unrelated to the primary ice formation. This explanation was supported by observations of explosive enhancements of the concentration of small ice particles at early stages of cloud glaciation as described in the aforementioned studies. Several possible mechanisms were proposed to explain such so-called secondary production of ice crystals.

Despite the efforts of several recent reviews on ice multiplication (e.g. Cantrell and Heymsfield, 2005; Field et al., 2017), little attention has been devoted to exploring the existing inconsistencies between previously published laboratory studies on SIP mechanisms. In order to bridge this gap, we provide an extended review of these studies in order to facilitate an understanding of the current status of our knowledge of the SIP mechanisms.

### 1.1 Fragmentation of freezing drops

Historically, the first proposed mechanism to explain SIP focused on droplet fragmentation during freezing (e.g. Langham and Mason, 1958; Mason and Maybank, 1960; Kachurin and Bekryaev, 1960). During freezing of a cloud droplet, isolated pockets of liquid water may become trapped inside an ice shell. The expansion of water during subsequent freezing results in an increase of pressure inside the ice shell. If the pressure exceeds a critical point, then the ice shell may crack to relieve the internal pressure. The release of internal pressure may be accompanied by a formation of spikes or bulges due to the exiting freezing water (Dorsey, 1948; Blanchard, 1951) or by a breaking of the ice shell into fragments. Newly formed ice fragments may serve as INPs and result in an enhancement of ice concentration.

Subsequent laboratory studies demonstrated that fragmentation of freezing drops depends on many factors such as droplet temperature before freezing, environmental temperature, droplet size, concentration of CO<sub>2</sub> and other gases dissolved in water, crystalline nature of the ice shell (i.e. monocrystalline or polycrystalline), drop rotation during freezing, the type of INP employed for droplet freezing and the manner of droplet suspension in the laboratory (Muchnik and Rudko 1961; Evans and Hutchinson 1963; Stott and Hutchinson 1965; Dye and Hobbs 1966, 1968; Johnson and Hallett 1968; Brownscombe and Thorndike 1968; Hobbs and Alkezweeney 1968; Takahashi and Yamashita 1968, 1970; Pitter and Pruppacher 1973; Takahashi 1975, 1976; Wildeman et al. 2017; Lauber et al. 2018).

One of the critical conditions for fragmentation of a freezing droplet is the formation of an ice shell around a liquid water core. No pressure builds inside a droplet freezing from inside to outside. However, if the droplet freezes inward, then the pressure inside the ice shell may reach 80 bars (Visagie, 1969; King and Fletcher, 1973). Laboratory



80 experiments by Stott and Hutchinson (1965), Takahashi (1975), and Lauber et al. (2018) classified different patterns of droplet response to the release of the internal pressure during freezing: jetting, cracking, splitting, bubble-bursting and breakup. The last of these is usually referred to as droplet shattering.

Analysis of the laboratory studies of droplet freezing showed a large diversity of reported results. Depending on the experimental setup, the number of fragments formed for the same size drop during its freezing may vary from  
85 zero (e.g. Dye and Hobbs 1966; Johnson and Hallett, 1968; Pena et al. 1969) to a few hundred (Mason and Maybank, 1960).

### 1.2 Splintering during riming

Splintering during ice particle riming is another mechanism that can potentially explain apparent SIP. Macklin (1960) observed splinter production in a small wind tunnel during the collection of droplets on an ice rod at speed of  
90 2.5 m/s and air temperature  $T_a = -11^\circ\text{C}$ . Latham and Mason (1961) observed freezing of droplets on a hailstone simulator, accompanied by the ejection of ice splinters. They established that the splinter production varied with the air temperature, drop diameter and impact velocity. A maximum production rate of 14 splinters per drop, on average, was observed in droplets with a diameter of 70  $\mu\text{m}$  impacting at 10 m/s at the air temperature of  $-15^\circ\text{C}$ .

Later, Hallett and Mossop (1974) and Mossop and Hallett (1974) observed splinter formation during riming in a  
95 cloud chamber with liquid water content of  $\sim 1 \text{ g/m}^3$  and droplet concentration  $500 \text{ cm}^{-3}$ . They found that splinter production is active in the air temperature range from  $-3^\circ\text{C}$  to  $-8^\circ\text{C}$ , and its rate has a pronounced maximum at an air temperature of  $-5^\circ\text{C}$  and drop impact velocity of 2.5 m/s. At these conditions, one splinter was produced per 250 droplets of diameter  $D > 24 \mu\text{m}$ . The phenomenon of splinter production during riming is usually referred to as the Hallett-Mossop (HM) mechanism. Mossop (1978, 1985) found that the presence of droplets with  $D < 12 \mu\text{m}$  in  
100 addition to those  $D > 24 \mu\text{m}$  increase the splinter production further.

Several studies have aimed at understanding the physical mechanism responsible for the splinter production. For instance, Macklin (1960) documented that fine ice structures formed during riming could be easily detached from the rimer and form splinters. Choularton et al. (1978, 1980) suggested that, if droplets  $D > 25 \mu\text{m}$  are accreted on the ice substrate by a thin neck, they will minimize the heat transfer towards the rimer. Such an arrangement may induce  
105 symmetrical heat loss to the air, which then leads to the formation of a complete ice shell around a droplet as it freezes. The following freezing of liquid will result in a pressure build up inside the droplet, which may result in cracking the shell, along with an expulsion of ice fragments. Emersic and Connolly (2017) found that with increasing rime depth, which is more commonly associated with graupel, growing rime spikes protrude from the surface into the airflow around the rimer. They hypothesized that rime spikes that develop with continuing droplet accretion could  
110 break off during particle tumbling, leading to SIP particularly if hinged by a smaller droplet.

Analysis of the literature indicates that, with the exception of some early studies (Hobbs and Borrows, 1966; Aufremeraud and Jonson, 1972), most laboratory experiments on the HM-process confirmed splinter production during riming. However, there was a lack of consistency in the rate of the rime splintering observed by different groups and the air or rimer skin temperature range over which it may be active. This inconsistency may be explained  
115 by different laboratory setups and techniques used for simulating riming and for splinter identification. Despite nearly seven decades of study and the inclusion of this process in a growing number of weather and climate models, the physical mechanism underlying this phenomenon is still under debate.



### 1.3 Fragmentation due to ice-ice collision

Collision of ice particles may result in their mechanical fragmentation and production of secondary ice (Langmuir, 1948, p.186). This hypothesis was stimulated by observations of ice particle fragments collected during airborne studies (e.g. Hobbs and Farber, 1972; Takahashi, 1993) or ground-based (Juisto and Weikmann, 1973).

To our knowledge, there are only two laboratory works dedicated to collisional ice fragmentation. Vardiman (1978) explored fragmentation of natural cloud ice particles on impact with a metal mesh. Takahashi et al. (1995) studied the dependence of mechanical fragmentation resulting from collision of 2 cm diameter rimed ice spheres attached to 10 cm long spinning metal rods. Vardiman (1978) also argued that pairwise collisions of dissimilar habits, specifically collisions of graupel and rimed dendrites, which have not been investigated in the laboratory, could be most efficient in producing fragments.

Collisional ice fragmentation has also been studied theoretically. The Hobbs and Farber (1972), Vardiman (1978), Phillips et al. (2017), Yano and Phillips, (2011), Yano et al. (2016) and Phillips et al. (2018) studies were based on the consideration of collisional kinetic energy and linear momentum. Such considerations would be complete only for cases of direct central impact. More generally, angular momentum and rotational energy should also be taken into consideration. Since oblique particle collisions are more frequent than central collisions, the efficiency of SIP obtained in these works is expected to be underestimated.

In summary of this subsection, it can be concluded that the role of the ice-ice collisional fragmentation in SIP remains uncertain. Additional laboratory studies are required to explore the efficiency of ice-ice collisional fragmentation of free-falling ice particles with different habits. Ice fragments observed in-situ should be considered cautiously due to potential particle breakup artifacts induced by the sampling (described further below).

### 1.4 Fragmentation due to thermal shock

When an ice crystal collides with a supercooled drop it will experience thermal shock due to release of latent heat of the freezing drop. This will cause a differential expansion of the ice crystal and may result in its fragmentation (Koenig, 1963, p.35).

During their laboratory studies, Dye and Hobbs (1968) observed that when ice crystals became attached to a freezing drop, they often broke into 5 to 10 pieces as the drop freezes. Hobbs and Farber (1972) observed in the laboratory shattering of a dendritic crystal into several pieces after contact with a 2 mm diameter supercooled drop. This observation is of considerable interest, as it suggests that the breaking up of ice crystals that collide and nucleate supercooled drops may play an important role in increasing the concentration of ice particles.

Using thermoelastic theory, King and Fletcher (1976a) calculated thermal stresses in idealised ice shapes on impact with liquid droplets, when a small area was warmed to 0°C. They concluded that a thermal shock mechanism is unlikely to be responsible for SIP at temperatures  $T_a > -5^\circ\text{C}$ . Experiments on thermal shock breakup with large polycrystalline spheres (<3 cm) and thin ice slabs showed no fragmentation for temperatures warmer than  $-35^\circ\text{C}$  (King and Fletcher 1976b). The results obtained by King and Fletcher (1976ab) are not consistent with the laboratory observations of Gold (1963), Dye and Hobbs (1968) or Hobbs and Farber (1972).

Currently, the efficiency of ice particle fragmentation due to thermal shock caused by rimed freezing drops remains poorly understood. Therefore, the role of this effect on SIP remains inconclusive.



### 1.5 Fragmentation of sublimating ice particles

Ice particle fragmentation and formation of secondary ice may occur during sublimation in subsaturated areas near cloud edges or underneath the cloud base. Oraltay and Hallett (1989) studied sublimation of ice particles suspended on a fiber at a wind speed emulating their fall velocity. They observed fragmentation of dendritic ice shapes at  
160 subfreezing temperatures only when relative humidity over ice was  $RH_i < 70\%$ . However, no sublimation breakup was observed for columnar and plate-like crystals. Dong et al. (1994) studied fragmentation of rimed ice and needles at  $50\% < RH_i < 90\%$  and  $-18^\circ\text{C} < T_a < -5^\circ\text{C}$ . In their experiments, they found that a rimed ice a few millimeters in length may generate up to 100 fragments during evaporation at  $RH_i < 70\%$  within 1-2 minutes. Bacon et al. (1998) studied fragmentation of sublimating ice particles suspended in an electrodynamic balance inside a thermodiffusional  
165 chamber at  $85\% < RH_i < 100\%$  and  $-30^\circ\text{C} < T_a < 0^\circ\text{C}$ . The observed fragmentation tended to affect prolate ice particles with an aspect ratio higher than 3. All three studies concluded that breakup rates depend on temperature and humidity but are largely determined by the initial shape of the ice particle.

During their observation of metamorphosis of shapes of sublimating ice particles in natural clouds, Korolev and Isaac (2004) came to the conclusion that particle fragmentation during sublimation does not play an important role in  
170 SIP.

In order for the ice fragments detached from sublimating particles to explain observed conditions of apparent ice multiplication, they have to be transported into an ice supersaturated cloud area. Since small ice fragments have lower fall speeds, their residence time in the subsaturated environment may be long enough to result in their complete sublimation before they can be transported into an ice supersaturated environment. This appears to be a significant  
175 limitation on the efficacy of sublimation breakup as a SIP mechanism.

### 1.6 Activation of INPs in transient supersaturation around freezing drops

Muchnik and Rudko (1961) and Dye and Hobbs (1968) reported on the observation of a halo of small droplets formed around a freezing drop immediately following ice nucleation. Dye and Hobbs (1968) explained the origin of small droplets by the activation of cloud condensation nuclei (CCN) in the region of high transient supersaturation  
180 formed around a freezing drop. After nucleation, the freezing drop temperature rises to  $0^\circ\text{C}$ . If the surrounding air is colder than  $0^\circ\text{C}$ , the surface of the freezing drop acts as a source of water vapor to a colder environment. The resulting water vapor diffuses radially outward. Depending on the air humidity, it may create at some distance from the droplet a region with supersaturated air. Nix and Fukuta (1974) developed a theoretical framework for the calculation of the supersaturation field around a freezing drop.

Later on, Gagin (1972) proposed a mechanism for SIP due to activation of INP in high transient supersaturation areas around freezing drops. He argued that high supersaturation may result in activation of insoluble INPs, which normally do not activate at typical cloud supersaturations ( $SS < 1\%$ ). Rosinski et al. (1975) and Gagin and Nozyce (1984) studied nucleation of INPs around suspended freezing drops with 1–2 mm diameter.  
185

The activation of INPs in the vicinity of freezing drops is expected to be most effective at air temperatures  $T_a < -10^\circ\text{C}$ , at which maximum ice supersaturation corresponds to  $SS_{\text{max}} > 15\%$ . However, Baker (1991) argued that even if  $T_a$  is low enough, the volume around a freezing drop is too small compared to regions with high concentrations of ice. Therefore, he concluded that INP activation in transient supersaturation around freezing drops is unlikely a significant SIP mechanism.  
190



195 However, simply due to limited laboratory studies, the effect of INP activation around freezing drops on SIP remains insufficiently quantified.

### 1.7 Spurious enhancement of ice concentration during sampling

200 The hypothesis that ice concentration measurements are widely subject to artifacts induced by airborne instruments has been discussed over a long period of time. Larger ice particles may bounce off a forward probe's tips or inlet, and shatter into smaller fragments. After rebounding, the shattered fragments may travel into the sample area and cause multiple artificial counts of small ice.

Cooper (1977) was the first to recognize the potential significance of particle shattering, and suggested filtering the shattered artifacts based on the characteristically short interarrival times. Several subsequent works based on comparisons with other instruments (Gardiner and Hallett, 1985; Gayet et al., 1996; Heymsfield, 2007; McFarquhar et al. 2007; Jensen et al. 2009) or analysis of the particles' interarrival time (Field et al., 2003) posed the question of whether observed high concentrations of ice particles are real or primarily artifacts.

205 Field et al. (2006) applied an interarrival time algorithm to identify and filter out shattering artifacts in 2D Optical Array Probe (OAP-2DC) and Cloud Imaging Probe (CIP) measurements. It was found that after filtering artifacts, the OAP-2DC and CIP concentrations were reduced by up to a factor of four, when the mass-weighted mean size exceeded 3mm.

210 Direct experimental support for the shattering hypothesis has been provided by a series of high-speed videos, which documented that after rebounding from the probes tips, shattered small fragments can, in fact, travel several centimeters across the airflow and reach the probe's sample volume (Korolev et al. 2011, 2013b). Korolev et al. (2011, 2013a), Lawson (2011), Korolev and Field (2015) showed that the effect of shattering can be mitigated by using both antishattering K-tips (Korolev et al. 2013b) and the interarrival time algorithm (Field et al. 2006). Korolev et al. (2013a) showed that a measured concentration of ice particles smaller than 200µm can be enhanced due to the shattering effect by up to two orders of magnitude, whereas the concentration of ice particles larger than 400µm remains mainly unaffected.

220 The latter finding brings up a question that some early airborne studies that pointed out the discrepancy between concentrations of ice particles and INPs might be contaminated by shattering artifacts, which resulted in an enhancement of the measured concentration of small ice. However, numerous recent in-situ measurements, which applied the antishattering techniques, are in general consistent with the early SIP observations and they also showed that in many clouds, ice particle concentrations are still much higher than the INP concentration (e.g. Croiser et al. 2011, 2014; Crawford et al. 2012; Stith et al. 2014; Lawson et al. 2015; 2017; Lloyd et al. 2015; Lasher-Trapp et al. 2016; Keppas et al. 2017; Ladino et al. 2017; Sullivan et al. 2017, 2018; and others)

225 Most observations of an enhanced concentration of ice particles have been attributed to the HM-process. The list of these studies extends over 30 publications, so we name only a few of them here (e.g. Ono, 1971, 1972; Harris-Hobbs and Cooper, 1987; Bower et al. 1996; and others). In these studies, the conclusions about the HM-process were obtained based on the observed association with graupel and columnar ice crystals. Fewer studies attributed observations of high ice concentration to drop shattering (e.g. Koenig 1963, 1965; Braham, 1964; Rangno 2008; Lawson et al. 2017). Ice-ice collisional fragmentation was identified as a source of SIP in natural clouds by Hobbs and Farber (1972), Takahashi (1993), Schwarzenboeck et al. (2009). As can be seen, the identification of SIP



gravitates towards the HM-process. The question that arises is, could these observations reflect an actual occurrence of different types of SIP?

## 235      **2. Objectives and data sets**

The present study is focused on an analysis of SIP in mature tropical mesoscale convective systems (MCS) and in frontal clouds. Both types of cloud systems were heavily seeded by aged recirculating ice particles. Cloud regions with ongoing ice multiplication were identified with the help of a new technique based on identification of small faceted ice crystals smaller 60-100 $\mu\text{m}$ . Based on the results obtained the authors attempt to revisit the role of different SIP mechanisms and identify conditions favorable for SIP. One of the important finding of this study is that melting layers in many cases work as a source of large liquid drops, which then ascended to a supercooled environment via convective or turbulent updrafts. After impaction freezing by preexisting ice, the drops may shatter and initiate a chain reaction of secondary ice particle production.

Measurements were conducted from the National Research Council (NRC) Convar580 research aircraft during two field campaigns: High Ice Water Content (HIWC) and the Buffalo Area Icing and Radar Study 2/Weather Radar Validation Experiment (BAIRS 2/WERVEX).

The HIWC flight operations were conducted out of Cayenne (French Guiana) in May 2015. A total of fourteen Convar580 research flights were conducted in the frame of the HIWC campaign with the average flight endurance of approximately 4 hours. Most of the flights were performed in oceanic MCS in the altitudes ranging from 6500m to 7200m and temperatures from 0°C to -15°C. The observations of MCSs from the Convair-580 were performed during their mature stages, when the area of clouds with longwave brightness temperatures colder than -50°C from GOES13 approached or surpassed its maximum. At that stage, most of the volume of the MCS above the freezing level was nearly glaciated, with embedded mixed phase regions mainly associated with vertical updrafts. However, the studied MCSs during the observations remained dynamically active with updrafts peaking at 15-20m/s.

The BAIRS2/WERVEX flight operations were conducted over Southern Ontario and Upstate New York from January to March 2017. A total of five research flights were conducted in precipitating frontal cloud systems. In the framework of this study, the analysis will be focused on two flights performed in the range of altitudes from 1500m to 3000m and temperature ranges from +5°C to -10°C.

The NRC Convair-580 was equipped with state-of-the-art cloud microphysical and thermodynamic instrumentation. Size distributions of aerosol particles were measured by a DMT UHSAS (Cai et al. 2008). Measurements of ice particle number concentration and ice water content (IWC) were extracted from composite particle size distributions measured by 2D imaging probes a PMS 2DC (Knollenberg, 1981), a SPEC 2-Dimensional Stereo 2DS (Lawson et al. 2006) and a DMT Precipitation Imaging Probe PIP (Baumgardner et al. 2001). Cloud droplet size distributions were measured by a PMS Forward Scattering Spectrometer Probe FSSP (Knollenberg, 1981) and a DMT Cloud Droplet Probe CDP (Lance et al. 2010). Cloud particle images were measured with the SPEC CPI. Bulk liquid water content (LWC) and total water content (TWC) were measured with a SkyPhysTech Nevzorov probe (Korolev et al. 1998) and a SEA IsoKinetic probe (IKP) (Davison et al. 2011). A Rosemount Icing Detector was used for detection of presence of liquid water at  $T < -5\text{C}$  (Mazin et al. 2001). The extinction coefficient was measured with the ECCC Cloud Extinction Probe (Korolev et al. 2014). Vertical velocity



270 was measured by Rosemount 858 and Aventech AIMMS-20 (Beswick et al. 2008). The Convair-580 was also  
equipped with ProSensing W-band and X-band radars with Doppler capability. The UHSAS and IKP were employed  
only during the HIWC project and were not used during BAIRS 2/WERVEX.

In order to mitigate the effect of shattering artifacts on ice particle measurements (Korolev et al. 2011), all cloud  
particle probes were equipped with anti-shattering K-tips (Korolev et al. 2013). The remaining shattering artifacts  
275 were filtered out during data post-processing with the help of the modified interarrival time algorithm (Korolev and  
Field, 2015).

The collected cloud microphysical data were processed and analysed with the help of the ECCC D2G software.  
This software allowed analysis and visualization of cloud microphysical, thermodynamical, radar, and aircraft data  
probes.

280

### 3. Methodology

#### 3.1 Basic assumptions

If initiation of secondary ice occurs in supersaturated environment, then the newly formed ice particles start  
growing through water vapor diffusion and some fraction of secondary ice particles may turn into faceted ice crystals.  
285 If the growth time is shorter than certain characteristic time  $\tau_{corr}$ , then these faceted ice crystals may still be  
associated with the environment of their origin. At time scale  $t > \tau_{corr}$  the size and shape of ice crystals may undergo  
significant metamorphosis, and secondary ice particles may lose their spatial correlation with the environment of their  
origin due to horizontal and/or vertical advection and turbulent diffusion. This process is schematically shown in  
**Fig.1.**

290 This concept was used to develop a method for the identification of SIP regions. This method is based on the  
following assumptions:

- (1) Small faceted ice crystals (hexagonal plates or columns) originate from secondary ice production.
- (2) During some time  $\tau_{corr}$ , the newly formed ice crystals remain associated with the environment where they  
originated.

295 If these assumptions are valid, then small pristine ice crystals can be used as tracers of the environmental  
conditions favorable to secondary ice production. The following subsections aim to assess  $\tau_{corr}$  and the characteristic  
size of small faceted ice crystals.

#### 3.2 Ice crystal habits

In order for an ice crystal to grow as a hexagonal prism, its growth begins as a monocrystalline ice particle.

300 As discussed in the introduction, most potential SIP mechanisms are related to fragmentation of existing ice  
particles. Since water drops frozen at  $T_a > -15^\circ\text{C}$  tend to be monocrystalline (e.g. Pitter and Pruppacher, 1973;  
Hallett 1964), their fragments will also be monocrystalline. In addition, if a large ice particle is polycrystalline, the  
probability of its small fragment to be monocrystalline remains high. Therefore, the condition of monocrystallinity is  
expected to be satisfied for most small ice fragments with  $L_{\max} < 40\text{-}50\mu\text{m}$ . Formation of ice fragments with  
305 characteristic sizes down to  $20\mu\text{m}$  is supported by video material of the breakup of freezing drops from Wildeman et  
al. (2017) and Lauber et al. (2018)



### 3.3 Assessment of spatial correlation time

Condition (2) in section 2a, requires assessment of a characteristic time ( $\tau_{corr}$ ) such that for time  $t < \tau_{corr}$ , the changes of cloud environment parameters (e.g. air temperature ( $T_a$ ), humidity ( $RH$ ), ice particle concentration ( $N_i$ ), droplet concentration ( $N_d$ ), liquid water content ( $LWC$ ), ice water content ( $IWC$ ), etc.) are insignificant, and the SIP-generated ice particles remain within this environment.

In order to assess  $\tau_{corr}$ , the main characteristic time scales of cloud dynamics and kinetics, such as the time of phase relaxation  $\tau_p$ , glaciation time  $\tau_{gl}$ , turbulent diffusion time  $\tau_t$  vertical advection time  $\tau_v$ , and particle residence time  $\tau_r$ , have to be estimated.

The time scale  $\tau_p$  characterizes the response of the cloud environment to changes of in-cloud humidity (e.g., due to entrainment, vertical motion, interaction between liquid and ice phases). So, in order for  $RH$  to relax to its steady state value, it is required that

$$\tau_p < \tau_{corr} \quad (1)$$

For mixed phase clouds, after neglecting the effect of the vertical velocity,  $\tau_p$  can be written as (Korolev and Mazin, 2003)

$$\frac{1}{\tau_p} = \frac{1}{\tau_{p\ ice}} + \frac{1}{\tau_{p\ liq}} \quad (2)$$

where  $\tau_{p\ ice} = \frac{a_i(T,P)}{N_i \bar{r}_i}$  is the time of phase relaxation in the ice clouds,  $\tau_{p\ liq} = \frac{a_l(T,P)}{N_l \bar{r}_l}$  is the time of phase relaxation in liquid clouds,  $N_i, N_l, \bar{r}_i, \bar{r}_l$  are the concentrations and average radii of ice particles and liquid droplets, and  $a_i, a_l$  are coefficients dependent of pressure  $P$  and temperature  $T$ .

The glaciation time scale characterizes the transit time of the mixed phase cloud into an all-ice cloud due the WBF process (Wegener, A., 1911; Bergeron, T., 1935). This process results in complete evaporation of liquid droplets ( $N_d(t > \tau_{gl}) = 0$ ) and changes of steady state relative humidity ( $RH(t > \tau_{gl}) \rightarrow RH_{s\ ice}$ ).

Therefore, it is required that

$$\tau_{corr} < \tau_{gl} \quad (3)$$

The glaciation time scale can be estimated as (Korolev and Mazin, 2003)

$$\tau_{gl} = \frac{b(T,P)}{S_i} \left( \left( \frac{W_{i0} + W_{l0}}{N_i} \right)^{\frac{2}{3}} - \left( \frac{W_{i0}}{N_i} \right)^{\frac{2}{3}} \right) \quad (4)$$

where  $S_i$  is the supersaturation over ice at saturation over water;  $W_{i0}, W_{l0}$  are the initial liquid and ice water content, respectively;  $N_i$  is the concentration of ice particles;  $b(T,P)$  is the coefficient dependent of pressure  $P$  and temperature  $T$ .

Turbulent mixing results in a spatial transport of the SIP particles and a decrease in their concentration. Turbulent mixing may result in biases in the assessment of the spatial scales of the SIP regions and the concentration of the SIP particles. Therefore,  $\tau_{corr}$  should relate to the turbulent mixing time as

$$\tau_{corr} < \tau_t \quad (5)$$

The characteristic time of turbulent mixing of a cloud parcel with a spatial scale  $L$  can be estimated as

$$\tau_t = \varepsilon^{-\frac{1}{3}} L^{\frac{2}{3}} \quad (6)$$



where  $\varepsilon$  is the turbulent energy dissipation rate.

Vertical transport of a cloud parcel affects  $T_a$  and  $RH$ . Assuming an adiabatic temperature change  $\Delta T$ , the characteristic time of vertical transport can be written as

$$\tau_v = \frac{\Delta T}{u_z \gamma_w} \quad (7)$$

where  $u_z$  is the vertical velocity, and  $\gamma_w$  is the moist adiabatic lapse rate. So, in order to limit the amplitude of  $T_a$  and  $RH$ ,  $\tau_{corr}$  and  $\tau_v$  should relate as

$$\tau_{corr} < \tau_v \quad (8)$$

Residence time of an ice particle is determined by the fall velocity  $u_{ice}$  and cloud parcel size  $L$  and is equal to

$$\tau_{res} = \frac{L}{u_{ice}} \quad (9)$$

In order that the ice particle remains in the cloud volume, it is required that

$$\tau_{corr} < \tau_{res} \quad (10)$$

Summarizing Eqs.(1),(3),(5),(8) yields the condition for  $\tau_{corr}$

$$\tau_p < \tau_{corr} < \min(\tau_{gl}, \tau_t, \tau_v, \tau_{res}) \quad (11)$$

Characteristic values of  $\tau_p$ ,  $\tau_{gl}$ ,  $\tau_t$ ,  $\tau_v$ ,  $\tau_{res}$  will be assessed for the following conditions:  $T_a = -5^\circ\text{C}$ ,  $P = 700$  mb,  $N_i = 200 \text{ L}^{-1}$ ,  $N_d = 100 \text{ cm}^{-3}$ ,  $\bar{r}_d = 8 \mu\text{m}$ ,  $\bar{r}_i = 100 \mu\text{m}$ ,  $L = 200\text{-}300 \text{ m}$ ,  $\varepsilon = 10^2 \text{ m}^2/\text{s}^3$ ,  $u_z = 1\text{-}4 \text{ m/s}$ , temperature change limit  $|\Delta T| < 2^\circ\text{C}$ , vertical fall velocity of a solid column with  $L_{\max} = 100 \mu\text{m}$  and  $u_{ice} = 0.1 \text{ m/s}$ .

Substituting  $T$ ,  $P$ ,  $L$ ,  $\varepsilon$ ,  $N_d$ ,  $N_i$ ,  $\bar{r}_d$ ,  $\bar{r}_i$ ,  $\Delta T$ ,  $u_{ice}$  in Eqs.(2),(4),(6),(7),(9) yields to  $\tau_p \approx 5 \text{ s}$ ,  $\tau_{gl} \approx 320 \text{ s}$ ,  $\tau_t \approx 160 \text{ s}$ ,  $\tau_v \approx 80 \text{ s}$ ,  $\tau_{res} \approx 2000 \text{ s}$ . It should be noted that  $\tau_p$ ,  $\tau_{gl}$ ,  $\tau_t$ ,  $\tau_v$  are sensitive to the above parameters and may be different from the obtained estimates. However, the above assessment provides the magnitude of the characteristic times for SIP cloud regions. Based on the above estimates, it would be reasonable to assume that  $\tau_{corr}$  should not exceed 60-120s.

### 3.4 Assessment of ice particle sizes

The estimate of  $\tau_{corr}$  allows for the assessment of ice particles sizes that they may grow up to during this time. Since SIP is expected to occur in liquid or mixed phase clouds, then the water vapor humidity will be close to saturation over water (Korolev and Isaac, 2006).

**Figure 2** shows the calculated length of columns, which were grown by water vapor deposition at saturation over liquid water at different temperatures. The results of the calculations are in a good agreement with the laboratory studies of ice growth in Fukuta and Takahashi (1999).

As shown in **Fig. 2**, during  $\tau_{corr}$  the length of hexagonal columns  $L_{\max}$  may reach  $50 \mu\text{m}$  to  $150 \mu\text{m}$  depending on the temperature and the aspect ratio ( $R = h/2a$ ). Based on this assessment, for the following identification of SIP, the size of small faceted crystals will be limited by  $L_{\max} < 100 \mu\text{m}$ .

### 3.5 Identification of SIP particles

Acquisition of small ice particles images was conducted with the help of the SPEC Cloud Particle Imager (CPI) (Lawson et al. 2001). The CPI was designed for recording 256 grey-level images of ice particles with  $2.3 \mu\text{m}$  resolution at a rate up to approximately 500 images per second. Even though the acquisition rate of particle images is



lower than that for 2D-imaging optical array probes, the CPI provides high-resolution, photographic quality, crisp images of small ice particles. This feature is critical for the goals of this study, and it is superior compared to the OAP probes (e.g. SPEC 2DS, DMT CIP, PMS 2DC). Binary OAP images have lower pixel resolution (from 10 $\mu$ m to 25 $\mu$ m), and their appearance may be significantly modified by diffraction effects (e.g. Korolev 2007; Vaillant de Guélis et al. 2019).

Identification of small pristine ice particles from the CPI imagery was performed with the help of a pre-trained convolutional neural network (Krizhevsky et al., 2017) fine-tuned for the identification of small hexagonal faceted ice crystals. The habit of faceted ice particles was limited by hexagonal prism type crystals: columns, short columns and plates. Examples of CPI images that were used in the final tuning are presented in **Fig.3a**.

Validation, based on hand-labeled images held out from training (950 from each of the three categories), showed that only 4% were misclassified. Although the occurrence of small faceted ice crystals was rare, since they also tended to appear in clusters, a clear signal of their occurrence could be seen above noise from false positives.

Examples of images of small ice particles falsely identified as pristine faceted ice are shown in **Fig.3b**. As it is seen from **Fig.3b**, the centers of growth of the ice crystals are absent in the images. From a crystallographic viewpoint, such crystals cannot be formed during vapor deposition growth, and they are most likely the result of breakups after impact with the CPI inlet (Appendix B). Such particles were excluded from the following analysis.

It is worth noting that some or similar images with irregular shapes as in **Fig.3b** could be a result of SIP, and therefore have a natural origin. Thus, fragments of droplets shattered during freezing may appear as irregular shaped ice before they develop facets. So, the assessment of the concentration of the SIP particles based on the estimates of the concentration of small faceted ice particles can be considered as a lower limit.

In this study, the sizes of particle images are estimated from the maximum size of the image measured in all possible directions ( $L_{\max}$ ). Note, that for randomly oriented hexagonal thin plates  $L_{\max}$  provides an estimate of the diameter of the prism base ( $a$ ) with accuracy better 15%. For hexagonal columns  $L_{\max}$  is not representative of the prism height  $h$ , and depending on the column orientation, it can be either  $L_{\max} > h$  or  $L_{\max} < h$ .

Due to uncertainty of the CPI sample area definition affected by the settings of acceptance out-of-focus images during sampling and post processing, we will be using counting rate ( $s^{-1}$ ) of small faceted ice particles to characterize their concentration. The assessment of concentration of faceted ice provided in the foregoing discussion will be done based on the comparisons of the CPI counting rate of droplets with  $D > 40\mu$ m and that measured by 2DS. The accuracy of such estimation of concentration of small ice particles is estimated as  $\pm 30\%$ .

## 4. Results

### 4.1 SIP observations in tropical MCSs

In this section, we present the observations of SIP during the Convair-580 flight in a tropical MCS on May 15, 2015. The MCS was located off the shore of French Guiana with its center approximately 350km north-east of Cayenne. **Figure 4** shows two GOES13 infrared images of the MCS with an overlay of Convair-580 flight tracks. During the flight leg in **Fig.4a** (UTC 09:23-10:22) the altitude varied between 5600m and 5700m with the air temperature ranging from  $-4^{\circ}\text{C}$  to  $-6^{\circ}\text{C}$ . As it is seen in **Fig.4a**, the Convair-580 crossed three convective cells with the cloud top brightness temperatures ranging between approximately  $-55^{\circ}\text{C}$  and  $-65^{\circ}\text{C}$  (marked by dashed circles).



The flight leg in **Fig.4b** (UTC 11:23 - 12:07) was performed at altitudes ranging from 7000m to 7300m and  
405 temperatures from -11°C to -15°C. Despite its decaying stage, the MSC remained dynamically active at the Convair-  
580 flight level (dashed circle). As will be discussed below, it was found that SIP was observed in convective cloud  
regions indicated by circles in **Fig.4a,b**.

**Figure 5** presents a time series of cloud microphysical parameters corresponding to the flight leg in **Fig.4a**. The  
top panel (**Fig.5a**) shows the CPI counting rate of small faceted ice crystals with  $L_{\max} < 60\mu\text{m}$  and  $100\mu\text{m}$ . Grey  
410 vertical strips indicate cloud sections identified as SIP regions. In this cloud segment, the concentration of small  
pristine ice with  $L_{\max} < 100\mu\text{m}$  attains values up to  $N_{pr100} \approx 480\text{L}^{-1}$ . Based on the discussion in section 3 the origin  
of these small pristine ice crystals is attributed to the vicinity of the level of their observation.

After including aged pristine ice crystals with  $L_{\max} < 200\mu\text{m}$ , the concentration of faceted ice crystals reached  
 $N_{pr200} \approx 900\text{L}^{-1}$ . As was shown in Ladino et al. (2017) the estimated INP concentration remained nearly constant  
415 during the flight operations in French Guiana, and for the temperature range  $-6^\circ\text{C} < T < -4^\circ\text{C}$  it was approximately  
 $N_{INP} \sim 10^{-2}\text{L}^{-1}$ . So, estimated  $N_{INP}$  is nearly four to five orders of magnitude lower than the concentration of small  
pristine ice particles  $N_{pr100}$  and  $N_{pr200}$ . Therefore, the observed small ice particles cannot be explained by  
heterogeneous ice nucleation, and the most likely pathway of their formation is SIP.

To address the question regarding conditions favorable for SIP, we explore the correlations of different  
420 microphysical parameters. As seen from Table 1, the ice particle concentration has the highest correlation coefficient  
with droplets  $D > 60\text{--}80\mu\text{m}$ . In many apparent SIP regions, droplets over  $300\mu\text{m}$  in diameter were registered by the  
CPI. However, in some cloud regions with  $D > 60\mu\text{m}$ , small faceted ice was not observed. Such cloud regions in  
**Fig.5** are indicated by pink strips.

425 **Table 1.** Correlation coefficient between droplet concentration in different size ranges and concentration of small  
faceted ice crystals with  $D_{\max} < 100\mu\text{m}$  for the cloud segment in **Fig.5** for 30 s and 60 s averaging.

Dropl. Conc.	$D > 20\mu\text{m}$	$D > 40\mu\text{m}$	$D > 60\mu\text{m}$	$D > 80\mu\text{m}$	$D > 100\mu\text{m}$
Corr. Coeff. (30s)	0.48	0.66	0.85	0.77	0.69
Corr. Coeff. (60s)	0.56	0.71	0.9	0.85	0.8

The analysis of the entire HIWC data set showed that, as a rule, SIP was not observed or was very unproductive in  
supercooled liquid clouds with droplets  $D_{\max} < 40\mu\text{m}$ . One of such cases in **Fig.5** is indicated by a yellow strip. In  
430 this specific cloud region, the maximum size of droplets measured by FSSP and CDP did not exceed  $D_{\max} = 30\mu\text{m}$ .  
So, this observation suggests that the presence of droplets with  $D_{\max} > 40\mu\text{m}$  is a necessary, but not sufficient  
condition for SIP.

Comparing **Fig.5a,f** also indicates that intense SIP was observed in cloud regions with enhanced turbulence or  
vertical updrafts. Yet in the regions on the left side of **Fig.5a** (UTC 09:33-09:38), SIP was observed in the absence of  
435 any significant turbulence or updraft ( $u_z < 0.2\text{m/s}$ ).

**Figure 6** shows CPI images of cloud particles from a 5-second cloud segment (UTC 09:40:33 – 09:40:38) in  
**Fig.5**. This cloud segment is characterized by an enhanced concentration of small faceted ice particles ( $L_{\max} <$



100 $\mu\text{m}$ ) estimated as approximately  $N_{pr100} \approx 450 \text{ L}^{-1}$ . The majority of the CPI images of droplets are larger than  
40 $\mu\text{m}$  diameter with drizzle size drops up to 200 $\mu\text{m}$  (**Fig.6a**). The droplet concentration measured by FSSP and CDP  
440 is quite low and varies from  $2\text{cm}^{-3}$  to  $6\text{cm}^{-3}$ , whereas the concentration of droplets with  $D > 40\mu\text{m}$  assessed from the  
CPI and 2DS data varies between  $1\text{cm}^{-3}$  and  $3\text{cm}^{-3}$ .

Some of the droplets, identified as frozen and indicated in **Fig.6a** by blue frames, have distorted shapes and  
bulges. As documented by Lauber et al. (2018) the formation of bulges may be accompanied by bubble bursting or  
jetting, which may be a primary source of SIP particles. A few other droplets in the red frames appear as fragments of  
445 shattered droplets. Altogether, the presence of droplet fragments and frozen droplets with bulges are supportive of  
SIP from shattering of freezing drops.

The concentration of frozen drops in **Fig.6a** is estimated as  $N_{frd} \sim 6\text{L}^{-1}$ . This concentration is still much higher  
than the concentration of INP  $N_{INP} \sim 10^{-2}\text{L}^{-1}$  at  $T = -5^\circ\text{C}$  (Ladino et al. 2016), and therefore, droplet freezing cannot be  
explained by heterogeneous nucleation on INPs alone. This gap serves as a basis for explaining droplet freezing due  
450 to impact with splinters produced by shattered freezing drops.

It is worth noting that the concentration of frozen droplets in **Fig.6a** may be higher than  $N_{frd}$ , since some drops  
may freeze without deformation, and after complete freezing they may become transparent again and appear as liquid  
drops (e.g. Mason and Maybank, 1960). The phase state of such drops cannot be unambiguously identified and, for  
the purposes of this study, are considered to be liquid.

**Figure 6a** shows images of aged ice particles sampled in the same cloud volume as the newly generated SIP ice  
particles. The aged ice particles come in two distinct types: faceted columns with  $L_{\text{max}} < 400\mu\text{m}$  and graupel with  
 $L_{\text{max}} < 1000\mu\text{m}$ . Presence of graupel is a necessary conditions for the HM process (Hallett and Mossop 1974).  
However, visual analysis of graupel images (**Fig.6b**) shows that their surfaces appear smooth without small-scale  
features. This appearance suggests that liquid droplets spread over the graupel's surface and freeze as a film. The way  
460 in which the droplets spread is determined primarily by the droplet's size and air temperature (Macklin and Payne,  
1969; Dong and Hallett, 1989).

The surface of graupel in **Fig.6b** appears different than the surfaces of rimed ice cylinders in lab experiments on  
secondary ice production (Macklin, 1960; Choulaton and Latham, 1978; Choulaton et al. 1980; Emersic and  
Connolly 2017). The surfaces of the rimed ice cylinders were highly inhomogeneous with distinct images of frozen  
465 droplets and small features down to  $10\mu\text{m}$ , which presumably serve as a source of splintering. Comparing these  
observations with laboratory studies poses a question regarding whether graupel without small scale features, as in  
**Fig.6b**, could produce splinters.

Another condition for the HM process is presence of droplets smaller than  $12\mu\text{m}$  (Mossop, 1978, 1985). For the  
case in **Fig.6b**, the concentration of droplets with  $D < 15\mu\text{m}$  is estimated from the CDP and FSSP data to be  $0.5\text{cm}^{-3}$   
470 to  $1\text{cm}^{-3}$ . The probability of graupel collision with droplets at such a small concentration is likely too low to have any  
significant effect on the HM process.

**Figure 7a** shows another 5-second segment with successive cloud particle images measured by the CPI in another  
SIP region (UTC 09:46:39-09:46:44). Enlarged cloud droplets and SIP particles from **Fig.7a** are shown in **Fig.7b**.  
The concentration of SIP particles is estimated as  $70\text{L}^{-1}$ , which is lower than the previous case. The concentration of



475 droplets with  $D > 40\mu\text{m}$  is also lower, and it is estimated from the 2DS and CPI measurements as  $0.2\text{--}0.3\text{cm}^{-3}$ .  
However, no droplets larger than  $70\mu\text{m}$  were observed in this cloud segment. The droplet concentration measured by  
FSSP and CDP is approximately  $1\text{cm}^{-3}$ . Due to the large concentration of ice, half of the FSSP and CDP measured  
concentration ( $\sim 0.5\text{cm}^{-3}$ ) may be caused by shattering artifacts (Korolev et al. 2013b).

480 As seen from **Fig.7a**, the background aged ice is represented by columnar shaped particles with well-developed  
facets with minor riming. Some ice particles highlighted by purple frames have features of recirculation. These  
particles started their growth as columns at  $-8^\circ\text{C} < T_a < -4^\circ\text{C}$ , then they were ascended to a plate growth condition  
(e.g.  $-18^\circ\text{C} < T_a < -12^\circ\text{C}$ ) and turned into capped columns. Then they were brought down by a downdraft or  
sedimented back to the columnar growth environment ( $-8^\circ\text{C} < T_a < -4^\circ\text{C}$ ) and developed columns growing out of the  
plate edges.

485 What is important about the case in **Fig.7** is that no graupel, heavily rimed ice or significant amount of liquid  
droplets were observed here. Therefore, the SIP in this specific cloud region does not meet the HM-process criteria.

**Figure 8** shows a time series of microphysical and state parameters in the same cloud area as in **Fig.5** but at a  
higher altitude ( $7000\text{m} < H < 7300\text{m}$ ) and lower temperature ( $-14^\circ\text{C} < T_a < -12^\circ\text{C}$ ). This locale offers the opportunity  
to consider the evolution of ice crystals initiated at lower levels, and to explore the initiation of new ice in colder  
490 environments. **Fig.8a** shows that small faceted particles are spread horizontally over the entire cloud environment.  
The clustering of the small ice parties and their association with updrafts and liquid droplets is less pronounced than  
at the temperature level of  $-4^\circ\text{C}$  to  $-6^\circ\text{C}$  (Figure 5). As follows from **Figs.8b-f**, the liquid phase appears in  
horizontally narrow segments associated with vertical updraft regions. As discussed in Korolev (2007) updrafts may  
extend the maintenance of the liquid phase in mixed phase clouds or completely suppress the WBF process. The  
majority of the cloud segment in **Fig.8** is associated with high IWC peaking up to  $3\text{g/m}^3$  within an ice number  
495 concentration up to  $1\text{cm}^{-3}$ . Liquid phase with no updraft in this kind of environment can exist only for a short time  
period. For example, a mixed phase cloud with  $LWC \sim 0.1\text{g/m}^3$  and  $u_z = 0$  will be glaciated within 50s.

**Fig.9a** presents a sequence of cloud particle images measured during a 10 second time interval (UTC 12:05:31-  
12:05:41) at  $T_a = -14^\circ\text{C}$  and  $H = 7250\text{m}$ . The measurements were conducted within a moderate updraft  $2\text{m/s} <$   
500  $u_z < 6\text{m/s}$ . As it is seen, aged ice particles are represented by graupel, a few lightly rimed particles and numerous  
columns. The origin of columns is related to nucleation at lower levels ( $\sim 5300\text{--}5700\text{m}$ ) at temperatures corresponding  
to columnar growth ( $-10^\circ\text{C} < T_a < -4^\circ\text{C}$ ).

**Figure 9b** shows a subset of zoomed-in images of droplets and small faceted ice particles extracted from **Fig.9**.  
The majority of the small faceted ice particles are hexagonal plates. According to Magono and Lee (1966), these  
505 types of plates are expected to form in the near-saturated-over-water air within the temperature range  $-12^\circ\text{C} < T_a < -$   
 $18^\circ\text{C}$ . Hence, the growth habit of the observed plates is consistent with the temperature range where they were  
sampled.

The concentration of droplets with  $D < 15\mu\text{m}$  is estimated from FSSP and CDP as less than  $1\text{cm}^{-3}$ , and the  
concentration of droplets with  $D > 40\mu\text{m}$  is estimated from 2DS as  $\sim 2\text{cm}^{-3}$ . Therefore, even though the ensemble of  
510 particles in **Fig.9** contains graupel, the rest of the parameters, such as temperature and concentration of small and



large droplets, are well outside the envelope of conditions required for the HM process, as documented in the literature.

**Figure 10a** shows another example of ice particles sampled approximately one kilometer away from those shown in **Fig.9**. This cloud region is characterized by the absence of liquid phase. However, the concentration of small ice particles in **Fig.10** appears to be even higher than that of the small ice in **Fig.9**, where liquid droplets were present. It is worth noting that, in most observational studies, the presence of liquid was considered as one of a necessary conditions for SIP. However, in this particular case, it can be argued that the absence of liquid droplets may be explained by their evaporation as a result of the WBF process just before the cloudy air arrived at the level of observation. The small ice plates in **Fig.10b** could be formed at lower levels with temperatures  $-14^{\circ}\text{C} < T_a < -12^{\circ}\text{C}$  when liquid droplets were still present in the parcel. After that, the plates were ascended in the glaciated updraft to a higher level.

The variety of ice particles in **Fig.9** and **Fig.10** show that SIP apparently occurred continuously during ascent through different levels, with temperatures ranging from  $-2^{\circ}\text{C}$  to  $-14^{\circ}\text{C}$  (at the level of observation).

**Figure 11** shows a summary of the concentrations of small faceted ice crystals and droplets averaged over the entire Convair-580 HIWC data set. This data was collected in ten tropical MCSs with a total sampling length of 9580km within the temperature range  $-15^{\circ}\text{C} < T_a < 0^{\circ}\text{C}$ . It should be noted that small faceted ice crystals, along with cloud drops, occurred in spatial clusters with a characteristic horizontal extension from a few hundred meters to a few kilometers. In many cases, regions with liquid droplets and regions with enhanced concentrations of the small ice may be separated by a few hundred meters or kilometers. In these SIP cloud regions, the concentration of drops and SIP particles is significantly higher than their average values shown in **Fig.11**.

**Figure 11** shows that, on average, the concentration of SIP particles increases, and the concentration of liquid droplets decreases with increasing height within the entire bulk of MCSs at  $-15^{\circ}\text{C} < T_a$ . These trends may be related to the cumulative effect of vertical advection of SIP particles by the convective updrafts.

#### 535 4.2 SIP observations in mid-latitude frontal clouds

The next observation of SIP was conducted in clouds associated with mid-latitude winter frontal systems during the BAIRS2/WERVEX project on March 24<sup>th</sup>, 2017. **Figure 12** shows GOES 16 IR image (a) and Buffalo NEXRAD reflectivity (b) overlaid with the Convair-580 flight track. The cloud regions identified as SIP are indicated by dashed circles.

**Figure 13** shows a one-hour segment of in-situ cloud microphysical measurements sampled from the Convair-580. During these measurements, the Convair-580 performed a series of porpoise and spiral ascents and descents in the vicinity of the melting layer with altitude and temperature changing in the ranges of  $2400\text{m} < H < 4200\text{m}$ , and  $-6^{\circ}\text{C} < T_a < +2^{\circ}\text{C}$ , respectively.

It turned out that in mid-latitude frontal clouds the correlation between the concentration of small faceted ice crystals and liquid droplets is similar to that obtained in tropical MCSs at  $T_a > -6^{\circ}\text{C}$ . The correlation coefficients between the droplet concentrations with different diameters and the count rate of small faceted ice particles are shown in Table 2. As seen from Table 2 the best correlation is reached for droplets with  $D > 40\mu\text{m}$ . This optimal droplet size threshold is smaller than the  $60\mu\text{m}$  found for the tropical MCS (Table 1).



Similar to tropical MCSs, in frontal clouds SIP was not observed in liquid and mixed phase clouds with  
550  $D < 30\mu\text{m}$ . Such cloud segments are indicated by yellow strips in **Fig.13**. Most cases of SIP in **Fig.13** were associated  
with cloud regions with enhanced turbulence ( $u_z \sim \pm 3\text{m/s}$ ).

**Table 2.** Correlation coefficient in different size ranges between droplet concentration and concentration of small  
faceted ice crystals with  $L_{\text{max}} < 100\mu\text{m}$  for the cloud segment in **Fig.13** with 30s and 60s averaging.

Dropl.Conc.	$D > 20\mu\text{m}$	$D > 40\mu\text{m}$	$D > 60\mu\text{m}$	$D > 80\mu\text{m}$	$D > 100\mu\text{m}$
Corr.Coeff. (30s)	0.44	0.51	0.48	0.26	0.11
Corr.Coeff. (60s)	0.65	0.71	0.59	0.29	0.18

555

**Figure 14** shows a sequence of CPI images of cloud particles from a 40s cloud segment with enhanced  
concentrations of small faceted ice crystals. In this cloud region, the concentration of small ice crystals with  $L_{\text{max}} <$   
 $100\mu\text{m}$  peaked up to approximately  $N_{pr100} \approx 1500\text{L}^{-1}$ . Like the case in **Fig.6**, a number of frozen drops with  
deformed shapes (blue frames) were observed in this SIP region. The concentration of visually identified frozen drops  
560 is estimated at approximately  $N_{frd} \approx 30\text{L}^{-1}$ . During the BAIRS2/WERVEX project, the UHSAS probe was not  
installed on the Convair-580, and therefore, the concentration of INP could not be assessed using the approach from  
Ladino et al. (2017). However, the estimate concentrations  $N_{pr100}$  and  $N_{frd}$  still appear to be much higher than  
expected INP concentrations of  $10^{-6}$  to  $10^{-3}\text{L}^{-1}$  at a  $-2^\circ\text{C}$  to  $-5^\circ\text{C}$  temperature range (e.g. Kanji et al., 2017, DeMott et  
al. 2016; Price et al. 2018; Welti et al. 2018; Creamean et al. 2018; Wex et al. 2019).

565 The aged ice particles in **Fig.14b** are represented by rimed columns and graupel-like particles. Therefore, this case  
is consistent with the conditions required for the HM process.

In **Fig.14b**, there are a few ice particles with small faceted crystals stuck to their surfaces, which are indicated  
using brown frames. The origin of small faceted ice on the surface of large particles may have the following reasons:  
(1) vapor deposition regrowth of rime into faceted crystals, or (2) aggregation of newly formed small and pre-existing  
570 large ice particles. Option (1) may not be relevant to the particles in **Fig.14b**, since a closer look at the small particles  
reveals that the centers of their growth are separated from the surface of the large ice particle.

Another argument supporting aggregation is that droplets  $D < 100\mu\text{m}$ , at  $T_a > -10^\circ\text{C}$  tend to freeze as monocrystals  
(e.g. Hallett, 1964; Pitter and Pruppacher, 1973). Small droplets freezing on the surface of a monocrystalline particle  
usually have the same orientation of principal crystallographic axis (e.g. Pitter and Pruppacher 1973; Iwabuch and  
575 Magono, 1973; Uyeda and Kikuchi, 1978). If the rimed droplets continue to grow through vapor deposition, they will  
regrow into faceted crystals with the orientation of principal axes the same as that of the ‘host’ crystal. Examples of  
such ice crystals can be found in **Figs.7** and **9** (brown frames). The alternative to this arrangement is when small  
faceted ice crystals on the surface of a frozen drop, (brown-red frame) **Fig.14b**, have clearly multi-directional  
crystallographic orientations. Therefore, these small ice crystals most likely formed independently of the frozen drop  
580 before they were aggregated.

It is worth noting that the ice particles in the brown-red frame includes five visible small faceted ice crystals  
attached to the surface of the frozen drop. Aggregation of the small crystals may be enhanced by electrostatic charges,



585 which fragmented particles may have after shattering. Charge separation during droplet shattering was observed in  
studies by many research groups (e.g. Mason and Maybank 1960; Kachurin and Bekryaev, 1960; Latham and Mason,  
1961; Evans and Hutchinson, 1963; Scott and Hutchinson, 1965; Kolomeychuk et al. 1975). Therefore, the  
observation of small faceted ice aggregated to the surface of large particles with different orientations of principal  
axis is supportive of their formation due to SIP.

590 **Figure 15** shows another example of a spatial sequence of particle images from a cloud region with enhanced  
concentrations of faceted ice particles apparently resulting from SIP. What is interesting about this is that the  
background aged ice particles were not observed here. Ice particles are either faceted ice crystals or frozen drops. The  
absence of small droplets and graupel suggests that the HM-process is not relevant to this case and that SIP most  
likely occurred here due to shattering of large drops. This hypothesis is supported by the presence of a large number  
of images of fragmented (red frames) and deformed frozen drops (blue frames). The presence of such droplets  
supports the SIP mechanism of shattering of freezing drops. It should be noted that most of the faceted ice crystals in  
595 **Fig.15** are aged and their sizes exceed 100-200 $\mu\text{m}$ . However, the purpose of this case is to show another example of  
SIP, in which the criteria for the HM process are not met.

**Figure 16** shows the average concentration of faceted ice crystals and droplets for two flights from the  
BAIRS2/WERVEX field campaign. As it is seen, the concentration of drops with  $D > 60\mu\text{m}$  decreases with the  
decrease of  $T_a$ . However, the concentration of faceted ice particles has a maximum at  $-3.5^\circ\text{C} < T_a < -1.5^\circ\text{C}$ . This type  
600 of behavior is different from those in tropical MCSs as shown in **Fig.11**. This difference is explained by the absence  
of well-defined convective regions present in MCSs, which transport liquid droplets to the upper levels and extend  
the temperature range of SIP. A narrower SIP temperature range in the studied frontal clouds is explained by SIP  
regions being associated with the mixed phase layer embedded into a deep ice cloud. The cloud top temperature of  
the mixed phase layers limited by  $T_a = -6^\circ\text{C}$  to  $-7^\circ\text{C}$ , which is well reflected in **Fig.16**.

605

## 5. Initial size of secondary ice particles

Knowledge about the initial size and number concentration of secondary ice is of great importance for the  
parameterization of SIP processes in atmospheric models, including weather prediction and climate models,  
particularly when using multi-moment microphysics schemes. The number and size of SIP particles determines the  
610 rate of water vapor depletion, release of latent heat, cloud dynamics, and glaciation time. Because of their slow fall  
velocity, small SIP particles will stay longer in the environment of their origin. Small fragments will also spread  
faster over clouds being transported by turbulent diffusion or vertical updrafts. On the contrary, large SIP fragments  
will precipitate down and have a shorter residence time in the cloud. Besides that, small ice fragments have higher  
probability to be monocrystalline, and therefore regrow into pristine faceted ice crystals. However, large ice  
615 fragments most likely keep an irregular shape during the subsequent growth by water vapor deposition. The size of  
the fragments also plays an important role in charge separation and cloud electrification in general (e.g. Jayarante et  
al. 1983). Altogether, the size distribution of primary SIP particles has a great significance for precipitation  
production, radiation properties and lifetime of clouds.

620 In this section, we will estimate characteristic initial sizes of the SIP particles. Identification of initial sizes of  
secondary ice from the CPI imagery may be problematic because of the limited pixel resolution, and ambiguity of



distinguishing secondary ice fragments from natural cloud particles. In order to address this issue, we will use an indirect assessment of the initial sizes of secondary ice.

**Figure 17** shows images of ice particles sampled in frontal clouds at temperatures ranging from  $-1^{\circ}\text{C}$  to  $-1.5^{\circ}\text{C}$ . All small faceted ice crystals in this cloud region appear to be thin plates (red frames in **Fig.17a**). The thickness of the plates  $h$  is estimated as varying in the range from  $10\mu\text{m}$  to  $20\mu\text{m}$ . Since the smallest size of drops in this region  $D_{\min} \approx 40\mu\text{m} > h$ , then the origin of these plates cannot be attributed to the deposition growth on frozen droplets.

The plates in **Fig.17a** have plane parallel basal surfaces without steps. None of these thin plates have a visually identifiable center of initial growth. Such a shape is suggestive that the secondary ice particles, on which these plates were formed, were monocrystalline and their initial sizes  $L_{\min 0}$  were smaller than the thickness of the plates, i.e.  $L_{\max 0} < h$ . In this case the secondary ice particles were completely embedded inside the plates and became part of the crystallographic lattice. So, there will be no additional refraction of transmitted light and the plates will appear uniform as in **Fig.17a**. Therefore, the smallest initial size of the secondary ice particles is estimated as  $L_{\min 0} \leq 10\mu\text{m}$ .

Secondary ice particles representing a large end of their initial sizes are shown in **Fig.18**, which presents images of fragments of shattered frozen drops. Most of these images were collected in SIP regions indicated by grey areas in **Fig.5**. The maximum size of droplet fragments **Fig.18** is limited by  $L_{\max 0} \approx 400\mu\text{m}$ . In general,  $L_{\max 0}$  is determined by the maximum size of ice particles that participate in SIP. Thus, for the case of freezing raindrops  $L_{\max 0}$  can be extended to a few millimeters.

The obtained estimates suggest that at the moment of initiation, secondary ice particles are represented by a cascade of sizes ranging from  $10\mu\text{m}$  (or smaller) to few hundred microns (or larger). This estimate of initial sizes of SIP particles is consistent with the videos by Wildeman et al. (2017) and Lauber et al. (2018), which showed a variety of fragments with different sizes formed during shattering of freezing drops.

## 6. Shapes of small secondary ice particles

The shapes of secondary ice particles that develop during  $\tau_{\text{corr}}$  may shed light on the environmental conditions associated with the SIP initiation.

A quick look at the ice particle images in **Figs.6,7,14,15,17** shows that the aspect ratio ( $R = h/a$ ) of small ice crystals (hexagonal prisms) may noticeably vary within the same SIP cloud region.

**Figure 19** shows small faceted ice crystals sampled in different SIP cloud regions (**Fig.5**) with narrow temperature ranges from  $-5.5^{\circ}\text{C} < T_a < -5^{\circ}\text{C}$ . As seen from **Fig.19**, despite the minor changes of  $T_a$ , the habits of small ice crystals varied from plates to long columns, and the aspect ratio changed in the range of  $0.3 < R < 6$ .

Based on laboratory studies,  $R$  depends on the air temperature  $T_a$  and supersaturation over ice  $S_i$  of the environment where the ice crystals were grown (e.g. Mason, 1971; Kobayashi, 1961; Bailey and Hallett, 2009). Therefore, it is expected that ice crystals that were formed in the same cloud volume and were exposed to the same  $T_a$  and  $S_i$ , should have the same  $R$ . Thus, the question arises, why do ice crystals with different habits form in the same cloud volume?



There are several possibilities as to how  $R$  may vary. The environment with  $T_a > -4\text{C}$  and  $S_w > 0$  corresponds to the plate growth condition. Therefore, the plates shown in the upper row in **Fig.19** could be formed a few hundred meters below at  $T_a > -4\text{C}$  and then be brought up to the level of observation with a convective updraft. The internal structure of some plates in the upper row (i.e. images ##8,9,11,14, and 15) is indicative of the changing  $T_a$  and  $S_i$  that ice crystals may experience during ascent.

As seen in **Fig.19**, most of the ice crystals are solid columns and thick plates. Following laboratory studies (*ibid*) such ice habits form at  $T_a \approx -5^\circ\text{C}$  in the environment supersaturated with respect to ice ( $S_i > 0$ ) but undersaturated with respect to water ( $S_w < 0$ ). Therefore, the cloudy air in the SIP region, despite any presence of liquid drops was undersaturated with respect to water. Such conditions may occur during the repartitioning of water between ice and liquid phases, when the WBF process is active (Korolev and Mazin, 2003, Pinsky et al. 2018).

Ice crystals with  $R \sim 1$  may be formed as a result frozen droplets developing facets and turning into isometric hexagonal prisms (e.g. Gonda and Yamazaki 1978; Magono et al. 1979; Takahashi and Mori, 2006).

Long columns with  $3 < R < 6$ , shown in the two bottom rows in **Fig.19**, correspond to the growth condition with  $S_w \geq 0$  and  $T_a \sim -5^\circ\text{C}$  (*ibid*).

Accordingly, the shape of secondary ice crystals during the early stage of their evolution, may vary from plates to solid columns. At a later stage, ice particles metamorphose in shape in accordance to their evolving  $T_a(t)$  and  $S_i(t)$ . Thus, **Fig.9** and **10** shows that columns tend to be the dominant shape of the aged secondary ice particles after ascending from 5600m ( $-5^\circ\text{C}$ ) to 7200m ( $-15^\circ\text{C}$ ). The aspect ratio and size of the aged columns vary in the ranges of  $2 < R < 4$  and  $150\mu\text{m} < L_{\text{max}} < 450\mu\text{m}$ , respectively.

## 7. Interaction of secondary ice with the cloud environment

Understanding the interaction between secondary ice particles and the cloud environment is an important part of developing cloud simulations. These interactions are specifically related to small secondary ice particles ( $L_{\text{max}} < 10\mu\text{m}$ ) just after their formation. There are four possible scenarios of how secondary ice particles may evolve after their production:

### 7.1 Vapor deposition growth

This scenario consists of vapor deposition growth of individual secondary ice particles, which requires supersaturation over ice. The necessary condition for this scenario is supersaturation over ice. This condition is satisfied in mixed phase clouds and in updrafts in ice clouds (Korolev and Mazin, 2003). Examples of the secondary ice particles regrown into hexagonal plates and columns are shown in **Figs.6,7,10,14,15,17**. This scenario conserves the concentration of SIP particles ( $N_{SIP}$ ).

### 7.2 Scavenging by liquid droplets

Because of the high concentration of droplets in mixed phase clouds (typically  $10^1\text{-}10^2\text{cm}^{-3}$ ), scavenging of secondary ice particles by liquid drops may have a high frequency of occurrence. Examples of images of frozen drops measured in SIP cloud regions are shown in **Fig.20**. Most of these images do not have any large ice crystals attached to them. Therefore, it would be reasonable to assume that they were nucleated by secondary ice particles, presumably smaller than  $10\text{-}20\mu\text{m}$ . More examples of frozen drops in SIP regions can be seen in **Figs.6,14,15,17** (indicated by



695 blue frames). Because of the high concentration of the frozen drops (section 3) their formation cannot be explained by nucleation via heterogeneous INP.

Scavenging of secondary ice particles by liquid droplets may result in shattered freezing drops and an increase in the concentration of secondary ice. This process induces a positive feedback loop and under certain conditions may result in an avalanche increase in the concentration of secondary ice particles. The possibility of ice multiplication due to a chain reaction was proposed in early studies (e.g. Kachurin and Bekryaev, 1960; Mason and Maybank, 1960; 700 Koenig, 1963; Braham, 1964, Mossop et al. 1964; and others). The observation of frozen and fragmented drops inside the SIP regions can be used as evidence that chain reactions are part of the ice multiplication process.

Droplet freezing may also occur without shattering. In this case, frozen drops keep growing through vapor deposition. Examples of frozen drops with developing facets are shown in **Fig.21**. Observations of frozen drops re-growing into hexagonal prisms, as in **Fig.21**, is indicative that these drops were nucleated by embryonic 705 monocrystalline secondary ice particles. As seen from **Fig.21**, depending on the stage of their growth, some frozen drops developed not only basal and prism faces, but also pyramidal faces. Such evolution of frozen drops was observed in laboratory studies by Gonda and Yamazaki (1978), Magono et al. (1979), Takahashi and Mori (2006). Additional examples of frozen drops with developed facets can be found in **Figs.14,15,17** (green frames).

### 7.3 Scavenging by aged ice particles

710 After their initiation, secondary ice particles may be scavenged by aged ice particles.

As follows from laboratory studies, shattering of freezing drops is usually accompanied by charge separation (e.g. Mason and Maybank, 1960; Kachurin and Bekryaev, 1960; Evans and Hutchinson, 1963; Stott and Hutchinson, 1965; Kolomeychuk et al. 1975). Static electric charges may significantly enhance the scavenging of secondary ice by liquid drops and/or pre-existing ice, and result in the rapid reduction of the concentration of secondary ice.

### 7.4 Sublimation of secondary ice

715 Small secondary ice particles may undergo complete sublimation, if SIP occurs in the environment undersaturated over ice. For example, at  $T_a = -5^\circ\text{C}$  and  $RH_w = 90\%$  ( $RH_{ice} = 95\%$ ) a  $10\mu\text{m}$  ice particle will completely sublimate during  $t_{ev} \approx 4\text{s}$ .

720 Subsaturated in ice or mixed phase clouds may occur due to entrainment of dry air. Thus, Pinsky et al. (2018) showed that in mixed phase cloud simulations complete sublimation of small ice crystals during entrainment and mixing of dry air may occur prior to the complete evaporation of liquid droplets.

Ice clouds may also become subsaturated in downdrafts (Korolev and Mazin 2003). Thus, in an ice cloud parcel with  $N_{ice} = 200\text{L}^{-1}$ , and  $D_{ice}(0) = 200\mu\text{m}$ ,  $RH_{ice}(0) = 100\%$ ,  $T_a(0) = -8^\circ\text{C}$ , descending with  $u_z = -4\text{m/s}$ , relative humidity over ice in  $t = 20\text{s}$  will be  $RH_{ice}(t) = 95\%$ . If such a parcel contained ice splinters with  $D_{ice} \approx 10\mu\text{m}$ , they 725 would completely sublimate. Downdrafts frequently accompany vertical updrafts in dynamically active regions inside MCSs (e.g. **Figs.5f** and **8f**)

The above examples demonstrate that sublimation of newly formed small secondary ice particles may play an important role in suppressing ongoing SIP and the reduction of  $N_{SIP}$ .

**Figure 22** summarises potential interactions of newly formed secondary ice with a cloud environment.

730



## 8. Feasibility of different SIP mechanisms

This section revisits the discussion of the SIP mechanisms, which might be responsible for the enhanced concentration of small ice particles.

### 735 8.1 Droplet fragmentation/shattering during freezing

Images of fragmented frozen drops in **Figs.6,14,15** collocated with secondary ice particles explicitly indicate that the SIP mechanism due to shattering of freezing drops is a contributing factor in ice multiplication. A collection of fragments of frozen drops from other SIP regions is shown in **Fig.17**. Fragments of frozen drops were also documented through in-situ observations reported by Korolev et al. (2004) and Rangno (2008).

740 It should be noted that small fragments of frozen droplets may not be identified from the CPI imagery due to limited pixel resolution and issues related to segregation of irregular shaped fragments from natural particles. Fragments of large frozen drops may also not be found in the SIP region, since they rapidly leave the region of their origin due to the fast sedimentation. For these reasons the fragments of shattered frozen droplets may not be always seen in the SIP cloud regions associated with shattering of freezing drops (e.g. **Figs.7,9,10,17**).

745 Drop freezing by impaction of ice splinters is supported by observations of single frozen drops with deformed shapes (**Fig.20**), and frozen drops with partially developed facets (**Fig.21**). Because of the absence of any visible large ice particles attached to them, these drops must have been nucleated by small ice particles.

As it is seen from **Figs.11** and **16**, secondary ice particles were observed at temperatures both warmer than  $-2^{\circ}\text{C}$  and colder than  $-8^{\circ}\text{C}$ . These temperatures are outside of the HM and riming-splintering temperature range. However, shattering of freezing drops may explain the observation of SIP in a greater temperature range. Such an explanation is consistent with the laboratory observation of the frequency of droplet shattering by Takahashi and Yamashita (1970), Takahashi (1975) and Lauber et al. (2018).

### 750 8.2 Splintering during riming and HM mechanism

As discussed in section 3, some SIP cloud regions comprised both liquid droplets and graupel and therefore, they formally satisfy conditions for the HM process (i.e. **Figs.6** and **14**). However, in a number of SIP cases, graupel was not observed (i.e. **Figs.7,15** and **17**). Whereas in cases like in **Figs.9** and **10** is present, but LWC is very low or absent. Hence, such cases did not meet the formal conditions for the HM process.

760 These inconsistencies of the environmental conditions imply the existence of another SIP mechanism, one that does not involve graupel. One of such mechanisms could be splintering during riming (Ono, 1971; Choulaton et al. 1978; Mossop, 1980). After sticking to an ice surface, some drops during freezing may form an ice shell around a liquid core and rupture, ejecting splinters. Such a scenario is supported by the observation in SIP regions of both liquid droplets and rimed ice.

765 However, Macklin and Payne (1969) and Dong and Hallett (1989) showed that droplets spread out after hitting an ice surface at temperatures warmer than  $-3^{\circ}\text{C}$ . Therefore, an ice shell does not form, and it limits the riming-splintering mechanism at the high temperature end. On the other hand, Griggs and Choulaton (1983) argued that the ice shell might be too strong to break from internal pressure at temperatures  $T_a < -9^{\circ}\text{C}$ . So, these laboratory studies suggest that the temperature range of the splintering during riming remains approximately the same as for the HM process.



Unfortunately, in the framework of this study, it is not possible to segregate droplet shattering, rime splintering,  
770 and HM mechanisms and assess their occurrences.

### 8.3 Fragmentation due to ice-ice collisions

Ice-ice collisional fragmentation depends of many parameters such as the type, size and masses of both ice  
particles involved in the collision, the coefficient of restitution, the relative velocities, the contact time of the  
collision, and the collision force as a function of time. The difference of the fall velocities of the two colliding  
775 particles is one of the critical parameters that determines frequency of their collision and kinetic energy of their  
interaction during impact (Vardiman, 1978). Takahashi (1993) argued that a collision between large graupel grown by  
riming and small graupel grown by deposition (or a rimed snowflake) results in SIP. In laboratory experiments,  
Takahashi (1995) found that collision between large and small graupel might be an efficient source of secondary ice  
particles.

780 Formally, the condition for presence of graupel and rimed ice particles is satisfied in the cases shown in  
**Figs.6,7,9,10,14,17**. Therefore, formation of the small faceted ice particles in these cases can be attributed to the  
collision-fragmentation mechanism.

However, analysis of the CPI imagery in ice clouds lacking graupel and far away from any sources of liquid or  
updrafts did not reveal any noticeable presence of small faceted ice crystals. This observation suggests that collision-  
785 fragmentation mechanism most likely has low significance for SIP for the cases of deposition grown ice crystals.  
Another possible explanation of the absence of evidence of the collision-fragmentation SIP is that the ice fragments  
formed due to ice-ice collision do not regrow into small faceted ice particles. In cases like that, the employed method  
cannot be used for identification of secondary ice formed due to this mechanism.

790 So, in the frame of the obtained observations, the contribution of the collision-fragmentation mechanism to SIP  
remains uncertain.

### 8.4 Ice fragmentation during thermal shock

Laboratory studies by Dye and Hobbs (1968) and Hobbs and Farber (1972) yielded positive results on  
fragmentation of ice particles due to thermal shock caused by a droplet freezing on the surface of an ice particle. This  
mechanism is expected to be active at  $T_a < -5^\circ\text{C}$  (King and Fletcher, 1976a). Since a large fraction of our  
795 observations of SIP can be related to originating temperatures  $T_a > -5^\circ\text{C}$ , it is expected that the thermal shock  
mechanism has low importance for this study. However, for lower temperatures, the role of this mechanism in SIP  
remains uncertain.

### 8.5 Ice fragmentation during sublimation

800 A cloud environment subsaturated with respect to ice is a necessary condition for initiating the mechanism of ice  
fragmentation during sublimation. As it was discussed in section 3, most of the SIP events were observed in mixed  
phase clouds. Such clouds are supersaturated with respect to ice, and therefore, the necessary condition is not  
satisfied. Hence, the fragmentation during sublimation mechanism can be ruled out.

### 8.6 INP activation in transient supersaturation around freezing drops

805 Maximum supersaturation formed around a freezing droplet with  $D = 200\mu\text{m}$  at  $T_a = -4^\circ\text{C}$  is estimated as  $S_w = 1\%$   
(Nix and Fukuta, 1974). Such supersaturation can also be achieved in moderate vertical updrafts (e.g.  $u_z = 4\text{m/s}$ ,  
 $N_{dr} = 50\text{cm}^{-3}$  and  $D = 30\mu\text{m}$ ), which are typical for convective regions in MCSs (e.g. **Fig.5**). Therefore, if activation



of INPs around freezing drops has any significance at  $T_a > -4^\circ\text{C}$ , it should be observed in the bulk of convective updrafts, since the total volume with  $S_w \sim 1\%$  is much higher there compared to that around a freezing drop. However, many MCS regions (not shown here) with vertical updrafts exceeding 4m/s lacked notable concentrations of small ice particles at temperatures close to  $-4^\circ\text{C}$ . Therefore, the mechanism of INP nucleation in transient supersaturation around freezing drops is unlikely to be responsible for the observed concentration of small ice observed in this study at  $T_a > -4^\circ\text{C}$ . However, this mechanism may be active at lower temperatures.

### 9. Effect of the melting layer

One of the most striking findings of this study is the persistent observation of SIP immediately above the melting layer. This phenomenon was observed in clouds in different geographical regions and clouds with different dynamics. So, the question arises: what are the conditions that make the cloud environment above the melting layer favorable for SIP?

One possible explanation is the formation of large drops ( $D \sim 80\text{--}500\mu\text{m}$ ) due to recirculation of ice and liquid through the melting layer. Thus, ice particles turn into drops after falling through the melting layer. Then these drops are brought back above the melting layer by convective or turbulent updrafts. After that, drops collide with aged ice particles and some of these drops may form ice shells during freezing and shatter. This may result in initiation of SIP.

Images of large drops frozen on the surface of aged ice particles observed above the melting layer are shown in **Fig.23**. Most of the drops have deformed shapes with bulges. Formation of bulges may be accompanied by production of ice splinters by jetting or bubble bursting (Lauber et al. 2018).

In laboratory studies (Takahashi, 1975; Lauber et al., 2018), large drops have higher occurrence of shattering compared to small ones. Therefore, shattering of a large drop may play the role of a trigger in initiating SIP. As follows from Tables 1 and 2, the concentration of small ice particles has the highest correlation with the droplets from the size range  $40\text{--}60\mu\text{m}$ . Therefore, it is expected that the droplets from this size range will be a contribution to SIP through maintenance of a chain reaction. **Fig.24a** shows a conceptual model of this process.

In order for a drop to ascend through the melting layer, the velocity of the updraft ( $u_z$ ) should exceed the drop fall velocity ( $u_{fall}$ ). **Figs.5f** and **13f** show that vertical velocity above the melting layer in MCS reached  $u_z \approx 8\text{m/s}$  and in frontal clouds  $u_z \approx 3\text{m/s}$ . Such updraft velocity is sufficient to move through the melting layer drops with  $D = 100\text{--}200\mu\text{m}$  ( $u_{fall} = 1\text{--}2\text{m/s}$ ) during a reasonable time of few tens of seconds to a few minutes.

The conceptual model of the effect of the melting layer of SIP is shown in **Fig.24b**.

### 10. Conclusions

The conclusions obtained in this study are based on the interpretation of observations, which have limited statistics and were obtained along needle-like penetrations of large cloud systems at some time of their evolution. The fact that initial and boundary conditions of the studied cloud systems are poorly known, and the trajectories of cloud volumes and cloud particles are not identifiable, brings a certain ambiguity into the interpretation of the obtained observations. So, in many ways the conclusions in this work bears a qualitative character and the emphasis of this study is on the observational part. The obtained results are expected to contribute in our understanding of SIP, and



they may be used by cloud modeling studies for evaluation of secondary ice production in the numerical simulations  
845 of clouds.

In microphysics schemes that predict the number concentration of ice crystals, i.e. spectral (bin) and multi-  
moment bulk schemes (e.g. Khain et al. 2004; Milbrandt and Yau 2005), SIP is most commonly modeled exclusively  
with a simple parameterization of the HM process. If riming of graupel is occurring in the temperature range between  
-3 and -8C, an ice splinter production rate is computed for this process, with a maximum at -5C, decreasing linearly to  
850 zero at the ends of the temperature range. Assumptions of the crystal number concentration tendency and the size of  
the new crystals are made, based broadly on the published results of Hallet and Mossop (1974). Parameterizations  
that exist for other mechanisms of secondary ice production have been less widely included in modeling efforts to  
explain apparent SIP in observed cloud systems, but when INP are treated rigorously in a prognostic manner, such  
mechanisms are generally found to be too weak to explain observed ice even when considered additively, including  
855 drop shattering and ice-ice collisions (e.g., Fridlind et al. 2007; Fu et al. 2019). It is perhaps unsurprising that such  
additional mechanisms are not more widely adopted if they provide only weak ice generation and still unsatisfactory  
results compared with observations, in addition to being highly uncertain owing to a paucity of robust laboratory data.  
Ultimately, it may be important in atmospheric models for some purposes to improve the representation of both  
primary and secondary ice production in microphysics parameterization schemes based on more recent observations  
860 and the hypothesized processes. It will be a topic of future research to apply the observations presented to develop  
new parameterizations of SIP. However, parameterizations based on field observations will necessarily remain to  
some degree speculative without a strong foundation of laboratory measurements that can provide clear and  
repeatable evidence of specific mechanism strengths.

In the frame of this study we explored the microphysics of SIP cloud regions in tropical MCSs at the mature stage  
865 of their development and mid-latitude frontal cloud systems within the temperature range  $-15^{\circ}\text{C} < T_a < 0^{\circ}\text{C}$ . SIP  
cloud regions were identified based on the presence of numerous small faceted ice crystals with  $L_{\text{max}} < 100\mu\text{m}$ . The  
concentration of such small crystals peaked at  $500\text{-}1000\text{ L}^{-1}$ . Such particles cannot be a result of recirculation or pre-  
existing aged ice. Based on the estimate that the age of such small crystals is limited by  $\tau_{cr} \sim 60\text{-}120\text{s}$ , it was deduced  
that such ice crystals are still associated with the environment of their origin. This assumption was employed to assess  
870 the environmental conditions associated with SIP. As discussed above, our method has a number limitations.

However, it allowed obtaining the following conclusions:

- 1) Most SIP cases were associated with:
  - (a) presence of liquid droplets in the SIP region or somewhere in the vicinity
  - (b) convective updrafts or regions of enhanced turbulence
  - 875 (c) aged rimed ice particles
- 2) The highest correlation between the concentration of small faceted ice crystals and liquid droplets was found  
for droplets in the range  $40\mu\text{m} < D < 60\mu\text{m}$  (Table 1 and 2).
- 3) In several cases, no liquid was observed in SIP cloud regions.
- 4) Graupel was not always present in the SIP cloud regions.
- 880 5) The shape of small faceted ice particles suggests that they were grown in conditions supersaturated with  
respect to ice, but subsaturated with respect to water.



6) Both in tropical MCSs and mid-latitude frontal clouds, secondary ice particles were observed immediately above the melting layer starting at  $T_a < -0.5^\circ\text{C}$ . In MCSs SIP was observed at temperatures down to  $-15^\circ\text{C}$ . No data points were available below this temperature.

885 7) In MCSs, SIP regions vertically correlate with the locations of the coldest tops. No such dependence was found for the frontal cloud systems we analyzed.

We hypothesize that the initiation of SIP above the melting layer is related to the circulation of liquid drops through the melting layer. Liquid drops formed via melting ice particles are advected by the convective updrafts above the melting layer, where they collide with aged ice, freeze and shatter. The ice splinters generated by shattering initialize the chain reaction of SIP.

890 In many cases, concentrations of frozen drops and their fragments exceeding expected concentrations of INPs by orders of magnitude were observed in SIP regions. This discrepancy implies that something other than heterogenous drop freezing must be contributing to SIP. The roles of mechanisms such as HM rime-splintering, ice-ice collisional breakup, thermal shock fragmentation, and INP activation around freezing drops cannot be confidently linked to SIP based on the collected data, for reasons explained at length. Thus, we conclude by process of elimination that the mechanism of droplet shattering during freezing is very likely a critical contributing factor to SIP in these cases.

The obtained results bring up a more general question about the limitations of airborne techniques in the identification of major mechanisms and their efficiencies in SIP. Airborne observations deal mostly with the results of SIP in the form of different stages of aged secondary ice. However, attempts to quantify or parameterize the secondary ice production from in-situ observations are limited because the initial and boundary conditions are mostly unknown. One of the fundamental limitations of airborne techniques is that they do not allow for monitoring and identifying the process of secondary ice directly. In this regard, the pursuit of SIP research lends itself well to laboratory experiments and should be emphasized in this area.

905 **Authors' contribution:**

A. Korolev led collection of the cloud microphysical data and data analysis. I. Heckman performed analysis of the CPI and cloud microphysical data. M. Wolde carried out the airborne data collection. L. Ladino supported the analysis of cloud microphysical data. E. Williams supported the airborne data collection during BAIRS2. A. Korolev prepared the manuscript with the co-authors contribution from, mainly from A. Ackerman, A. Fridlind, P. Lawson, J. Milbrandt.

*Acknowledgements*

The HIWC program was supported by Environment and Climate Change Canada (ECCC), National Research Council (NRC), Transport Canada (TC) and the Federal Aviation Administration (FAA). BAIRS2 program was supported by FAA. WERVEX program was supported by ECCC and TC. Participation of the Massachusetts Institute of Technology in BAIRS2 was supported by FAA under Air Force Contract FA8702-15-D-0001. Any opinions, findings, conclusions, or recommendations expressed in this material are those of the authors and do not necessarily reflect the views of the FAA and TC. Special thanks to the NRC FRL pilots Anthony Brown, Paul Kissman, and Rob Erdos for their outstanding cooperation during in-situ data collection during the HIWC and BAIRS2/WERVEX



920 projects. The authors are grateful for the technical support provided during the data collection period by ECCC and  
NRC technical and engineering teams. Authors acknowledge Ed Emery, Chris Lynch, and Quentin Schwinn NASA  
Glenn Research Center for supporting wind tunnel tests of CPI probe. CFD analysis of the flow around CPI was  
performed by Kirk Creelman Auriga Design Inc. We appreciate help of University of Waterloo student Keegan Cove  
who supported CPI data analysis. The data used in this study is available from ECCC upon request from Alexei  
925 Korolev ([alexei.korolev@canada.ca](mailto:alexei.korolev@canada.ca)).

## Appendix A

### Effect of ice particle shattering on CPI measurements

930 A set of tests in the Cox and Co. wind tunnel facility (Plainview, NY) was conducted to identify the performance  
of different airborne instruments in ice sprays. The primary objective of these tests was to identify and document the  
effect of shattering and bouncing on the measurements of airborne particle probes with different types of tips and  
inlets. More detail about the nature of this study can be found in Korolev et al. (2013b).

935 **Figure A1** shows two snapshots from a high-speed video of the CPI inlet in an ice spray at an air speed of 80m/s.  
The CPI sampling tube has diameter 2.5mm with a rounded edge having a radius of curvature of approximately  
0.5mm. The purpose of such sharpened edge is to mitigate the effect of shattering. However, as it is seen from **Figure**  
**A1**, despite of its relative sharpness, ice particles still shatter and rebound from the edge of the CPI inlet. **Figure A1**  
also shows that the rebound particles are deflected both outside and inside the CPI sampling tube. This observation  
led to the conclusion that the CPI measurements can be affected by mechanical shattering of ice particles on impact  
with the CPI inlet.

940 **Figure A2** presents results of the CFD simulations of the airflow around the CPI housing. The simulation was  
conducted for the airspeed 150m/s,  $P = 450\text{mb}$ ,  $T_a = -40\text{C}$ . As it is seen from **Figure A2c,d** the velocity of the air  
changes by approximately 30m/s at the distance of  $\sim 2\text{cm}$  when passing through the front part of the inlet tube. This  
will result in large aerodynamic stresses, which ice particles may experience when entering the CPI inlet. Another  
area where ice particles may experience strong aerodynamic stresses is located near the walls of the inlet tube (**Figure**  
945 **A2b**). Such aerodynamic stresses may result in deformation of the shape of liquid drops and fragmentation of large  
fragile ice particles and aggregates with weak bonding.

It is worth noting that the CPI used in this study had a modified shortened inlet tube. The original CPI front inlet  
tube is longer, and due to the inner step at the front edge, it has a higher velocity jump at the entrance compared to  
that in **Figure A2d**.

950 **Figure A3** shows examples of CPI images of fragmented ice particles sampled in clouds. The image frame in  
**Figure A3a** includes 55 fragments, which corresponds to a local concentration of approximately  $6 \times 10^3 \text{cm}^{-3}$  to  
 $7 \times 10^3 \text{cm}^{-3}$ . Such concentrations of ice particles does not seem to be possible in natural clouds. The only reasonable  
explanation is that these fragments result from ice particle shattering due to mechanical impact with the CPI inlet, and  
on immediately after shattering the fragments form a spatially dense cluster of particles with high local concentration.

955 The cluster of multiple images shown in **Figure A3b** is unlikely to occur in clouds due to significantly different  
fall velocities, which range from approximately 1cm/s (for the smallest particle in the image frame) to 1m/s (for the



largest particle). Most likely the images in **Figure A3b** are debris from shattered ice particle originated from impact with the CPI inlet.

960 The origin of fragmentation of the particle in **Figure A3c,d** is most likely related to fragmentation due to aerodynamic stresses. If such fragmentation occurs due to some natural causes, the fragments due to their different sizes are unlikely to stay together due to different fall velocities.

In the present study, CPI images similar to those in **Figure A4** were identified as shattered artifacts. The shapes of most of these particles conflict with the concept of growth of crystal lattice. However, their shapes can be explained by the fragmentation of ice crystals.

965 Images as in **Figure A4** usually form spatial clusters with close spacing, and they appear in CPI image frames (2.3 mm × 2.3 mm) as multiple images as in **Figure A3**. In this regard, the number of images in CPI image frames was used as an indicator of shattering. In this work, CPI image frames with more than one image were identified as shattering artifacts, and such frames were excluded from the analysis. The SPEC CPIview processing software was modified to recognize such image frames during the data processing and refute them.

970 It should be noted that some of the images as in **Figure A4** may have a natural origin. However, their exclusion from the analysis does not affect the conclusions obtained in this study.

975 The analysis of the CPI data showed that the number of shattering artifacts increases with the increase of particle size. Misalignment between the direction of local airflow and the axis of the CPI sampling tube also results in increase of the shattering artifacts and a decrease of the counting rate of intact particles. Thus, for a 4° angle between the airflow and axes of the sampling tube, the CPI sampling volume will be in the geometrical shadow. This will result in reduction of the counting rate of primarily large particles. Smaller particles will follow the airflow, and their counting rate will be less affected.

980 The orientation of the CPI sampling tube was aligned with the local flow at  $H = 3\text{km}$  and  $TAS = 100\text{m/s}$  at the mounting location on the Convair-580. For other flight conditions, the misalignment between the local airflow and the axis CPI inlet tube will persist.

## References

- Ackerman, A. S., Fridlind, A. M., Grandin, A., Dezitter, F., Weber, M., Strapp, J. W. and Korolev, A. V.: High ice water content at low radar reflectivity near deep convection - Part 2: Evaluation of microphysical pathways in updraft parcel simulations, *Atmos. Chem. Phys.*, 15(20), 11729–11751, doi:10.5194/acp-15-11729-2015, 2015.
- 985 Adkins, C. J.: The fragmentation and electrification of very small droplets, *Q. J. Roy. Meteor. Soc.*, 86(368), 186, doi:10.1002/qj.49708636807, 1960.
- Auer, A. H.: Observations of Ice Crystal Nucleation by Droplet Freezing in Natural Clouds, *J. Atmos. Sci.*, 28(2), 285–290, doi:10.1175/1520-0469(1971)028<0285:OOICNB>2.0.CO;2, 1971.
- 990 Aufdermaur, A. N. and Johnson, D. A.: Charge separation due to riming in an electric field, *Q. J. Roy. Meteor. Soc.*, 98(416), 369–382, doi:10.1002/qj.49709841609, 1972.
- Bacon, N. J., Swanson, B. D., Baker, M. B. and Davis, E. J.: Breakup of levitated frost particles, *J. Geophys. Res. Atmos.*, 103(D12), 13763–13775, doi:10.1029/98JD01162, 1998.



- 995 Bailey, M. P. and Hallett, J.: A Comprehensive Habit Diagram for Atmospheric Ice Crystals: Confirmation from the Laboratory, AIRS II, and Other Field Studies, *J. Atmos. Sci.*, 66(9), 2888–2899, doi:10.1175/2009JAS2883.1, 2009.
- Baker, B. A.: On the Nucleation of Ice in Highly Supersaturated Regions of Clouds, *J. Atmos. Sci.*, 48(16), 1904–1907, doi:10.1175/1520-0469(1991)048<1905:OTNOII>2.0.CO;2, 1991.
- 1000 Baumgardner, D., Jonsson, H. H., Dawson, W., O'Connor, D. P. and Newton, R.: The Cloud, Aerosol and Precipitation Spectrometer (CAPS) A New Instrument for Cloud Investigations, 2001.
- Beard, K. V.: Ice initiation in warm-base convective clouds: An assessment of microphysical mechanisms, *Atmos. Res.*, 28, 125–152, doi:10.1016/0169-8095(92)90024-5, 1992.
- Bentley, W. A. and Humphreys, W. J.: *Snow Crystals*, Dover Publications, New York, 266 pp., 1962.
- Bergeron, T.: On the physics of clouds and precipitation, in *Procès Verbaux de l'Association de Météorologie*, International Union of Geodesy and Geophysics, 156–178, 1935.
- 1005 Beswick, K. M., Gallagher, M. W., Webb, A. R., Norton, E. G. and Perry, F.: Application of the AVENTECH AIMMS20AQ airborne probe for turbulence measurements during the Convective Storm Initiation Project, *Atmos. Chem. Phys.*, 8(17), 5449–5463, doi:10.5194/acp-8-5449-2008, 2008.
- Bigg, E. K.: The fragmentation of freezing water drop, *Bull. l'Observatoire du Puy-de-Dôme*, N3, 65–69, 1957.
- 1010 Blanchard, D. G.: A verification of the Bally-Dorsey theory of spicule formation on sleet pellets, *J. Meteorol.*, 8(4), 268–269, doi:10.1175/1520-0469(1951)008<0268:AVOTBD>2.0.CO;2, 1951.
- Bower, K., J. Moss, S., W. Johnson, D., Choulaton, T., Latham, J., Brown, P., Blyth, A. and R. Cardwell, J.: A parametrization of ice water content observed in frontal and convective clouds, *Q. J. Roy. Meteor. Soc.*, 122, 1815–1844, doi:10.1002/qj.49712253605, 1996.
- 1015 Braham, R. R.: What is the Role of Ice in Summer Rain-Showers?, *J. Atmos. Sci.*, 21(6), 640–645, doi:10.1175/1520-0469(1964)021<0640:WITROI>2.0.CO;2, 1964.
- Brewer, A. W. and Palmer, H. P.: Condensation Processes at Low Temperatures, and the Production of New Sublimation Nuclei by the Splintering of Ice, *Nature*, 164(4164), 312–313, doi:10.1038/164312a0, 1949.
- 1020 Brownscombe, J. L. and Thorndike, N. S. C.: Freezing and Shattering of Water Droplets in Free Fall, *Nature*, 220(5168), 687–689, doi:10.1038/220687a0, 1968.
- Cai, Y., Montague, D. C., Mooiweer-Bryan, W. and Deshler, T.: Performance characteristics of the ultra high sensitivity aerosol spectrometer for particles between 55 and 800nm: Laboratory and field studies, *J. Aerosol Sci.*, 39(9), 759–769, doi:https://doi.org/10.1016/j.jaerosci.2008.04.007, 2008.
- 1025 Cantrell, W. and Heymsfield, A. J.: Production of Ice in Tropospheric Clouds: A Review, *B. Am. Meteorol. Soc.*, 86(6), 795–808, doi:10.1175/BAMS-86-6-795, 2005.
- Cheng, R. J.: Water Drop Freezing: Ejection of Microdroplets, *Science*, 170(3965), 1395–1396, doi:10.1126/science.170.3965.1395, 1970.
- Choulaton, T. W., Latham, J. and Mason, B. J.: A possible mechanism of ice splinter production during riming, *Nature*, 274(5673), 791–792, doi:10.1038/274791a0, 1978.
- 1030 Choulaton, T., Griggs, D., Y. Humood, B. and Latham, J.: Laboratory studies of riming, and its relation to ice splinter production, *Q. J. Roy. Meteor. Soc.*, 106, 367–374, doi:10.1002/qj.49710644809, 2007.



- Cooper, W. A.: Cloud physics investigations by the University of Wyoming in HIPLEX 1977 Bureau of Reclamation Rep. No. AS119, Laramie, WY: Dept. of Atmospheric Science, University of Wyoming, 1977.
- Crawford, I., Bower, K., Choullarton, T., Dearden, C., Crosier, J., Westbrook, C., Capes, G., Coe, H., Connolly, P., R. 1035  
Dorsey, J., Gallagher, M., Williams, P., Trembath, J., Cui, Z. and Blyth, A.: Ice formation and development in aged, wintertime cumulus over the UK: observations and modelling, *Atmos. Chem. Phys.*, 12, doi:10.5194/acp-12-4963-2012, 2012.
- Creamean, J. M., Kirpes, R. M., Pratt, K. A., Spada, N. J., Maahn, M., de Boer, G., Schnell, R. C. and China, S.: 1040  
Marine and terrestrial influences on ice nucleating particles during continuous springtime measurements in an Arctic oilfield location, *Atmos. Chem. Phys.*, 18(24), 18023–18042, doi:10.5194/acp-18-18023-2018, 2018.
- Crosier, J., Bower, K. N., Choullarton, T. W., Westbrook, C. D., Connolly, P. J., Cui, Z. Q., Crawford, I. P., Capes, G. L., Coe, H., Dorsey, J. R., Williams, P. I., Illingworth, A. J., Gallagher, M. W. and Blyth, A. M.: Observations of ice multiplication in a weakly convective cell embedded in supercooled mid-level stratus, *Atmos. Chem. Phys.*, 11(1), 257–273, doi:10.5194/acp-11-257-2011, 2011.
- 1045  
Crosier, J., Choullarton, T. W., Westbrook, C. D., Blyth, A. M., Bower, K. N., Connolly, P. J., Dearden, C., Gallagher, M. W., Cui, Z. and Nicol, J. C.: Microphysical properties of cold frontal rainbands, *Q. J. Roy. Meteor. Soc.*, 140(681), 1257–1268, doi:10.1002/qj.2206, 2014.
- Davison, C., Ratvasky, T. and Lilie, L.: Naturally Aspirating Isokinetic Total Water Content Probe: Wind Tunnel 1050  
Test Results and Design Modifications, in: SAE 2011 International Conference on Aircraft and Engine Icing and Ground Deicing, Chicago, Illinois, June 13–17, 2011.
- DeMott, P. J., Hill, T. C. J., McCluskey, C. S., Prather, K. A., Collins, D. B., Sullivan, R. C., Ruppel, M. J., Mason, R. H., Irish, V. E., Lee, T., Hwang, C. Y., Rhee, T. S., Snider, J. R., McMeeking, G. R., Dhaniyala, S., Lewis, E. R., Wentzell, J. J. B., Abbatt, J., Lee, C., Sultana, C. M., Ault, A. P., Axson, J. L., Diaz Martinez, M., Venero, I., Santos-Figueroa, G., Stokes, M. D., Deane, G. B., Mayol-Bracero, O. L., Grassian, V. H., Bertram, T. H., 1055  
Bertram, A. K., Moffett, B. F. and Franc, G. D.: Sea spray aerosol as a unique source of ice nucleating particles, *P. Natl. Acad. Sci.*, 113(21), 5797–5803, doi:10.1073/pnas.1514034112, 2016.
- DeMott, P. J., Prenni, A. J., Liu, X., Kreidenweis, S. M., Petters, M. D., Twohy, C. H., Richardson, M. S., Eidhammer, T. and Rogers, D. C.: Predicting global atmospheric ice nuclei distributions and their impacts on climate, *P. Natl. Acad. Sci.*, 107(25), 11217–11222, doi:10.1073/pnas.0910818107, 2010.
- 1060  
Dong, Y. Y. and Hallett, J.: Droplet accretion during rime growth and the formation of secondary ice crystals, *Q. J. Roy. Meteor. Soc.*, 115(485), 127–142, doi:10.1002/qj.49711548507, 1989.
- Dong, Y. Y., Oraltay, R. G. and Hallett, J.: Ice particle generation during evaporation, *Atmos. Res.*, 32(1–4), 45–53, doi:10.1016/0169-8095(94)90050-7, 1994.
- Dorsey, N. E.: The Freezing of Supercooled Water, *T. Am. Philos. Soc.*, 38(3), 247–328 [online] Available from: 1065  
<http://www.jstor.org/stable/1005602>, 1948.
- Dye, J. E. and Hobbs, P. V.: The Influence of Environmental Parameters on the Freezing and Fragmentation of Suspended Water Drops, *J. Atmos. Sci.*, 25(1), 82–96, doi:10.1175/1520-0469(1968)025<0082:TIOEPO>2.0.CO;2, 1968.



- 1070 Emersic, C. and Connolly, P. J.: Microscopic observations of riming on an ice surface using high speed video, *Atmos. Res.*, 185, 65–72, doi:10.1016/j.atmosres.2016.10.014, 2017.
- Evans, D. G. and Hutchinson, W. C. A.: The electrification of freezing water droplets and of colliding ice particles, *Q. J. Roy. Meteor. Soc.*, 89(381), 370–375, doi:10.1002/qj.49708938108, 1963.
- Field, P. R., Heymsfield, A. J. and Bansemer, A.: Shattering and Particle Interarrival Times Measured by Optical Array Probes in Ice Clouds, *J. Atmos. Ocean. Tech.*, 23(10), 1357–1371, doi:10.1175/JTECH1922.1, 2006.
- 1075 Field, P. R., Lawson, P., Brown, P., Lloyd, G., Westbrook, C., Moisseev, D., Miltenberger, A., Nenes, A., Blyth, A., Choulaton, T., Connolly, P., Bühl, J., Crosier, J., Cui, Z., Dearden, C., DeMott, P., Flossmann, A. I., Heymsfield, A. J., Huang, Y. and Sullivan, S.: Secondary Ice Production - current state of the science and recommendations for the future, in *Meteorological Monographs*, vol. 58, 7.1–7.20, 2017.
- 1080 Field, P. R., Wood, R., Brown, P. R. A., Kaye, P. H., Hirst, E., Greenaway, R. and Smith, J. A.: Ice Particle Interarrival Times Measured with a Fast FSSP, *J. Atmos. Ocean. Tech.*, 20(2), 249–261, doi:10.1175/1520-0426(2003)020<0249:IPITMW>2.0.CO;2, 2003.
- Findeisen, W.: Über die Entstehung der Gewitterelektrizität (On the origin of lightning electricity), *Meteorol. Z.*, 6, 201–221, 1940.
- 1085 Findeisen, W. and Findeisen, E.: Untersuchungen über die Eissplitterbildung an Reifschichten (Ein Beitrag zur Frage der Entstehung der Gewitterelektrizität und zur Mikrostruktur der Cumulonimbren). Investigations on the ice splinters formation on rime layers (A contribution to the problem of the origin of storm electricity and to the microstructure of cumulonimbus), *Meteorol. Z.*, 60, 145–154, 1943.
- Foster, T. and Hallett, J.: A laboratory investigation of the influence of liquid water content on the temperature dependence of secondary ice crystal production during soft hail growth, in: *Am. Met. Soc. Cloud Physics Conference*, Chicago, 123–126, 1982.
- 1090 Fridlind, A. M., Ackerman, A. S., McFarquhar, G., Zhang, G., Poellot, M. R., DeMott, P. J., Prenni, A. J. and Heymsfield, A. J.: Ice properties of single-layer stratocumulus during the Mixed-Phase Arctic Cloud Experiment: 2. Model results, *J. Geophys. Res. Atmos.*, 112(D24), doi:10.1029/2007JD008646, 2007.
- 1095 Fu, S., Deng, X., Shupe, M. D. and Xue, H.: A modelling study of the continuous ice formation in an autumnal Arctic mixed-phase cloud case, *Atmos. Res.*, 228, 77–85, doi:https://doi.org/10.1016/j.atmosres.2019.05.021, 2019.
- Fukuta, N. and Takahashi, T.: The Growth of Atmospheric Ice Crystals: A Summary of Findings in Vertical Supercooled Cloud Tunnel Studies, *J. Atmos. Sci.*, 56(12), 1963–1979, doi:10.1175/1520-0469(1999)056<1963:TGOAIC>2.0.CO;2, 1999.
- 1100 Gagin, A.: Effect of supersaturation on the ice crystal production by natural aerosols, *Journal de Recherches Atmosphériques*, 6, 175–185, 1972.
- Gagin, A. and Nozyce, N.: The nucleation of ice crystals during the freezing of large supercooled drops, *Journal de Recherches Atmosphériques*, 18, 119–129, 1984.
- Gardiner, B. A. and Hallett, J.: Degradation of In-Cloud Forward Scattering Spectrometer Probe Measurements in the Presence of Ice Particles, *J. Atmos. Ocean. Tech.*, 2(2), 171–180, doi:10.1175/1520-0426(1985)002<0171:DOICFS>2.0.CO;2, 1985.
- 1105



- Gayet, J.-F., Febvre, G. and Larsen, H.: The Reliability of the PMS FSSP in the Presence of Small Ice Crystals, *J. Atmos. Ocean. Tech.*, 13(6), 1300–1310, doi:10.1175/1520-0426(1996)013<1300:TROTPF>2.0.CO;2, 1996.
- Gold, L. W.: Crack formation in ice plates by thermal shock, *Can. J. Phys.*, 41(10), 1712–1728, doi:10.1139/p63-172, 1963.
- 1110 Gonda, T. and Yamazaki, T.: Initial Growth forms of Snow Crystals Growing from Frozen Cloud Droplets, *J. Meteorol. Soc. Japan*, 62(1), 190–192, doi:10.2151/jmsj1965.62.1\_190, 1984.
- Griggs, D. and Choullarton, T.: Freezing modes of riming drops with application to ice splinter production, *Q. J. Roy. Meteor. Soc.*, 109, 243–253, doi:10.1002/qj.49710945912, 1983.
- Hallett, J.: Experimental Studies of the Crystallization of Supercooled Water, *J. Atmos. Sci.*, 21, 671–682, doi:10.1175/1520-0469(1964)021<0671:ESOTCO>2.0.CO;2, 1964.
- 1115 Hallett, J. and Mossop, S. C.: Production of secondary ice particles during the riming process, *Nature*, 249(5452), 26–28, doi:10.1038/249026a0, 1974.
- Hallett, J., Sax, R. I., Lamb, D. and Murty, A. S. R.: Aircraft measurements of ice in Florida cumuli, *Q. J. Roy. Meteor. Soc.*, 104(441), 631–651, doi:10.1002/qj.49710444108, 1978.
- 1120 Harris-Hobbs, R. L. and Cooper, W. A.: Field Evidence Supporting Quantitative Predictions of Secondary Ice Production Rates, *J. Atmos. Sci.*, 44(7), 1071–1082, doi:10.1175/1520-0469(1987)044<1071:FESQPO>2.0.CO;2, 1987.
- Heymsfield, A. J.: On measurements of small ice particles in clouds, *Geophys. Res. Lett.*, 34(23), doi:10.1029/2007GL030951, 2007.
- 1125 Heymsfield, A. J. and Mossop, S. C.: Temperature dependence of secondary ice crystal production during soft hail growth by riming, *Q. J. Roy. Meteor. Soc.*, 110(465), 765–770, doi:10.1002/qj.49711046512, 1984.
- Hobbs, P. V.: Ice Multiplication in Clouds, *J. Atmos. Sci.*, 26(2), 315–318, doi:10.1175/1520-0469(1969)026<0315:IMIC>2.0.CO;2, 1969.
- Hobbs, P. V. and Alkezweeny, A. J.: The Fragmentation of Freezing Water Droplets in Free Fall, *J. Atmos. Sci.*, 25(5), 881–888, doi:10.1175/1520-0469(1968)025<0881:TFOFWD>2.0.CO;2, 1968.
- 1130 Hobbs, P. V. and Burrows, D. A.: The Electrification of an Ice Sphere Moving through Natural Clouds, *J. Atmos. Sci.*, 23(6), 757–763, doi:10.1175/1520-0469(1966)023<0757:TEOAIS>2.0.CO;2, 1966.
- Hobbs, P. V. and Cheng, R. J.: Microdroplets and Water Drop Freezing, *Science*, 173(3999), 849–850, doi:10.1126/science.173.3999.849, 1971.
- 1135 Hobbs, P. V. and Farber, R.: Fragmentation of ice particles in clouds, *Journal de Recherches Atmosphériques*, 6, 245–258, 1972.
- Hobbs, P. V. and Rangno, A. L.: Ice Particle Concentrations in Clouds, *J. Atmos. Sci.*, 42(23), 2523–2549, doi:10.1175/1520-0469(1985)042<2523:IPCIC>2.0.CO;2, 1985.
- Hobbs, P. V. and Rangno, A. L.: Rapid Development of High Ice Particle Concentrations in Small Polar Maritime Cumuliform Clouds, *J. Atmos. Sci.*, 47(22), 2710–2722, doi:10.1175/1520-0469(1990)047<2710:RDOHIP>2.0.CO;2, 1989.
- 1140 Iwabuchi, T. and Magono, C.: A Laboratory Experiment on the Freezing Electrification of Freely Falling Water Droplets, *J. Meteorol. Soc. Japan*, 53, 393–401, doi:10.2151/jmsj1965.53.6\_393, 1975.



- Jayarathne, E. R., Saunders, C. P. R. and Hallett, J.: Laboratory studies of the charging of soft-hail during ice crystal interactions, *Q. J. Roy. Meteor. Soc.*, 109(461), 609–630, doi:10.1002/qj.49710946111, 1983.
- 1145
- Jensen, E. J., Lawson, P., Baker, B., Pilon, B., Mo, Q., Heymsfield, A. J., Bansemer, A., Bui, T. P., McGill, M., Hlavka, D., Heymsfield, G., Platnick, S., Arnold, G. T. and Tanelli, S.: On the importance of small ice crystals in tropical anvil cirrus, *Atmos. Chem. Phys.*, 9(15), 5519–5537, doi:10.5194/acp-9-5519-2009, 2009.
- Jiusto, J. E. and Weickmann, H. K.: types of snowfall, *B. Am. Meteorol. Soc.*, 54(11), 1148–1162, doi:10.1175/1520-0477(1973)054<1148:TOS>2.0.CO;2, 1973.
- 1150
- Johnson, D. A. and Hallett, J.: Freezing and shattering of supercooled water drops, *Q. J. Roy. Meteor. Soc.*, 94(402), 468–482, doi:10.1002/qj.49709440204, 1968.
- Kachurin, L. G. and Bekryaev, V. I.: Investigation of the electrification of crystallizing water, *Dokl. Akad. Nauk. SSSR*, 130, 57–60, 1960.
- 1155
- Kanji, Z. A., Ladino, L. A., Wex, H., Boose, Y., Burkert-Kohn, M., Cziczo, D. J. and Krämer, M.: Overview of Ice Nucleating Particles, *Meteorol. Mon.*, 58, 1.1-1.33, doi:10.1175/AMSMONOGRAPHIS-D-16-0006.1, 2017.
- Keppas, S. C., Crosier, J., Choulaton, T. W. and Bower, K. N.: Ice lollies: An ice particle generated in supercooled conveyor belts, *Geophys. Res. Lett.*, 44(10), 5222–5230, doi:10.1002/2017GL073441, 2017.
- Kikuchi, K. and Uyeda, H.: On Snow Crystals of Spatial Dendritic Type, *J. Meteorol. Soc. Japan*, 57(3), 282–287, doi:10.2151/jmsj1965.57.3\_282, 1979.
- 1160
- Kimura, T. and Kajikawa, M.: An Observation of Ice Pellets, *J. Meteorol. Soc. Japan*, 62(5), 802–808, doi:10.2151/jmsj1965.62.5\_802, 1984.
- King, W. D. and Fletcher, N. H.: Pressures and stresses in freezing water drops, *J. Phys. D-Appl. Phys.*, 6(18), 2157–2173, doi:10.1088/0022-3727/6/18/302, 1973.
- 1165
- King, W. D. and Fletcher, N. H.: Thermal Shock as an Ice Multiplication Mechanism. Part I. Theory, *J. Atmos. Sci.*, 33(1), 85–96, doi:10.1175/1520-0469(1976)033<0085:TSAAIM>2.0.CO;2, 1976a.
- King, W. D. and Fletcher, N. H.: Thermal Shock as an Ice Multiplication Mechanism. Part II. Experimental, *J. Atmos. Sci.*, 33(1), 97–102, doi:10.1175/1520-0469(1976)033<0097:tsaaim>2.0.co;2, 1976b.
- Knollenberg, R. G.: Techniques for probing cloud microstructure, in *Clouds their Formation, Optical Properties, and Effects*, edited by P. V Hobbs and A. Deepak, 15–91, Academic Press, 1981.
- 1170
- Koenig, L. R.: The Glaciating Behavior of Small Cumulonimbus Clouds, *J. Atmos. Sci.*, 20(1), 29–47, doi:10.1175/1520-0469(1963)020<0029:TGBOSC>2.0.CO;2, 1963.
- Koenig, L. R.: Drop Freezing Through Drop Breakup, *J. Atmos. Sci.*, 22(4), 448–451, doi:10.1175/1520-0469(1965)022<0448:DFTDB>2.0.CO;2, 1965.
- 1175
- Kolomeychuk, R. J., McKay, D. C. and Iribarne, J. V.: The Fragmentation and Electrification of Freezing Drops, *J. Atmos. Sci.*, 32(5), 974–979, doi:10.1175/1520-0469(1975)032<0974:TFAEOF>2.0.CO;2, 1975.
- Korolev, A. V.: Reconstruction of the Sizes of Spherical Particles from Their Shadow Images. Part I: Theoretical Considerations, *J. Atmos. Ocean. Tech.*, 24(3), 376–389, doi:10.1175/JTECH1980.1, 2007.
- Korolev, A. V, Bailey, M. P., Hallett, J. and Isaac, G. A.: Laboratory and in situ observation of deposition growth of frozen drops, *J. Appl. Meteorol.*, 43(4), 612–622, 2004.
- 1180



- Korolev, A. V, Emery, E. F., Strapp, J. W., Cober, S. G. and Isaac, G. A.: Quantification of the Effects of Shattering on Airborne Ice Particle Measurements, *J. Atmos. Ocean. Tech.*, 30(11), 2527–2553, doi:10.1175/JTECH-D-13-00115.1, 2013b.
- 1185 Korolev, A. V, Emery, E. F., Strapp, J. W., Cober, S. G., Isaac, G. A., Wasey, M. and Marcotte, D.: Small Ice Particles in Tropospheric Clouds: Fact or Artifact? Airborne Icing Instrumentation Evaluation Experiment, *B. Am. Meteorol. Soc.*, 92(8), 967–973, doi:10.1175/2010BAMS3141.1, 2010.
- Korolev, A. V and Isaac, G. A.: Observations of sublimating ice particles in clouds, in: Proceedings of the 14th International Conference on Clouds and Precipitation, 808–811, 2004.
- 1190 Korolev, A. V and Isaac, G. A.: Relative humidity in liquid, mixed-phase, and ice clouds, *J. Atmos. Sci.*, 63(11), 2865–2880, 2006.
- Korolev, A. V and Mazin, I. P.: Zones of Increased and Decreased Droplet Concentration in Stratiform Clouds, *J. Appl. Meteorol.*, 32(4), 760–773, doi:10.1175/1520-0450(1993)032<0760:ZOIADD>2.0.CO;2, 1993.
- Korolev, A. V and Mazin, I. P.: Supersaturation of Water Vapor in Clouds, *J. Atmos. Sci.*, 60(24), 2957–2974, doi:10.1175/1520-0469(2003)060<2957:SOWVIC>2.0.CO;2, 2003.
- 1195 Korolev, A. V, Strapp, J. W., Isaac, G. A. and Nevzorov, A. N.: The Nevzorov Airborne Hot-Wire LWC–TWC Probe: Principle of Operation and Performance Characteristics, *J. Atmos. Ocean. Tech.*, 15(6), 1495–1510, doi:10.1175/1520-0426(1998)015<1495:TNAHWL>2.0.CO;2, 1998.
- Korolev, A., Emery, E. and Creelman, K.: Modification and Tests of Particle Probe Tips to Mitigate Effects of Ice Shattering, *J. Atmos. Ocean. Tech.*, 30(4), 690–708, doi:10.1175/JTECH-D-12-00142.1, 2013a.
- 1200 Korolev, A. and Field, P. R.: Assessment of the performance of the inter-arrival time algorithm to identify ice shattering artifacts in cloud particle probe measurements, *Atmos. Meas. Tech.*, 8(2), 761–777, doi:10.5194/amt-8-761-2015, 2015.
- Korolev, A., Shashkov, A. and Barker, H.: Calibrations and Performance of the Airborne Cloud Extinction Probe, *J. Atmos. Ocean. Tech.*, 31(2), 326–345, doi:10.1175/JTECH-D-13-00020.1, 2014.
- 1205 Krizhevsky, A., Sutskever, I. and Hinton, G. E.: ImageNet Classification with Deep Convolutional Neural Networks, *Commun. ACM*, 60(6), 84–90, doi:10.1145/3065386, 2017.
- Ladino, L. A., Korolev, A., Heckman, I., Wolde, M., Fridlind, A. M. and Ackerman, A. S.: On the role of ice-nucleating aerosol in the formation of ice particles in tropical mesoscale convective systems, *Geophys. Res. Lett.*, 44(3), 1574–1582, doi:10.1002/2016GL072455, 2017.
- 1210 Lance, S., Brock, C. A., Rogers, D. and Gordon, J. A.: Water droplet calibration of the Cloud Droplet Probe (CDP) and in-flight performance in liquid, ice and mixed-phase clouds during ARCPAC, *Atmos. Meas. Tech.*, 3(6), 1683–1706, doi:10.5194/amt-3-1683-2010, 2010.
- Langham, E. J. and Mason, B. J.: The Heterogeneous and Homogeneous Nucleation of Supercooled Water, in: Proceedings of the Royal Society A: Mathematical, Physical and Engineering Sciences, vol. 247, 493–504, 1958.
- 1215 Langmuir, I.: The Production of Rain by a Chain Reaction in Cumulus Clouds at Temperatures above Freezing, *J. Atmos. Sci.*, 5, 175–192, doi:10.1175/1520-0469(1948)005<0175:TPORBA>2.0.CO;2, 1948.



- Lasher-Trapp, S., Leon, D. C., DeMott, P. J., Villanueva-Birriel, C. M., Johnson, A. V., Moser, D. H., Tully, C. S. and Wu, W.: A Multisensor Investigation of Rime Splintering in Tropical Maritime Cumuli, *J. Atmos. Sci.*, 73(6), 2547–2564, doi:10.1175/JAS-D-15-0285.1, 2016.
- 1220 Latham, J. and Mason, B. J.: Generation of electric charge associated with the formation of soft hail in thunderclouds, in: *Proceedings of the Royal Society of London. Series A. Mathematical and Physical Sciences*, 260, 237–249, doi:10.1098/rspa.1961.0052, 1961.
- Lauber, A., Schätzle, M., Handmann, P., Kiselev, A. and Leisner, T.: Production of secondary ice particles and splintering of freezing droplets as a potential mechanism of ice multiplication, in: *Proceedings of the International Conference on Clouds and Precipitation*, Manchester, United Kingdom, available at: [https://bwsyncandshare.kit.edu/dl/fiCNioFokGC4zRCLdPongUXD/ICCP\\_2016\\_Kiselev.ppt](https://bwsyncandshare.kit.edu/dl/fiCNioFokGC4zRCLdPongUXD/ICCP_2016_Kiselev.ppt), 2016.
- 1225 Lauber, A., Kiselev, A., Pander, T., Handmann, P. and Leisner, T.: Secondary Ice Formation during Freezing of Levitated Droplets, *J. Atmos. Sci.*, 75(8), 2815–2826, doi:10.1175/JAS-D-18-0052.1, 2018.
- Lawson, P., Gurganus, C., Woods, S. and Brientjes, R.: Aircraft Observations of Cumulus Microphysics Ranging from the Tropics to Midlatitudes: Implications for a “New” Secondary Ice Process, *J. Atmos. Sci.*, 74(9), 2899–2920, doi:10.1175/JAS-D-17-0033.1, 2017.
- 1230 Lawson, R. P.: Effects of ice particles shattering on the 2D-S probe, *Atmos. Meas. Tech.*, 4(7), 1361–1381, doi:10.5194/amt-4-1361-2011, 2011.
- Lawson, R. P., Baker, B. A., Schmitt, C. G. and Jensen, T. L.: An overview of microphysical properties of Arctic clouds observed in May and July 1998 during FIRE ACE, *J. Geophys. Res. Atmos.*, 106(D14), 14989–15014, doi:10.1029/2000JD900789, 2001.
- 1235 Lawson, R. P., O’Connor, D., Zmarzly, P., Weaver, K., Baker, B., Mo, Q. and Jonsson, H.: The 2D-S (Stereo) Probe: Design and Preliminary Tests of a New Airborne, High-Speed, High-Resolution Particle Imaging Probe, *J. Atmos. Ocean. Tech.*, 23(11), 1462–1477, doi:10.1175/JTECH1927.1, 2006.
- 1240 Lloyd, G., Choulaton, T. W., Bower, K. N., Gallagher, M. W., Connolly, P. J., Flynn, M., Farrington, R., Crosier, J., Schlenczek, O., Fugal, J. and Henneberger, J.: The origins of ice crystals measured in mixed-phase clouds at the high-alpine site Jungfraujoch, *Atmos. Chem. Phys.*, 15(22), 12953–12969, doi:10.5194/acp-15-12953-2015, 2015.
- Macklin, W. C.: The Production of Ice Splinters During Riming, *Nubila*, 3, 30–33, 1960.
- Macklin, W. C. and Payne, G. S.: The spreading of accreted droplets, *Q. J. Roy. Meteor. Soc.*, 95, 724–730, doi:10.1002/qj.49709540606, 1969.
- 1245 Magono, C., Fujita, S.-I. and Taniguchi, T.: Unusual Types of Single Ice Crystals Originating from Frozen Cloud Droplets, *J. Atmos. Sci.*, 36, 2495–2501, doi:10.1175/1520-0469(1979)036<2495:utoc>2.0.co;2, 2002.
- Malkina, A. D. and Zak, E. G.: Mechanism of freezing of liquid droplets, *Transactions of the Central Aerological Observatory (Trudi TsAO)*, 9, 61–75, 1952.
- 1250 Mason, B. J. and Maybank, J.: The fragmentation and electrification of freezing water drops, *Q. J. Roy. Meteor. Soc.*, 86(176–185), doi:10.1002/qj.49708636806, 1960.
- Mazin, I. P. and Shmeter, S. M.: Turbulence within clouds and in the vicinity, in *Handbook of Clouds and Cloudy Atmosphere*, edited by I. P. Mazin and A. K. Khrgian, 277–294, Gidrometeoizdat, 1989.



- 1255 McFarquhar, G. M., Um, J., Freer, M., Baumgardner, D., Kok, G. L. and Mace, G.: Importance of small ice crystals to cirrus properties: Observations from the Tropical Warm Pool International Cloud Experiment (TWP-ICE), *Geophys. Res. Lett.*, 34, doi:10.1029/2007GL029865, 2007.
- Milbrandt, J. A. and Yau, M. K.: A Multimoment Bulk Microphysics Parameterization. Part II: A Proposed Three-Moment Closure and Scheme Description, *J. Atmos. Sci.*, 62(9), 3065–3081, doi:10.1175/JAS3535.1, 2005.
- 1260 Mossop, S. C.: Concentrations of Ice Crystals in Clouds, *B. Am. Meteorol. Soc.*, 51(6), 474–479, doi:10.1175/1520-0477(1970)051<0474:COICIC>2.0.CO;2, 1970.
- Mossop, S. C.: Some Factors Governing Ice Particle Multiplication in Cumulus Clouds, *J. Atmos. Sci.*, 35(10), 2033–2037, doi:10.1175/1520-0469(1978)035<2033:SFGIPM>2.0.CO;2, 1978.
- Mossop, S. C.: The Origin and Concentration of Ice Crystals in Clouds, *B. Am. Meteorol. Soc.*, 66(3), 264–273, doi:10.1175/1520-0477(1985)066<0264:TOACOI>2.0.CO;2, 1985.
- 1265 Mossop, S. C., Cottis, R. E. and Bartlett, B. M.: Ice crystal concentrations in cumulus and stratocumulus clouds, *Q. J. Roy. Meteor. Soc.*, doi:10.1002/qj.49709841509, 1972.
- Mossop, S. C. and Hallett, J.: Ice Crystal Concentration in Cumulus Clouds: Influence of the Drop Spectrum, *Science*, 186, 632–634, doi:10.1126/science.186.4164.632, 2006.
- Mossop, S. C., Ono, A. and Heffernan, K. J.: Studies of ice crystal in natural clouds, *Journal de Recherches Atmosphériques*, 3, 45–64, 1964.
- 1270 Muchnik, V. M. and Rudko, J. S.: Peculiarities of freezing supercooled water drops, *Trudy Ukrainsk Hydro Meteorological Institute*, 26, 64–73, 1961.
- Nix, N. and Fukuta, N.: Nonsteady-State Kinetics of Droplet Growth in Cloud Physics, *J. Atmos. Sci.*, 31(5), 1334–1343, doi:10.1175/1520-0469(1974)031<1334:NSKODG>2.0.CO;2, 1974.
- 1275 Ono, A.: Some Aspects of the Natural Glaciation Processes in Relatively Warm Maritime Clouds, *J. Meteorol. Soc. Japan*, 49A(0), 845–858, doi:10.2151/jmsj1965.49A.0\_845, 1971.
- Ono, A.: Evidence on the nature of ice crystal multiplication processes in natural cloud, *Journal de Recherches Atmosphériques*, 6, 399–408, 1972.
- Oraltay, R. G. and Hallett, J.: Evaporation and melting of ice crystals: A laboratory study, *Atmos. Res.*, 24(1–4), 169–189, doi:10.1016/0169-8095(89)90044-6, 1989.
- 1280 Pena, J. A., de Pena, R. G. and Hosler, C. L.: Freezing of Water Droplets in Equilibrium with Different Gases, *J. Atmos. Sci.*, 26(2), 309–314, doi:10.1175/1520-0469(1969)026<0309:FOWDIE>2.0.CO;2, 1969.
- Phillips, V. T. J., Patade, S., Gutierrez, J. and Bansemer, A.: Secondary Ice Production by Fragmentation of Freezing Drops: Formulation and Theory, *J. Atmos. Sci.*, doi:10.1175/jas-d-17-0190.1, 2018.
- 1285 Pinsky, M., Khain, A. and Korolev, A.: Theoretical Analysis of Liquid–Ice Interaction in the Unsaturated Environment with Application to the Problem of Homogeneous Mixing, *J. Atmos. Sci.*, doi:10.1175/jas-d-17-0228.1, 2018.
- Pitter, R. L. and Pruppacher, H. R.: A wind tunnel investigation of freezing of small water drops falling at terminal velocity in air, *Q. J. Roy. Meteor. Soc.*, doi:10.1002/qj.49709942111, 1973.
- 1290 Price, H. C., Baustian, K. J., McQuaid, J. B., Blyth, A., Bower, K. N., Choullarton, T., Cotton, R. J., Cui, Z., Field, P. R., Gallagher, M., Hawker, R., Merrington, A., Miltenberger, A., Neely, R. R., Parker, S. T., Rosenberg, P. D.,



- Taylor, J. W., Trembath, J., Vergara-Temprado, J., Whale, T. F., Wilson, T. W., Young, G. and Murray, B. J.: Atmospheric Ice-Nucleating Particles in the Dusty Tropical Atlantic, *J. Geophys. Res. Atmos.*, doi:10.1002/2017JD027560, 2018.
- 1295 Pruppacher, H. R.: On the growth of ice crystals in supercooled water and aqueous solution drops, *Pure Appl. Geophys.*, doi:10.1007/BF00874894, 1967.
- Pruppacher, H. R. and Klett, J. D.: *Microphysics of clouds and precipitation*, Kluwer academic, Dordrecht, 1997.
- Pruppacher, H. R. and Schlamp, R. J.: A wind tunnel investigation on ice multiplication by freezing of waterdrops falling at terminal velocity in air, *J. Geophys. Res.*, 80, 380–386, doi:10.1029/jc080i003p00380, 1975.
- 1300 Puzano, V. P. and Accuratov, V. I.: Towards formation mechanism of some types of hail, *Gidrologia i Meteorologia*, N6, 29–33, 1952.
- Rangno, A. L.: Fragmentation of Freezing Drops in Shallow Maritime Frontal Clouds, *J. Atmos. Sci.*, 65, 1455–1466, doi:10.1175/2007jas2295.1, 2008.
- Rosinski, J., Langer, G. and Nagamoto, C. T.: On the effect of microdroplets from the surface of a freezing water drop, *J. Appl. Meteorol.*, 11, 405–406, 1972.
- 1305 Rosinski, J., Nagamoto, C. T. and Kerrigan, T. C.: Heterogeneous nucleation of water and ice in the transient supersaturation field surrounding a freezing drop, *Journal de Recherches Atmosphériques*, 9, 107–117, 1975.
- Saunders, C. P. R. and Hosseini, A. S.: A laboratory study of the effect of velocity on Hallett-Mossop ice crystal multiplication, *Atmos. Res.*, 59, 3–14, doi:10.1016/S0169-8095(01)00106-5, 2001.
- 1310 Schaefer, V. J.: Formation of Ice Crystals in Ordinary and Nuclei-Free Air, *Ind. Eng. Chem.*, 44(6), 1300–1304, doi:10.1021/ie50510a033, 1952.
- Schaefer, V. J. and Cheng, R. J.: The production of ice crystal fragments by sublimation and electrification, *Journal de Recherches Atmosphériques*, 5, 5–10, 1971.
- Schwarzenboeck, A., Shcherbakov, V., Lefevre, R., Gayet, J. F., Pointin, Y. and Durooure, C.: Indications for stellar-crystal fragmentation in Arctic clouds, *Atmos. Res.*, 92, 220–228, doi:10.1016/j.atmosres.2008.10.002, 2009.
- 1315 Stith, J. L., Avallone, L. M., Bansemmer, A., Basarab, B., Dorsi, S. W., Fuchs, B., Lawson, R. P., Rogers, D. C., Rutledge, S. and Toohey, D. W.: Ice particles in the upper anvil regions of midlatitude continental thunderstorms: The case for frozen-drop aggregates, *Atmos. Chem. Phys.*, 14, 1973–1985, doi:10.5194/acp-14-1973-2014, 2014.
- Stott, D. and Hutchinson, W. C. A.: The electrification of freezing water drops, *Q. J. Roy. Meteor. Soc.*, 91, 80–86, doi:10.1002/qj.49709138711, 1965.
- 1320 Takahashi, C.: Deformations of Frozen Water Drops and Their Frequencies, *J. Meteorol. Soc. Japan*, 53(6), 402–411, doi:10.2151/jmsj1965.53.6\_402, 1975.
- Takahashi, C.: Relation between the Deformation and the Crystalline Nature of Frozen Water Drops, *J. Meteorol. Soc. Japan*, 54(6), 448–453, doi:10.2151/jmsj1965.54.6\_448, 1976.
- 1325 Takahashi, C. and Mori, M.: Growth of snow crystals from frozen water droplets, *Atmos. Res.*, 82(1–2), 385–390, doi:10.1016/j.atmosres.2005.12.013, 2006.
- Takahashi, C. and Yamashita, A.: Deformation and Fragmentation of Freezing Water Drops in Free Fall, *J. Meteorol. Soc. Japan*, 47(6), 431–436, doi:10.2151/jmsj1965.47.6\_431, 1969.



- 1330 Takahashi, C. and Yamashita, A.: Shattering of Frozen Water Drops in a Supercooled Cloud, *J. Meteorol. Soc. Japan*, 48(4), 373–376, doi:10.2151/jmsj1965.48.4\_373, 1970.
- Takahashi, T.: High ice crystal production in winter cumuli over the Japan Sea, *Geophys. Res. Lett.*, 20(6), 451–454, doi:10.1029/93GL00613, 1993.
- Takahashi, T., Nagao, Y. and Kushiyama, Y.: Possible High Ice Particle Production during Graupel–Graupel Collisions, *J. Atmos. Sci.*, 52(24), 4523–4527, 1995.
- 1335 Uyeda, H. and Kikuchi, K.: Freezing Experiment of Supercooled Water Droplets Frozen by Using Single Crystal Ice, *J. Meteorol. Soc. Jpn. Ser. II*, 56(1), 43–51, doi:10.2151/jmsj1965.56.1\_43, 1978.
- Vaillant de Guéllis, T., Schwarzenböck, A., Shcherbakov, V., Gourbeyre, C., Laurent, B., Dupuy, R., Coutris, P. and Duroure, C.: Study of the diffraction pattern of cloud particles and the respective responses of optical array probes, *Atmos. Meas. Tech.*, 12(4), 2513–2529, doi:10.5194/amt-12-2513-2019, 2019.
- 1340 Vardiman, L.: The Generation of Secondary Ice Particles in Clouds by Crystal–Crystal Collision, *J. Atmos. Sci.*, 35(11), 2168–2180, doi:10.1175/1520-0469(1978)035<2168:TGOSIP>2.0.CO;2, 1978.
- Vidaurre, G. and Hallett, J.: Particle Impact and Breakup in Aircraft Measurement, *J. Atmos. Ocean. Tech.*, 26(5), 972–983, doi:10.1175/2008JTECHA1147.1, 2009.
- Visagie, P. J.: Pressures Inside Freezing Water Drops, *J. Glaciol.*, 8(53), 301–309, doi:DOI: 10.3189/S0022143000031270, 1969.
- 1345 Wegener, A.: *Thermodynamik der Atmosphäre*, J. A. Barth, Leipzig, 1911.
- Welti, A., Müller, K., Fleming, Z. L. and Stratmann, F.: Concentration and variability of ice nuclei in the subtropical maritime boundary layer, *Atmos. Chem. Phys.*, 18(8), 5307–5320, doi:10.5194/acp-18-5307-2018, 2018.
- Wex, H., Huang, L., Zhang, W., Hung, H., Traversi, R., Becagli, S., Sheesley, R. J., Moffett, C. E., Barrett, T. E., Bossi, R., Skov, H., Hünerbein, A., Lubitz, J., Löffler, M., Linke, O., Hartmann, M., Herenz, P. and Stratmann, F.: Annual variability of ice-nucleating particle concentrations at different Arctic locations, *Atmos. Chem. Phys.*, 19(7), 5293–5311, doi:10.5194/acp-19-5293-2019, 2019.
- 1350 Wildeman, S., Sterl, S., Sun, C. and Lohse, D.: Fast Dynamics of Water Droplets Freezing from the Outside In, *Phys. Rev. Lett.*, 118(8), 84101, doi:10.1103/PhysRevLett.118.084101, 2017.
- 1355 Yano, J.-I. and Phillips, V. T. J.: Ice–Ice Collisions: An Ice Multiplication Process in Atmospheric Clouds, *J. Atmos. Sci.*, 68(2), 322–333, doi:10.1175/2010JAS3607.1, 2010.
- Yano, J.-I., Phillips, V. T. J. and Kanawade, V.: Explosive ice multiplication by mechanical break-up in ice–ice collisions: a dynamical system-based study, *Q. J. Roy. Meteor. Soc.*, 142(695), 867–879, doi:10.1002/qj.2687, 2016.
- 1360



**Table 1.** Correlation coefficient between droplet concentration in different size ranges and concentration of small faceted ice crystals with  $D_{\max} < 100\mu\text{m}$  for the cloud segment in **Fig.5** for 30 s and 60 s averaging.

Dropl.Conc.	$D > 20\mu\text{m}$	$D > 40\mu\text{m}$	$D > 60\mu\text{m}$	$D > 80\mu\text{m}$	$D > 100\mu\text{m}$
Corr.Coeff. (30s)	0.48	0.66	0.85	0.77	0.69
Corr.Coeff. (60s)	0.56	0.71	0.9	0.85	0.8



**Table 2.** Correlation coefficient in different size ranges between droplet concentration and concentration of small faceted ice crystals with  $L_{\max} < 100\mu\text{m}$  for the cloud segment in **Fig.13** with 30s and 60s averaging.

Dropl.Conc.	$D>20\mu\text{m}$	$D>40\mu\text{m}$	$D>60\mu\text{m}$	$D>80\mu\text{m}$	$D>100\mu\text{m}$
Corr.Coeff. (30s)	0.44	0.51	0.48	0.26	0.11
Corr.Coeff. (60s)	0.65	0.71	0.59	0.29	0.18

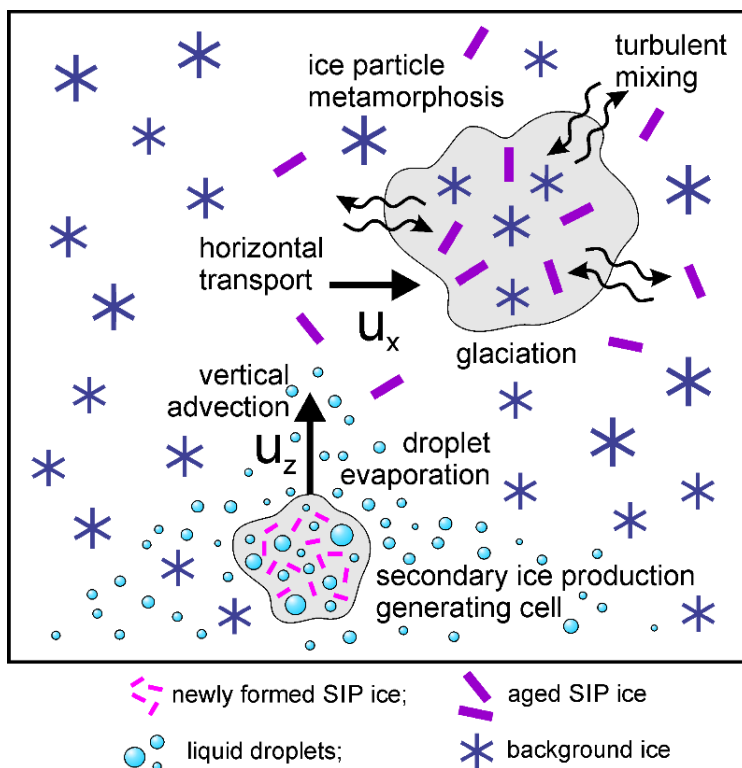


**Figure 1.** Conceptual diagram of the transport of secondary ice production particles in a cloud after its formation.

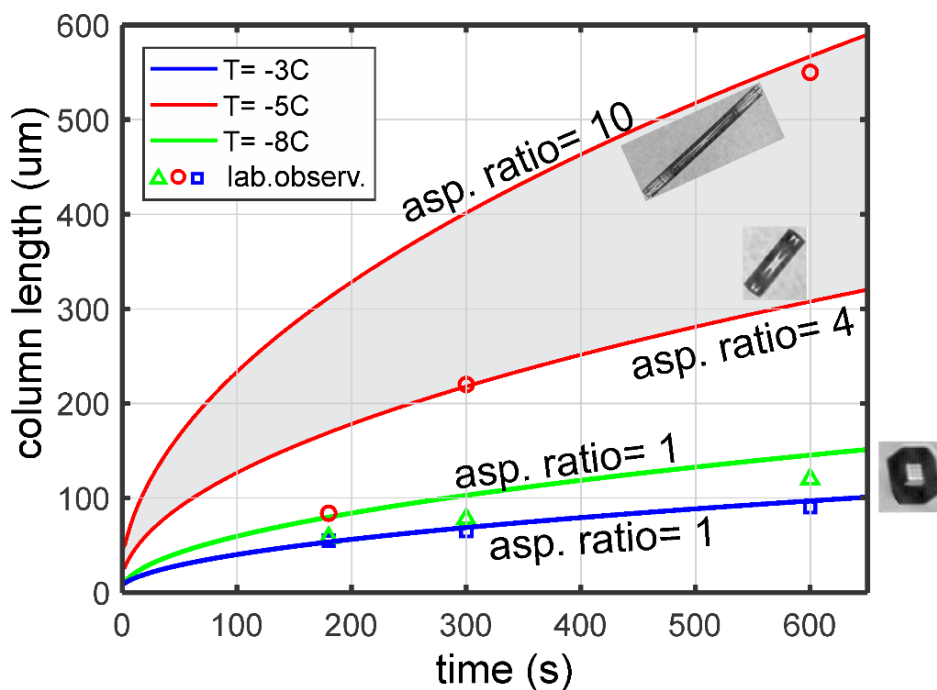


**Figure 2.** Calculated ice column growth at vapor saturation over water at -3C, -5C, -8C. Triangles, circles and squares are laboratory observations by Fukuta and Takahashi (1999).

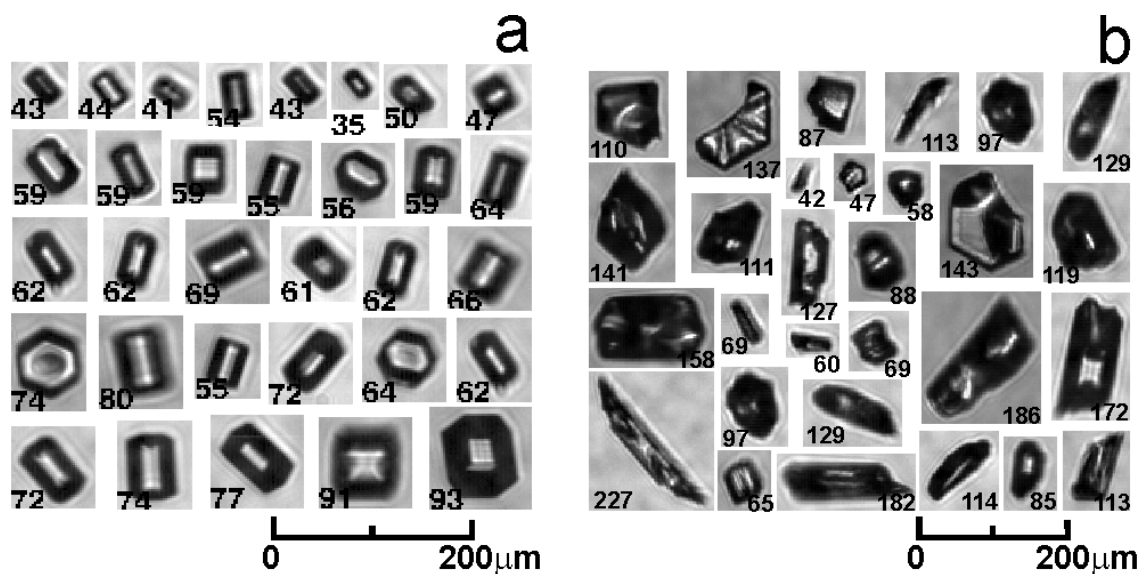


**Figure 3** (a) Examples of CPI images used for neural net training to identify small faceted ice crystals. These ice crystals were collected in the mesoscale convective clouds at altitudes  $6200 < H < 7000$  and temperature range  $-10\text{C} < T < -3\text{C}$ . (b) Examples of images misidentified by the image recognition software as pristine faceted ice. The numbers below each image frame indicate maximum size of the images in  $\mu\text{m}$ .

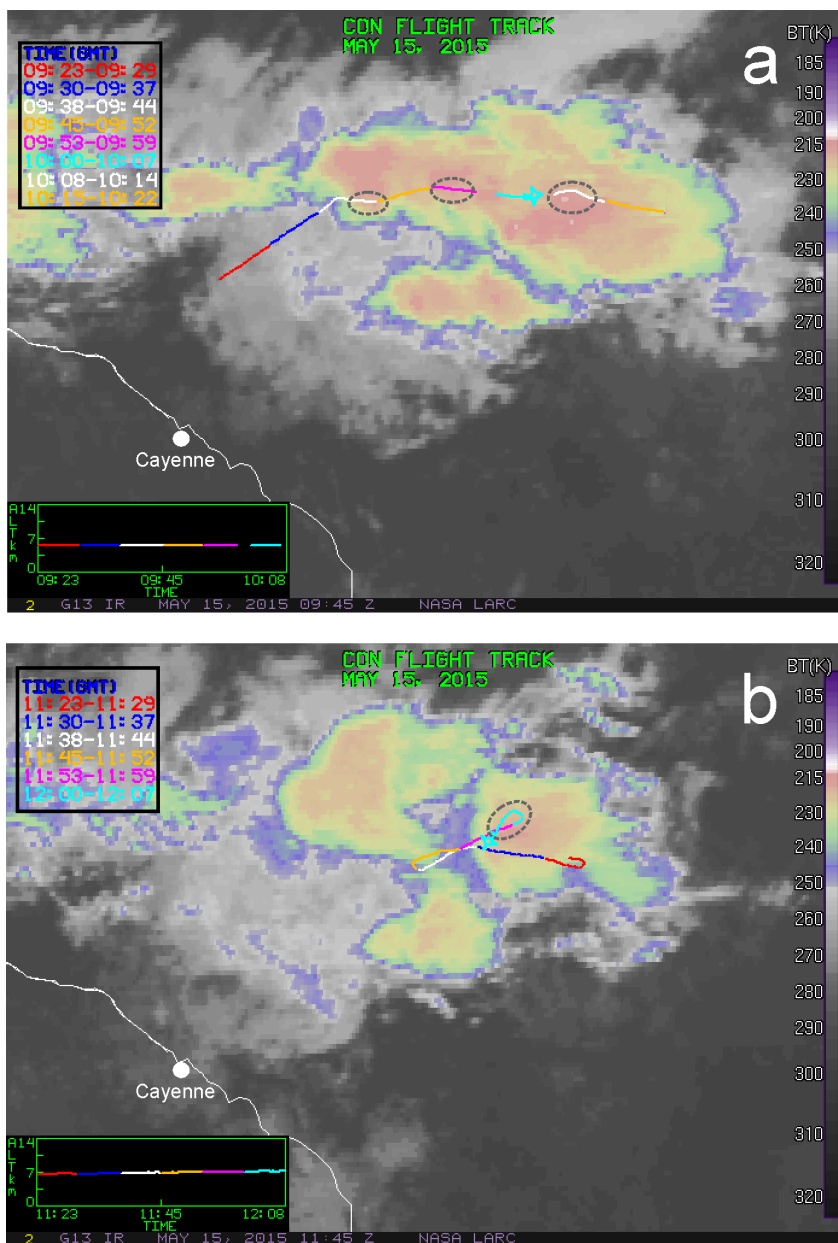


**Figure 4** GOES-13 infrared image of the MCS with the Convair-580 track (courtesy Pat Minnis). Circles indicate the cloud regions along the flight track where SIP was identified (see Figure 5). The marked regions also coincide with convective cloud regions (see text).

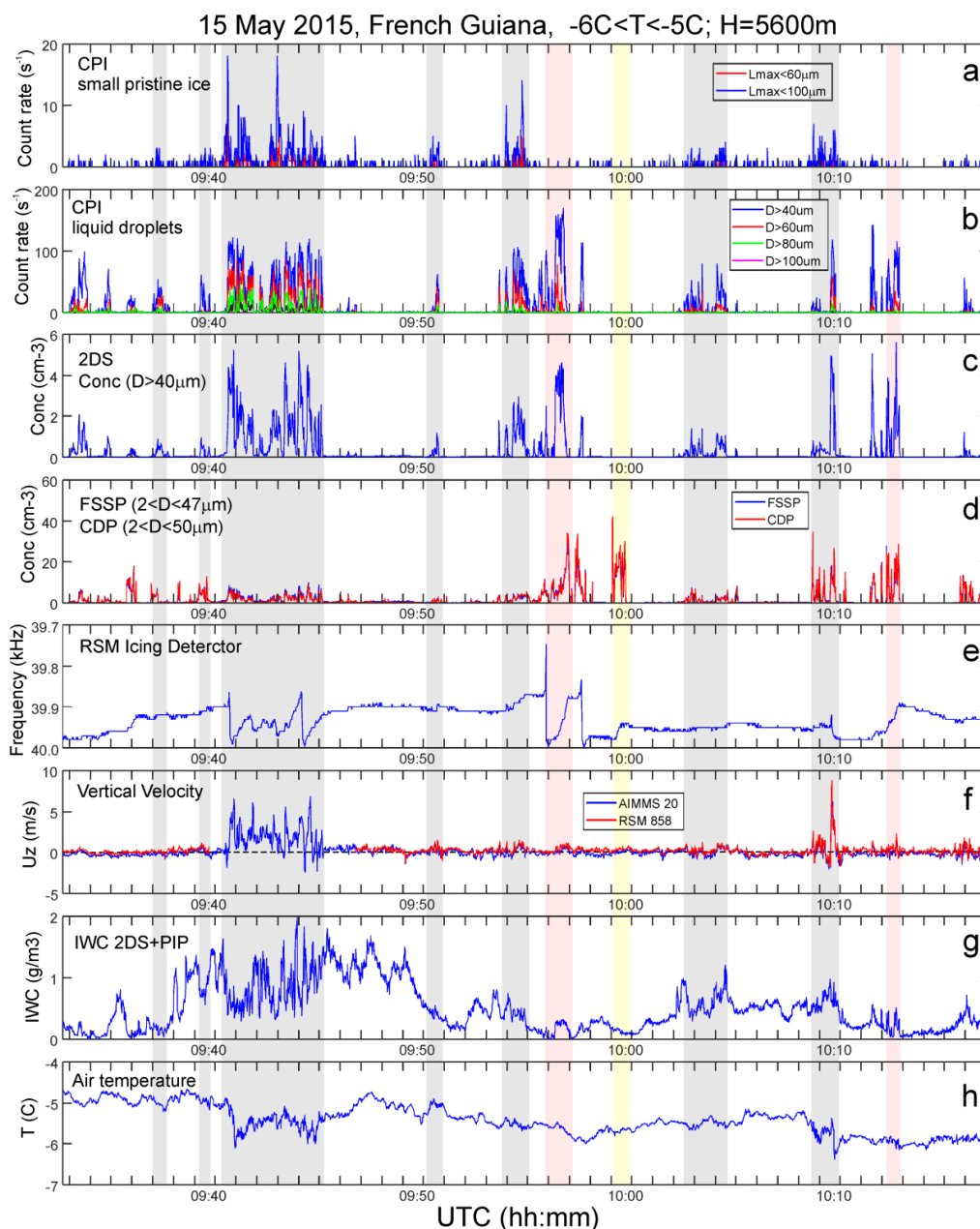


**Figure 5.** Time series of microphysical parameters collected in oceanic MCS offshore French Guiana on 15 May 2015. (a) CPI count rate of small pristine ice with  $D_{max} < 60\mu\text{m}$ ,  $100\mu\text{m}$ ; (b) CPI count rate of cloud droplets with  $D > 40\mu\text{m}$ ,  $60\mu\text{m}$ ,  $80\mu\text{m}$ ,  $100\mu\text{m}$ ; (c) concentration of cloud particles  $D > 40\mu\text{m}$  measured by 2DS; (d) concentration of cloud droplets measured by FSSP and CDP; (e) Rosemount Icing Detector frequency; (f) vertical velocity measured by AIMMS20 and Doppler velocity calculated from W-band radar; (g) IWC calculated from 2DS+PIP; (h) air temperature. Grey strips indicate cloud regions with enhanced concentration of small faceted ice particles; red and yellow strips indicate regions where ice and liquid were present, but no SIP was observed (see text). The altitude of measurements varied between 5600m and 5700m.

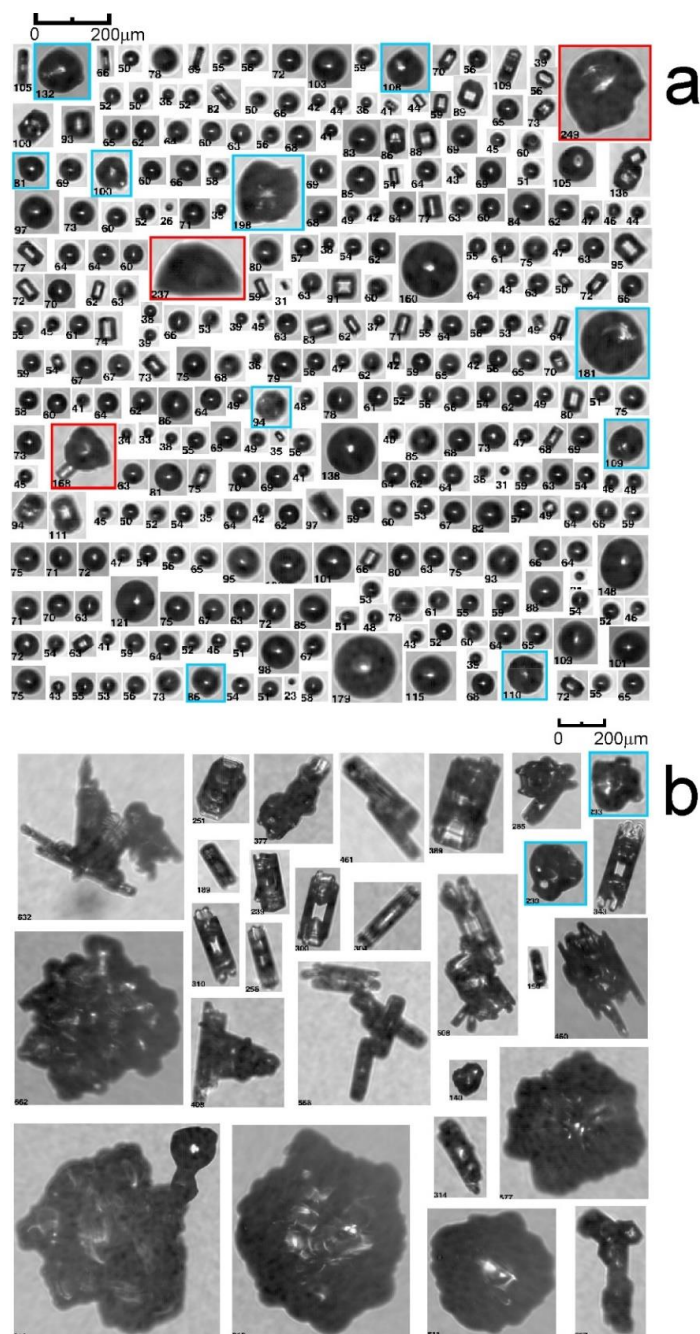


**Figure 6.** Spatial sequence of CPI images of (a) droplets and faceted ice crystals and (b) aged large ice particles. (a) Blue frames indicate frozen droplets with modified shapes, and red frames fragments of shattered frozen drops. Numbers under each image indicate their maximum sizes  $L_{max}$ . Cloud particles in (a) and (b) are spatially mixed, and they were split between two panels because of their difference in size. The images were sampled at  $T_a = -5\text{C}$  and  $H = 5650\text{m}$  during UTC 09:40:42 – 09:40:47 on 15 May 2015 during measurements shown in **Figure 5**.

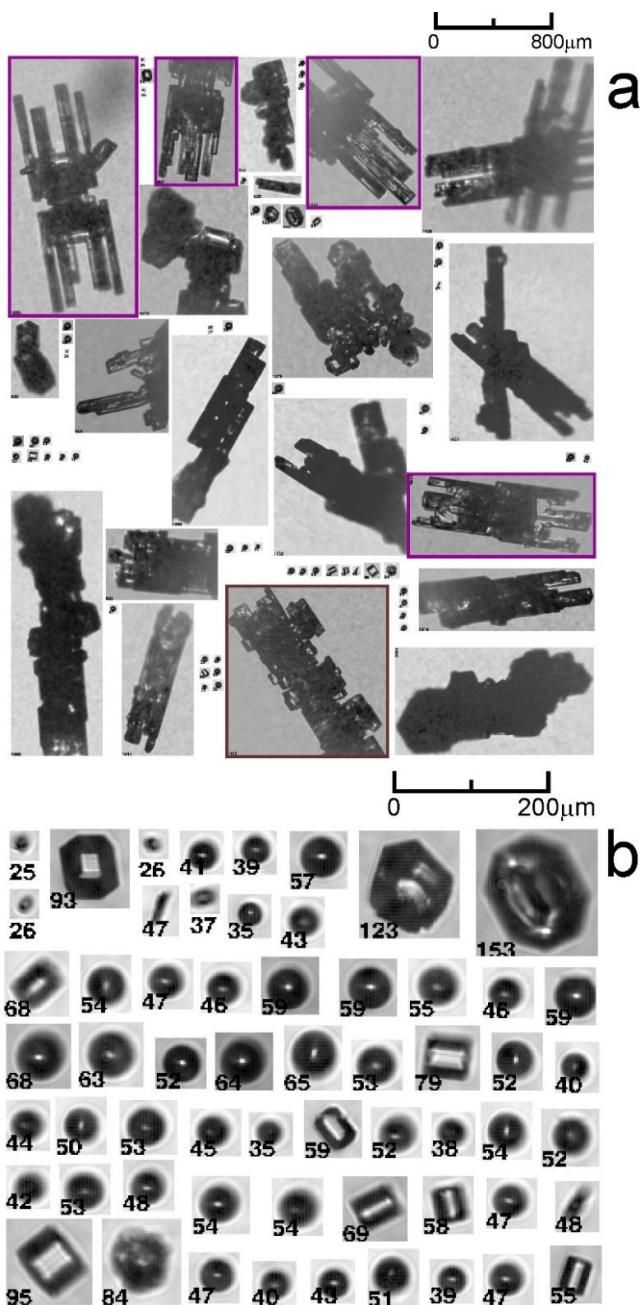


**Figure 7.** (a) Spatial sequence of CPI images; (b) Subset of droplets and faceted ice crystals from panel (a). Numbers under each image indicate their maximum sizes  $L_{max}$ . The images were sampled at  $T_a = -5\text{C}$  and  $H = 5620\text{m}$  during UTC 09:46:36 – 09:46:39 on 15 May 2015 during measurements shown in **Figure 5**. (a) Purple frames indicate images of ice particles with evidence for their vertical circulation in the storm.

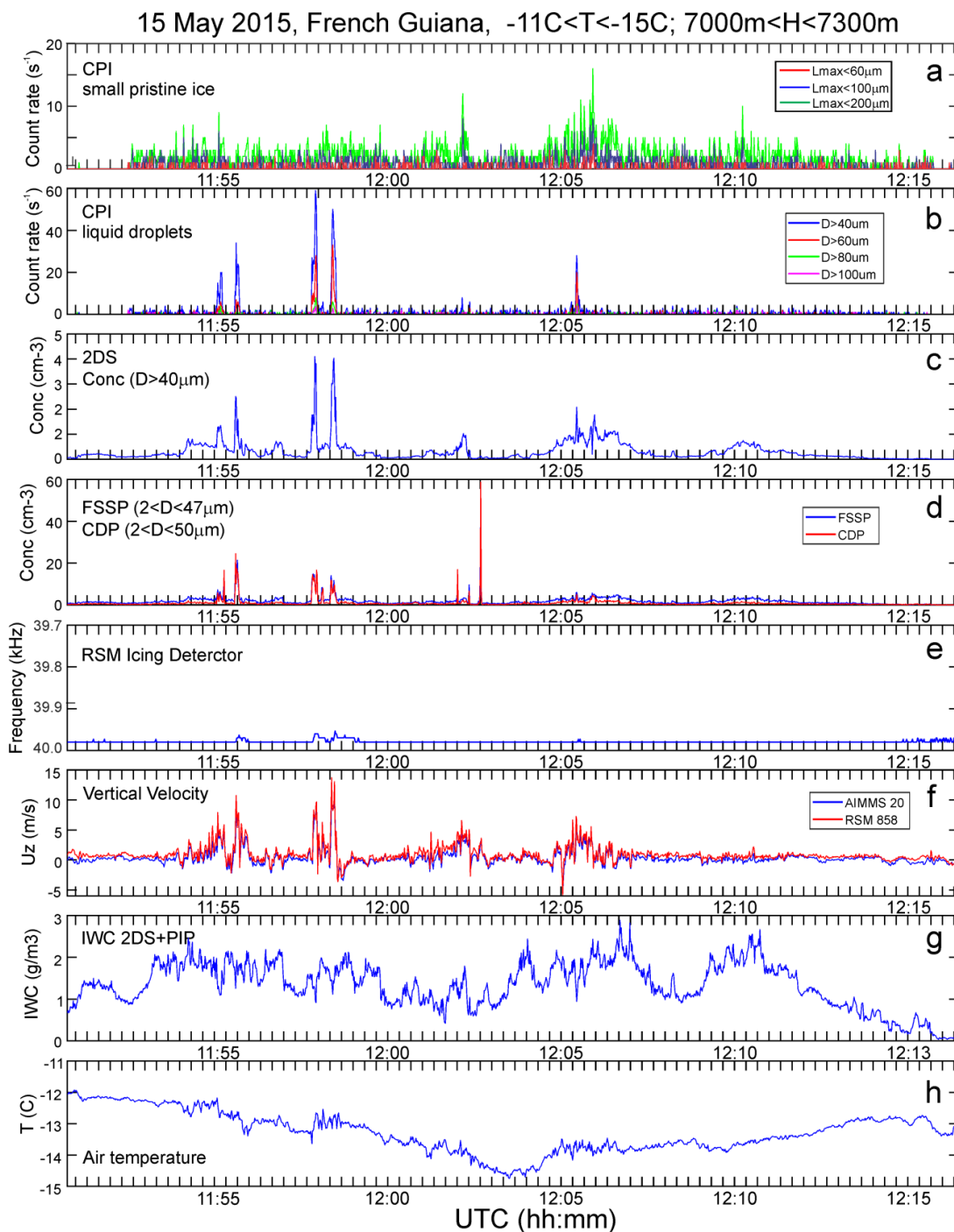
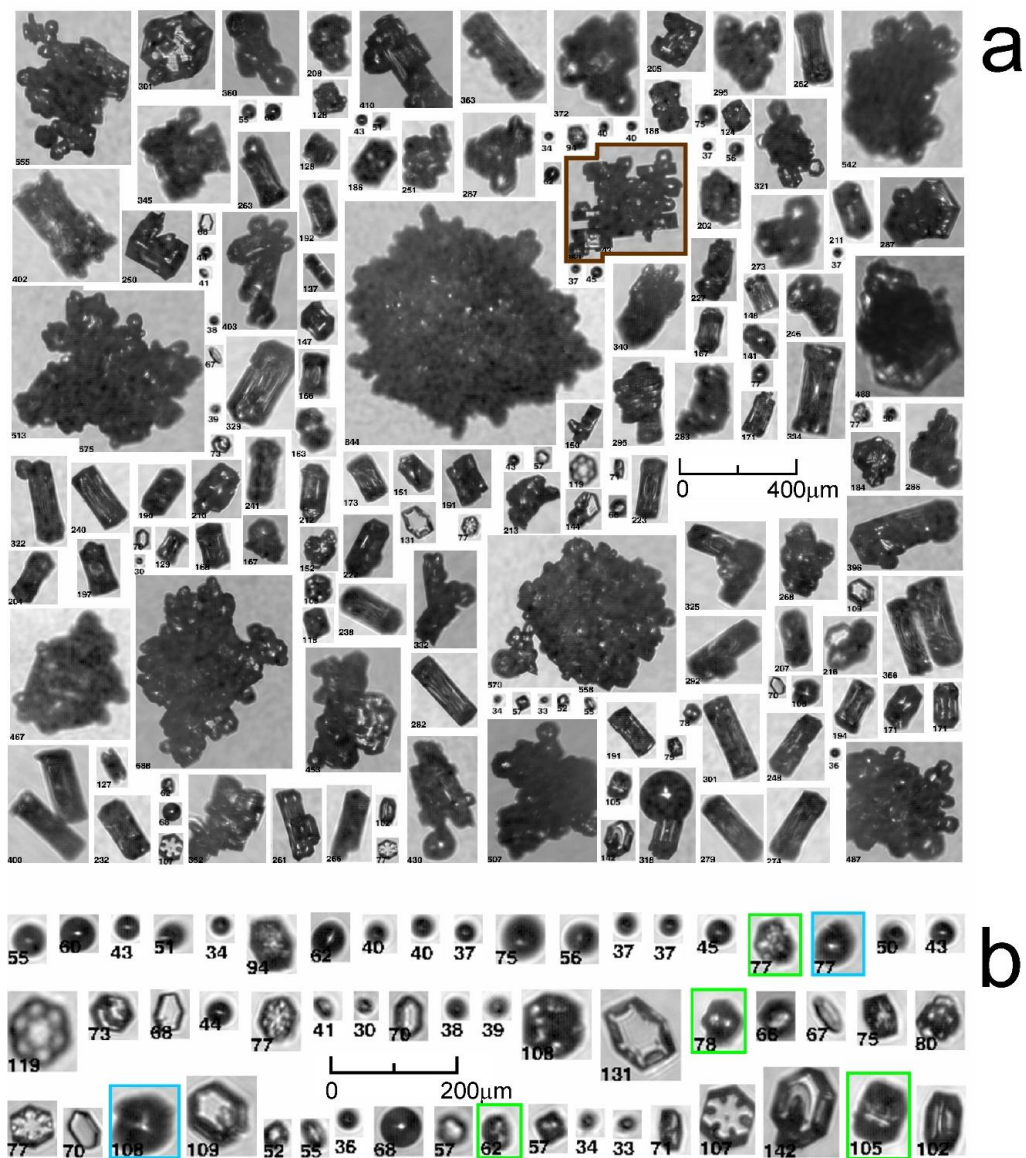
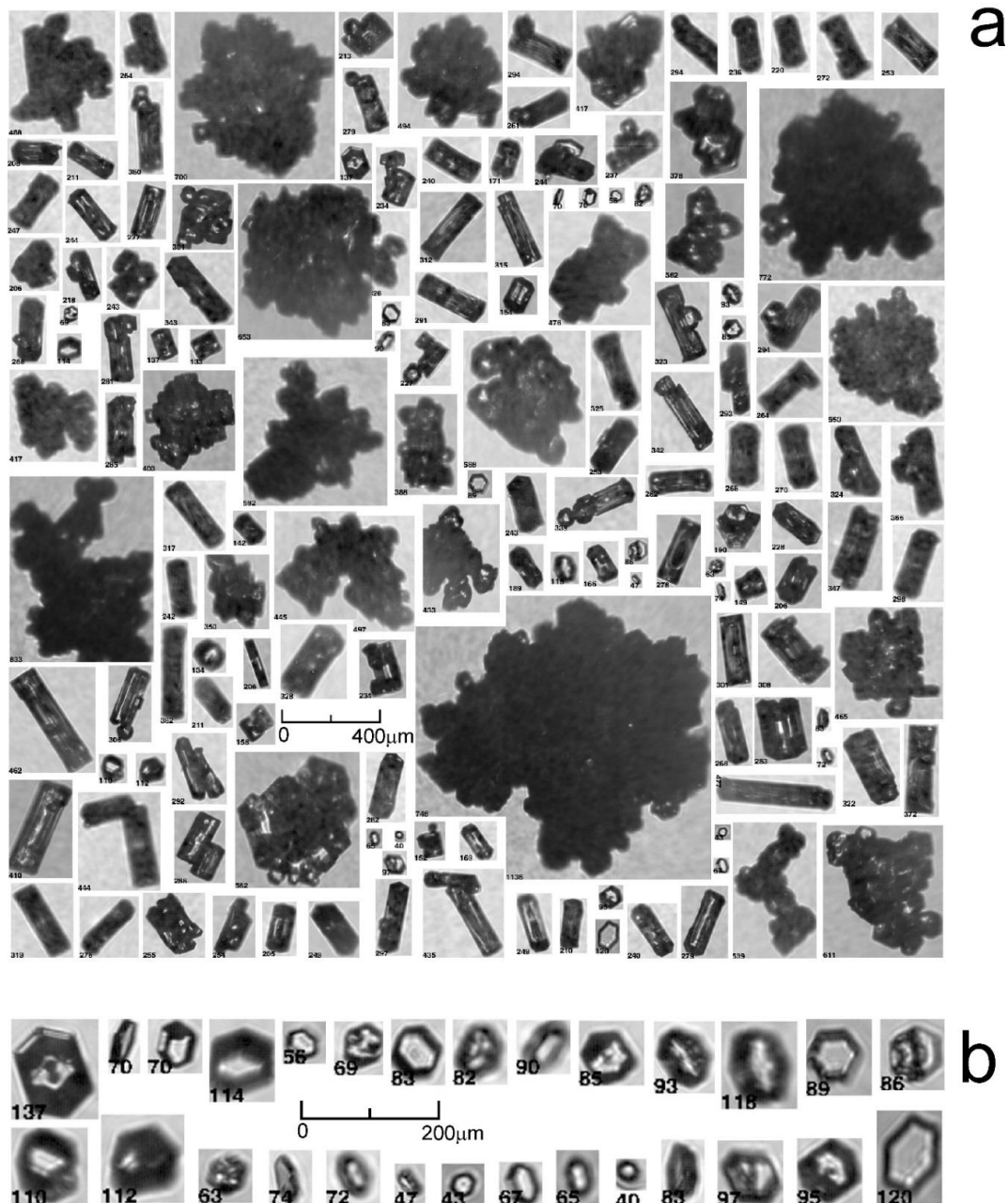


Figure 8. Same as in Fig.5. The altitude of measurements varied between 7000m and 7300m.



**Figure 9.** (a) Spatial sequence of CPI images; (b) Subset of droplets and faceted ice crystals from panel (a). (b) Blue frames indicate frozen droplets with modified shapes, and green frames frozen drops with developed facets. Numbers under each image indicate their maximum sizes  $L_{max}$ . The images were sampled at  $T_a = -14\text{C}$  and  $H = 7200\text{m}$  during UTC 12:05:27 – 12:05:38 on 15 May 2015 during measurements shown in **Figure 8**.



**Figure 10.** (a) Spatial sequence of CPI images; (b) Subset of droplets and faceted ice crystals from panel (a). Numbers under each image indicate their maximum sizes  $L_{max}$ . No liquid droplets were present in this cloud region. The images were sampled  $T_a = -14\text{C}$  and  $H = 7200\text{m}$  during UTC 12:05:47 – 12:05:53 on 15 May 2015 during measurements shown in **Figure 8**.

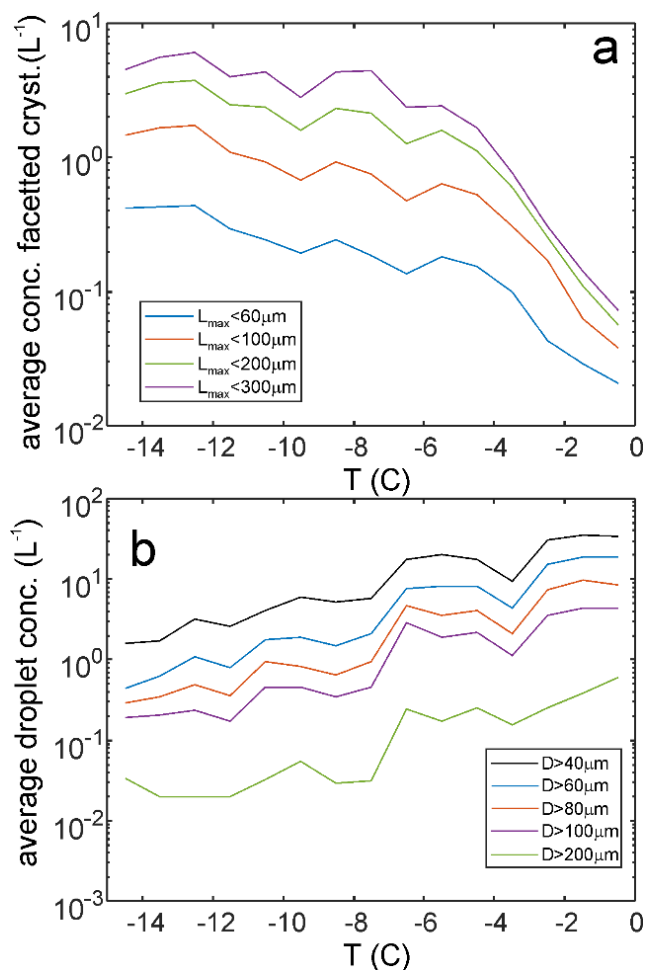


**Figure 11.** Average concentration of small faceted ice crystals (a) and drops (b) estimated from CPI measurements. The concentration was averaged over the entire flight length sampled during 13 flights in 10 tropical MCSs. The concentration was normalized on the sampling distance in each IC temperature interval. Total number of 1s average samples  $8.4 \times 10^4$ , total in-cloud length 9580km.

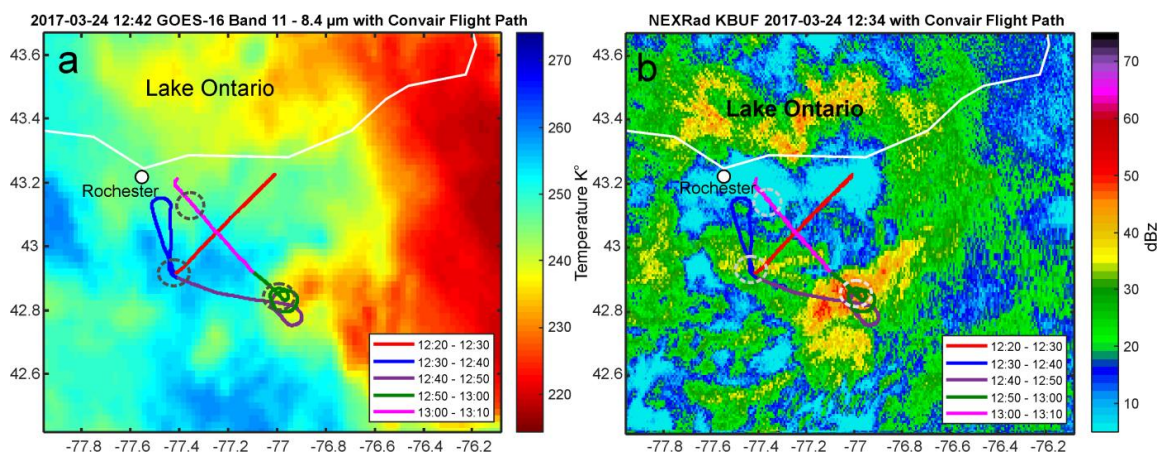


**Figure 12.** Flight track of the Convair-580 in the frontal cloud system on 24 March 2017 overlaid over (a) GOES-16 infrared image (download from Univ. Wisconsin); (b) KBUF (Buffalo, NY) NEXRAD reflectivity at elevation 0.46°. Dashed line circles indicate SIP cloud regions.

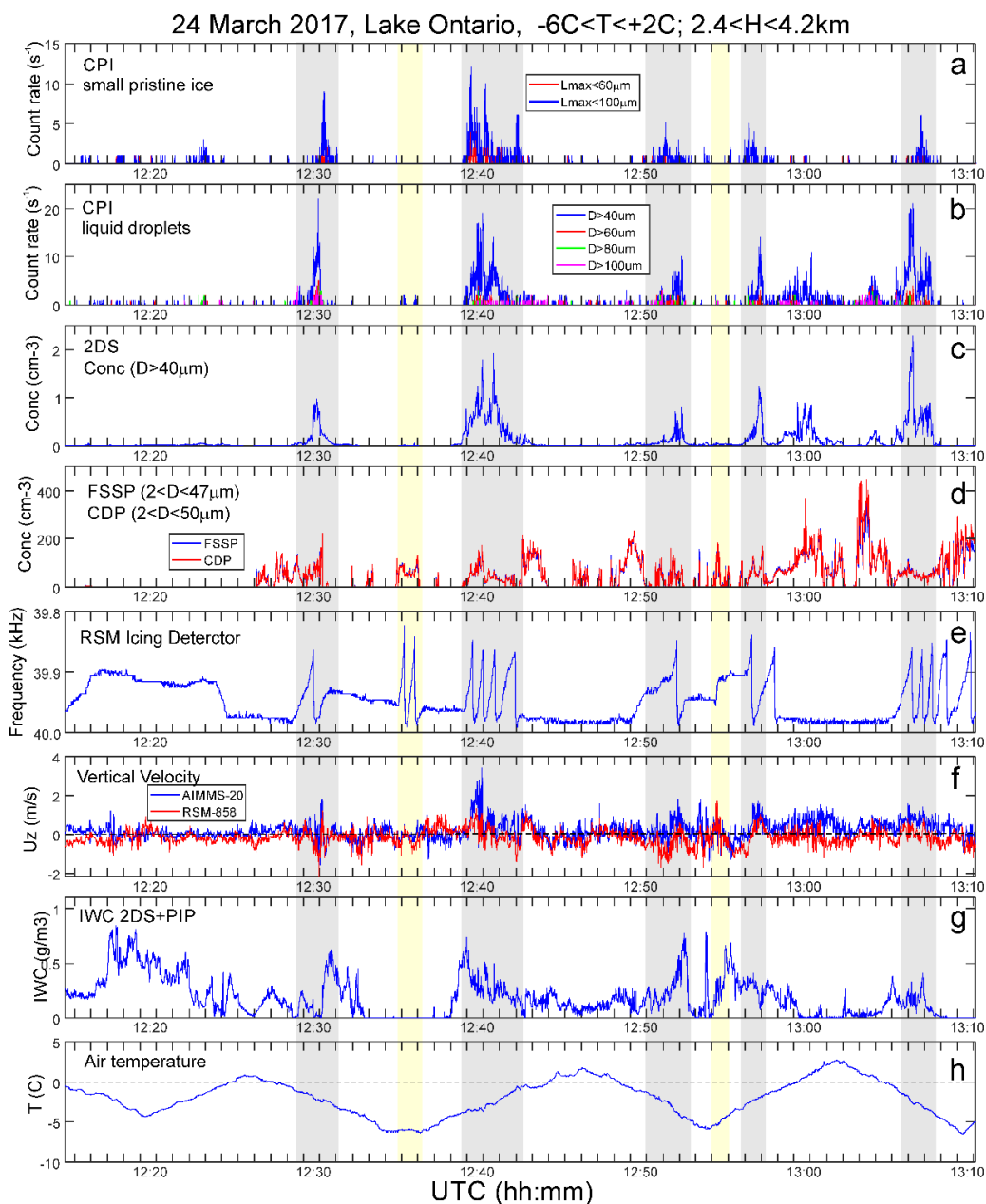


**Figure 13.** Time series of cloud microphysical parameters collected in a frontal cloud system over upstate NY on 24 March 2017. (a) CPI count rate of small pristine ice with  $D_{max} < 60\mu\text{m}$ ,  $100\mu\text{m}$ ; (b) CPI count rate of cloud droplets with  $D > 40\mu\text{m}$ ,  $60\mu\text{m}$ ,  $80\mu\text{m}$ ,  $100\mu\text{m}$ ; (c) concentration of cloud particles  $D > 40\mu\text{m}$  measured by 2DS; (d) concentration of cloud droplets measured by FSSP and CDP; (e) Rosemount Icing Detector frequency; (f) vertical velocity measured by AIMMS20 and Rosemount 858 probes; (g) IWC calculated from composite 2DS and PIP PSDs; (h) air temperature. Grey strips indicate cloud regions with enhanced concentration of small faceted ice particles; red and yellow strips indicate regions where ice and liquid were present, but no SIP was observed (see text).

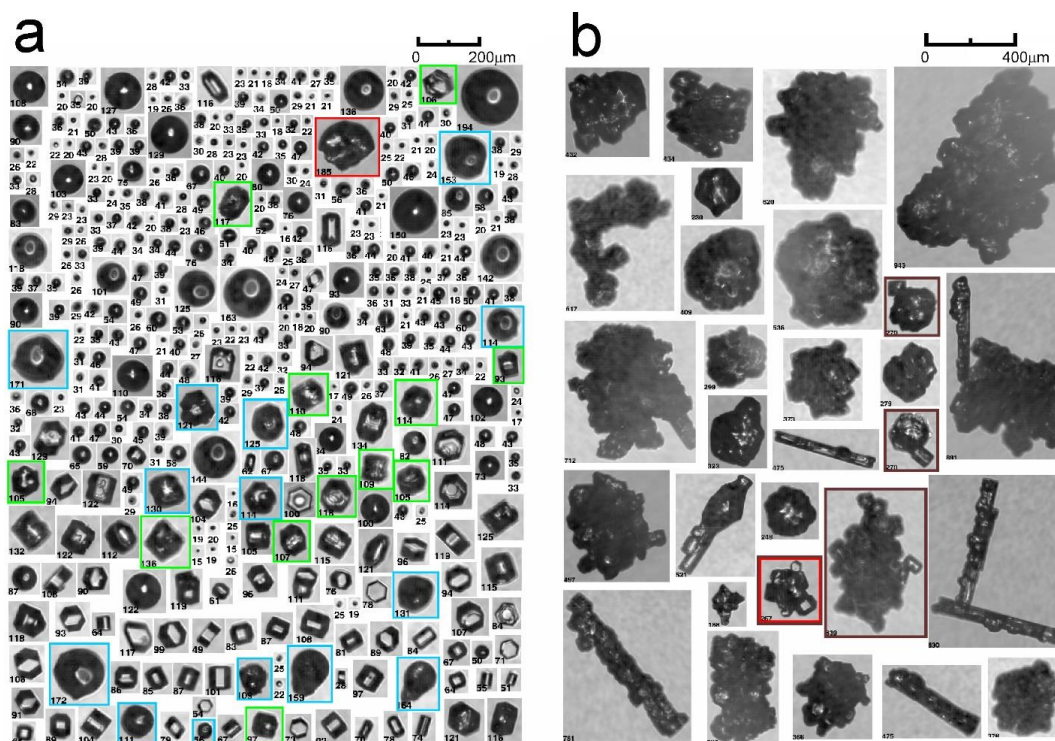


**Figure 14.** Spatial sequence of CPI images of (a) droplets and faceted ice crystals and (b) background large ice particles. (a) Blue frames indicate frozen droplets with modified shapes, green frames - frozen drops with developed facets, red frames - fragments of shattered drops. Numbers under each image indicate their maximum sizes  $L_{max}$ . Cloud particles in (a) and (b) are spatially mixed, and they were split between two panels because of their difference in sizes. The images were sampled at  $T_a = -2\text{C}$  and  $H = 3500\text{m}$  during UTC 12:29:20 – 12:30:00 on 24 March 2017 during measurements shown in **Figure 13**.

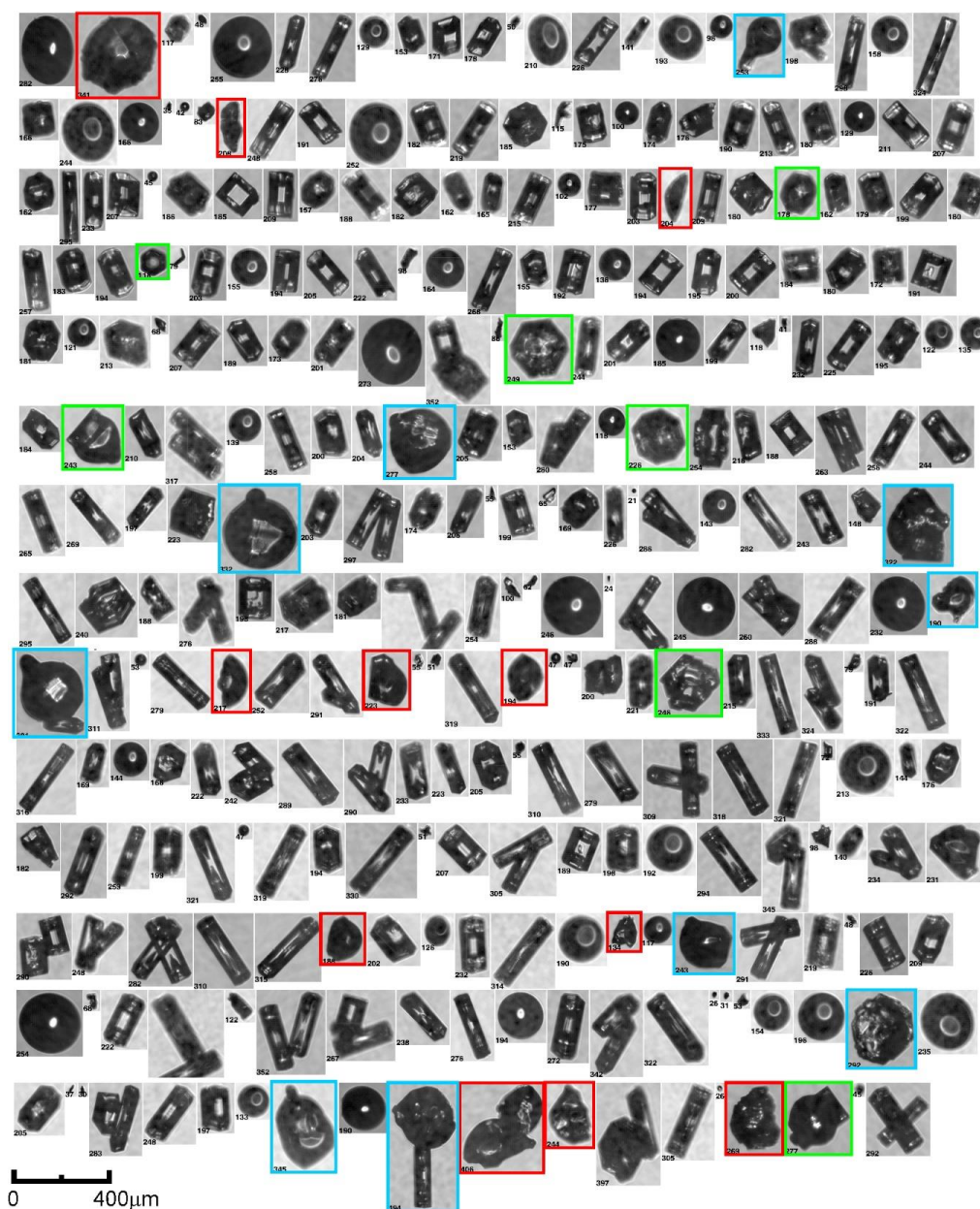


**Figure 15.** Spatial sequence of CPI images of droplets and faceted ice crystals. Blue frames indicate frozen droplets with modified shapes, green frames - frozen drops with developed facets, red frames - fragments of shattered drops. Numbers under each image indicate their maximum size  $D_{max}$ . The images were sampled during UTC 14:06:30-14:07:30 on 24 March 2017 (not shown in **Figure 13**),  $T_a = -3\text{C}$ ,  $H = 2100\text{m}$ .

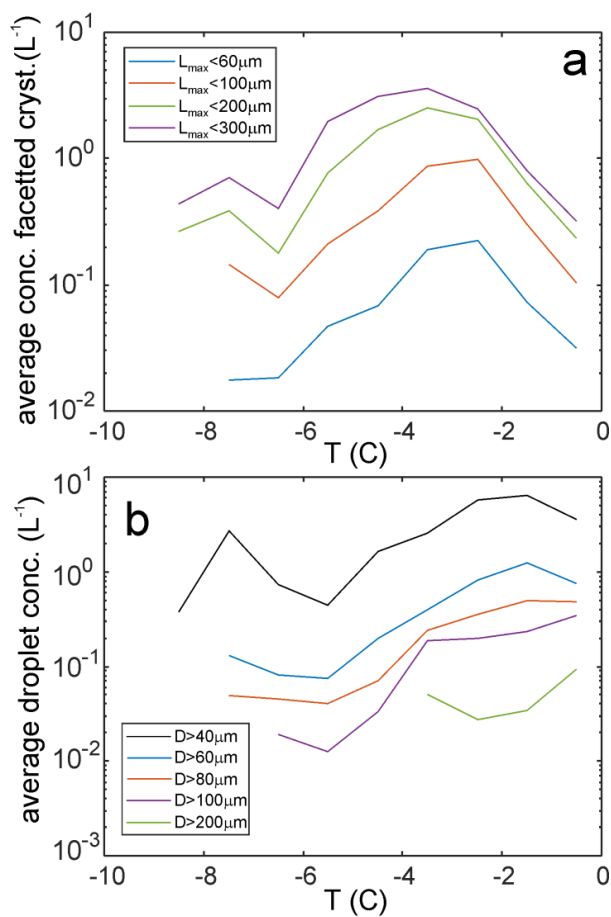


**Figure 16.** Average concentration of ice crystals (a) and drops (b) estimated from CPI measurements and normalized on the sampling distance in each temperature interval. The data were collected during two flights in mid-latitude frontal cloud systems with temperatures  $-10^{\circ}\text{C} < T_a < -0^{\circ}\text{C}$ . Total number of 1s average samples  $1.4 \times 10^4$ , total in-cloud aircraft path length 1380 km

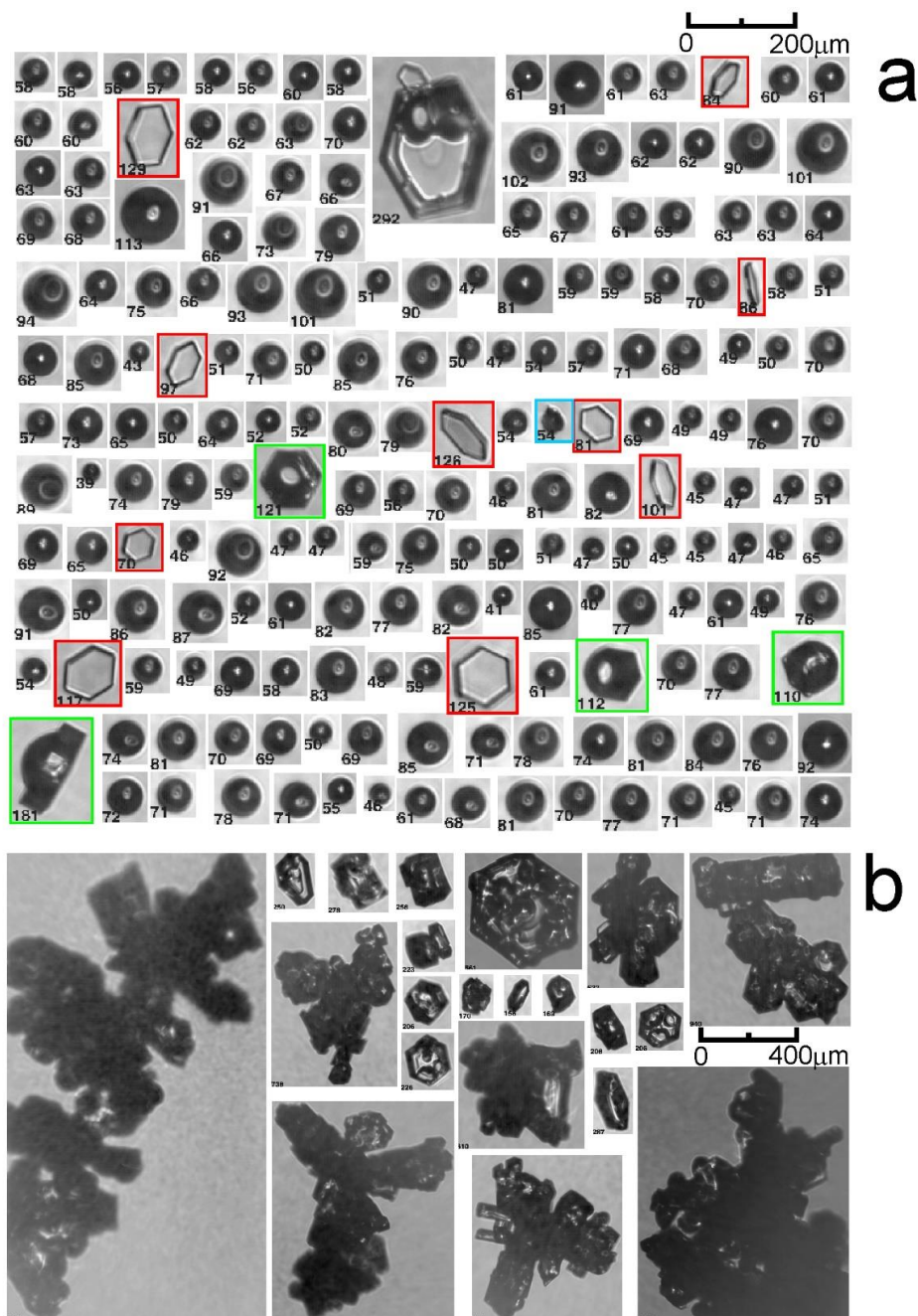


**Figure 17.** Spatial sequence of CPI images of (a) droplets and faceted ice crystals and (b) background large ice particles. (a) Blue frames indicate frozen droplets with modified shapes, green frames - frozen drops with developed facets, red frames - secondary ice particles developed into thin hexagonal plates. Numbers under each image indicate their maximum size  $D_{max}$ . Cloud particles in (a) and (b) are spatially mixed, and they were split between two panels because of their difference in sizes. The images were sampled during UTC 04:59:50-05:00:18, on 24 January 2017.  $T = -1.5\text{C}$ ,  $H = 2400\text{m}$

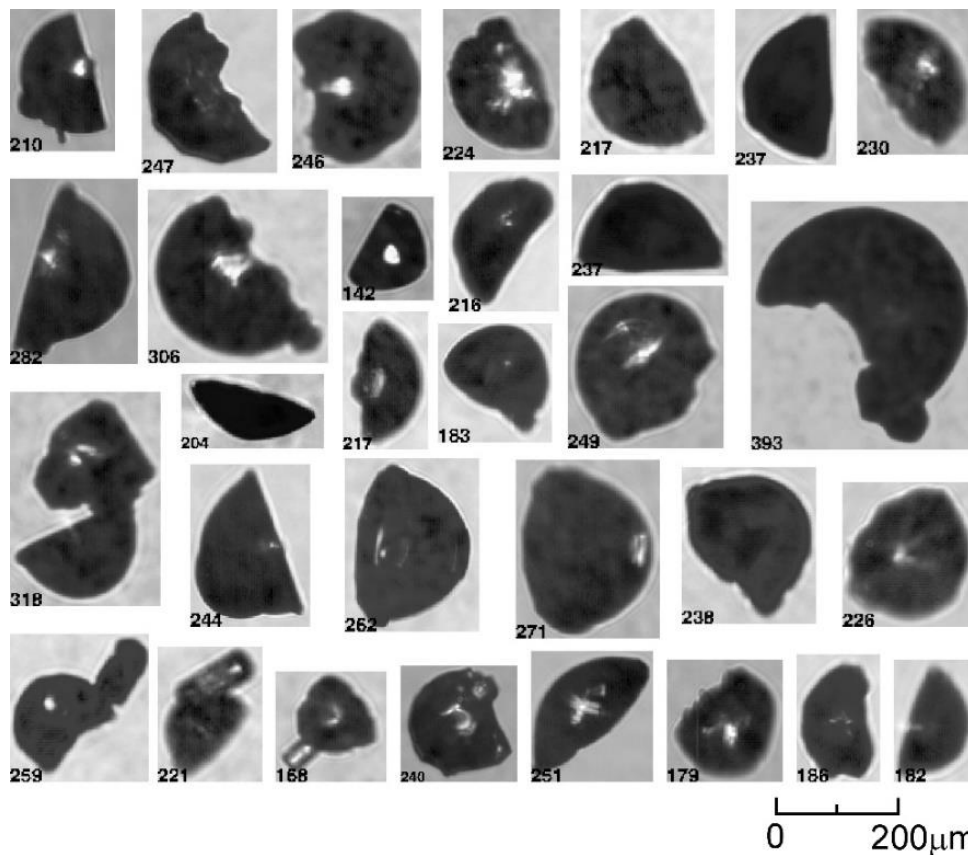


**Figure 18.** Images of fragmented frozen droplets collected in the SIP cloud regions indicated by grey areas in **Figure 5** and **Figure 13**.

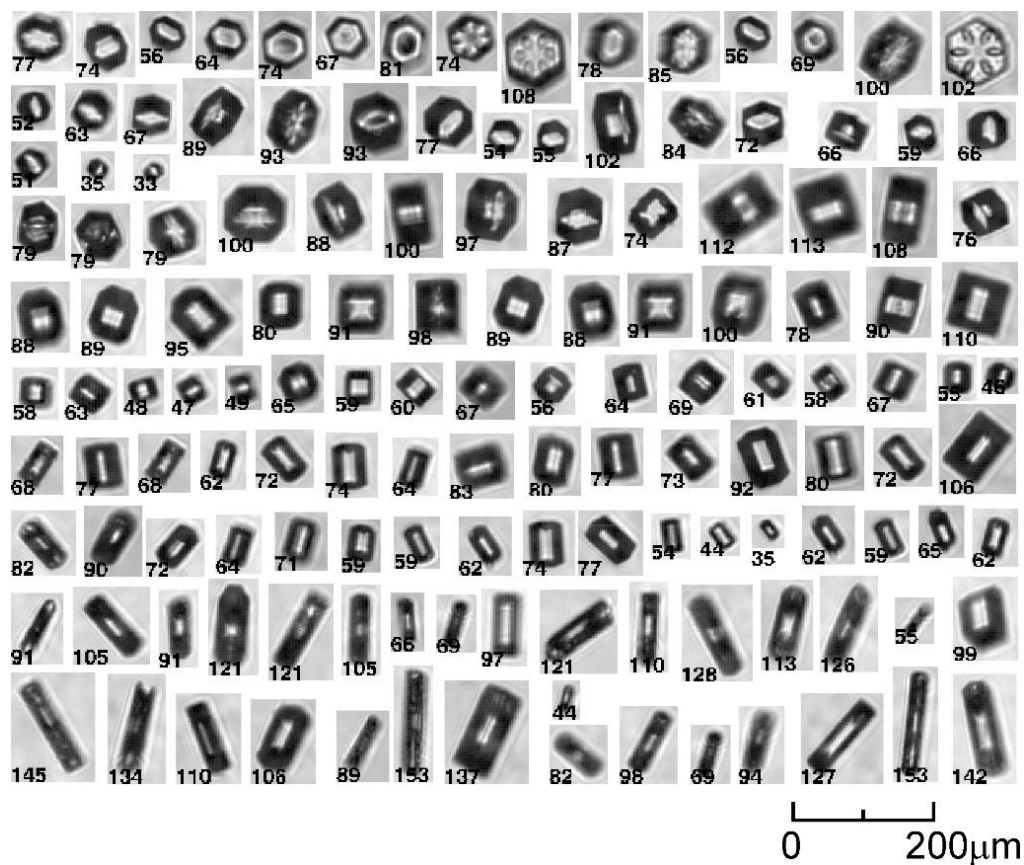


**Figure 19** Images of small faceted ice particles, which were sampled in SIP cloud regions at  $-5.5\text{C} < T_a < -5\text{C}$ ,  $H = 5600\text{m}$  indicated by grey color in **Figure 5**. The aspect ratio of the small hexagonal prisms varies in the range  $0.3 < R < 6$

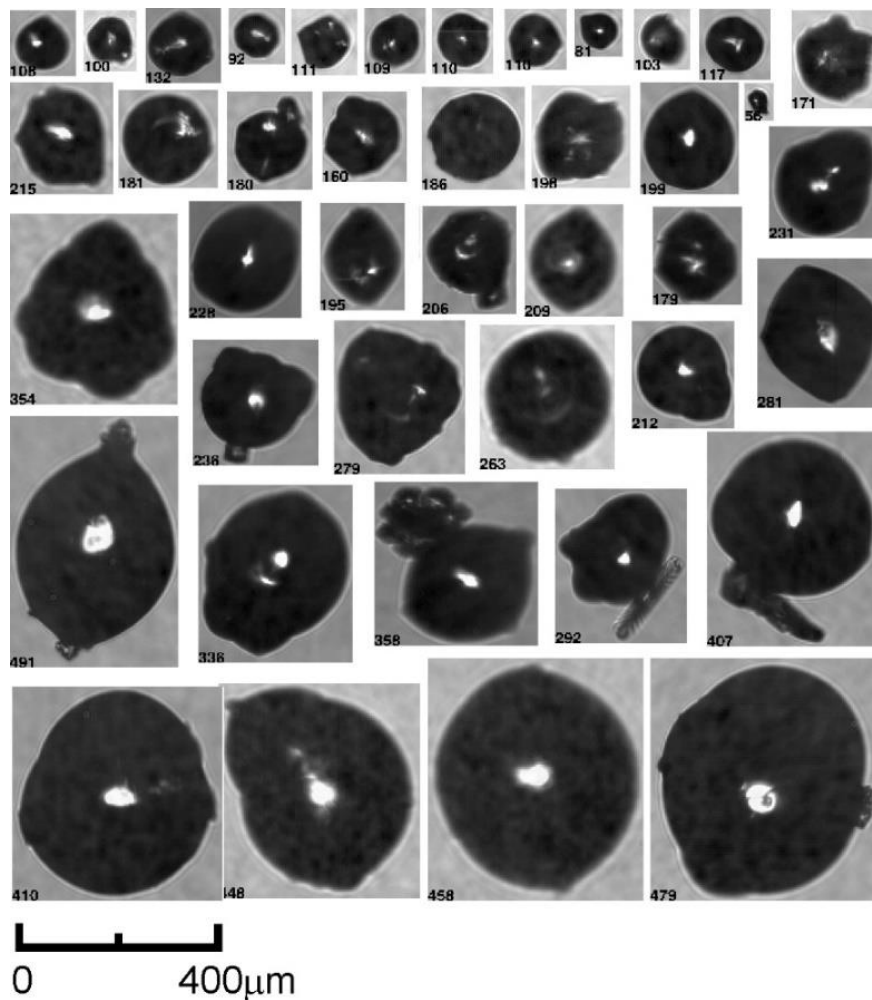


**Figure 20.** CPI images of single frozen droplets, which shape was modified during freezing.

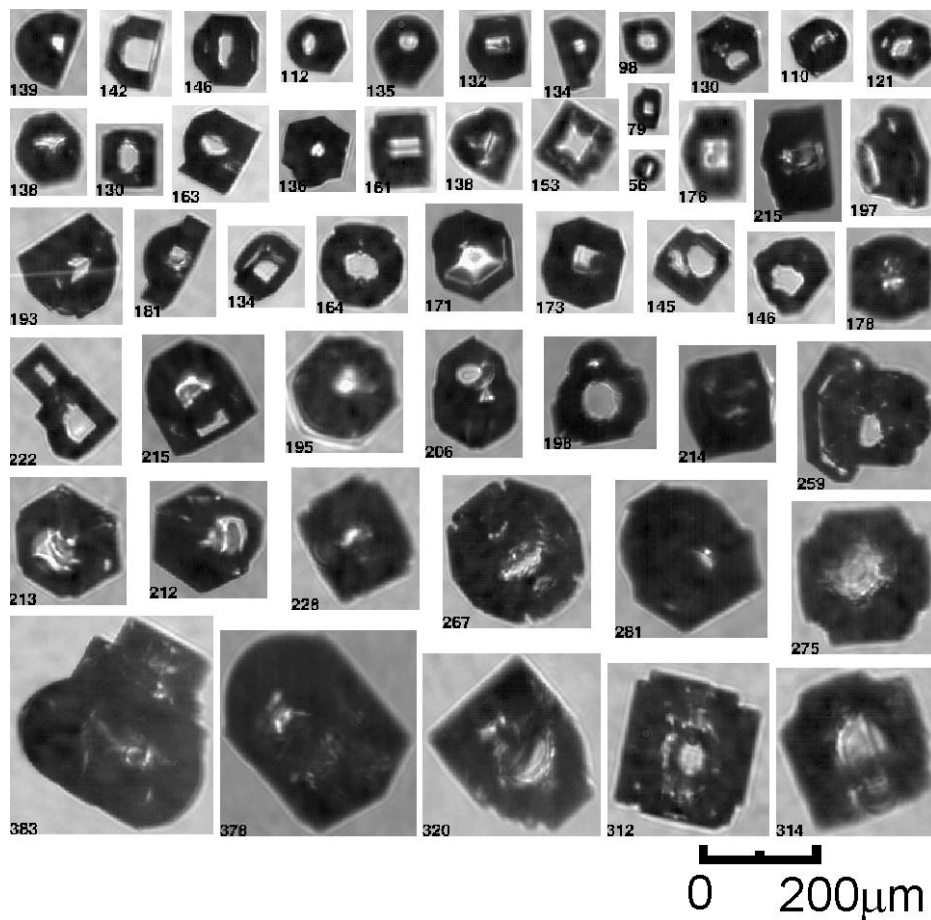


**Figure 21.** Images of frozen droplets partially regrown into faceted ice crystals.

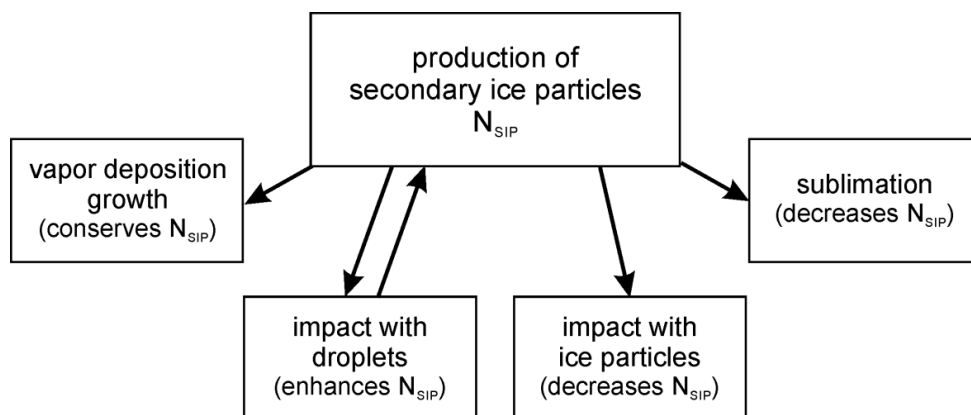


**Figure 22.** Different scenarios of evolution of SIP particles after their production.

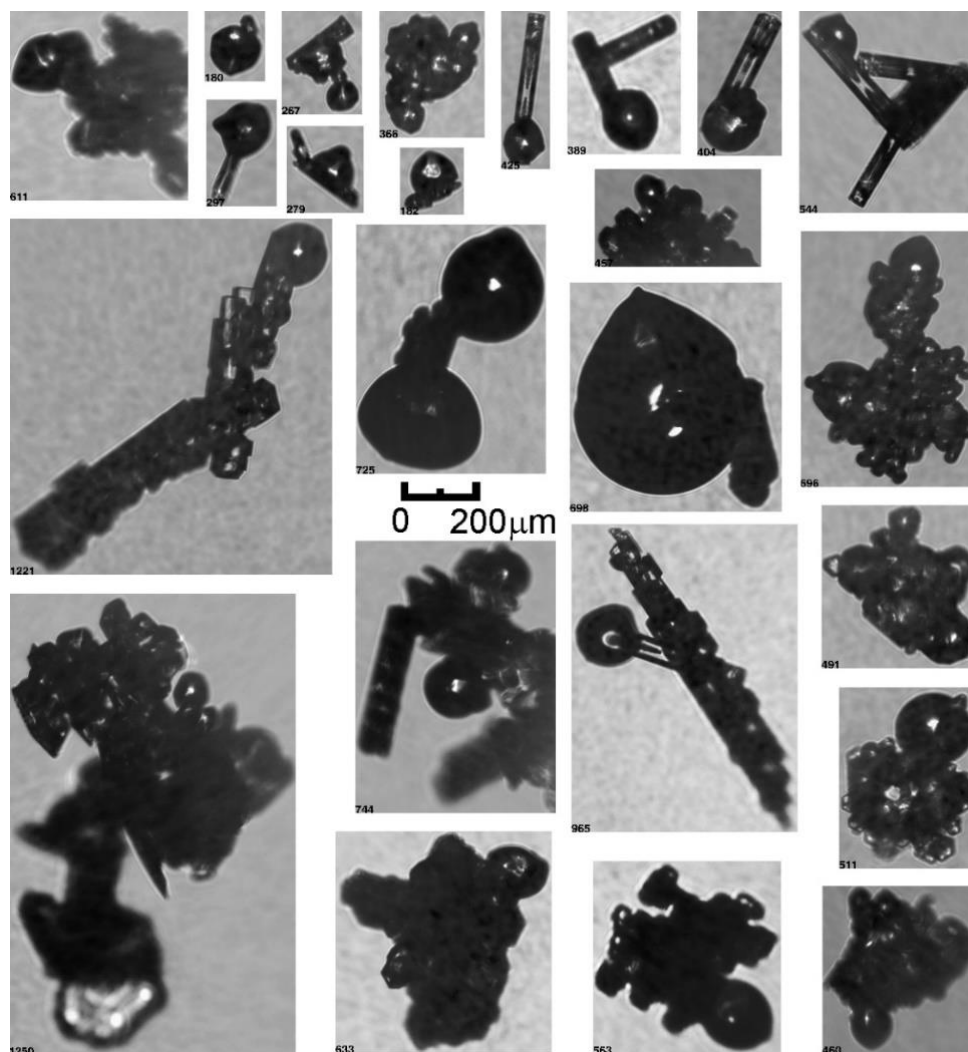


**Figure 23.** Images of frozen droplets attached to ice crystals that initiated their freezing. The shape of the frozen droplets was modified during freezing.

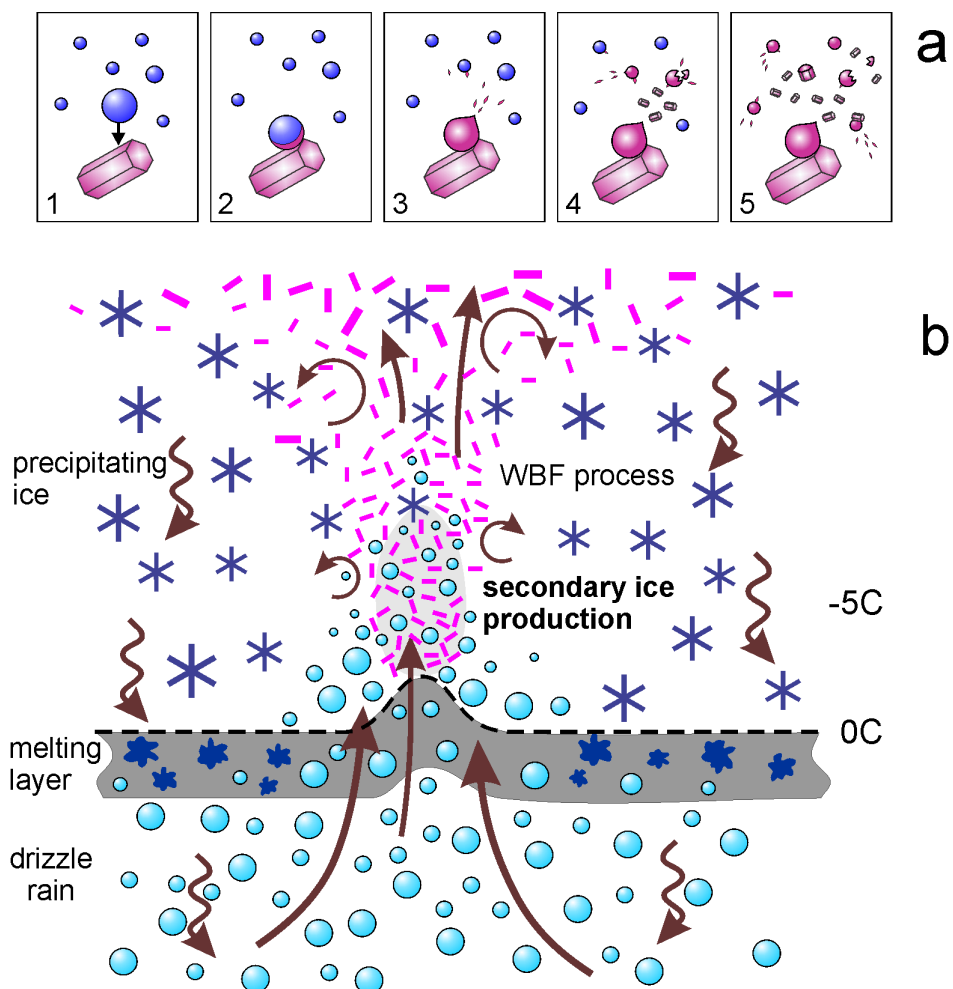


**Figure 24.** (a) conceptual model of secondary ice production due to shattering of freezing drops. (b) Conceptual model of the effect of melting layer on the secondary ice particle formation in MCSs and frontal clouds.

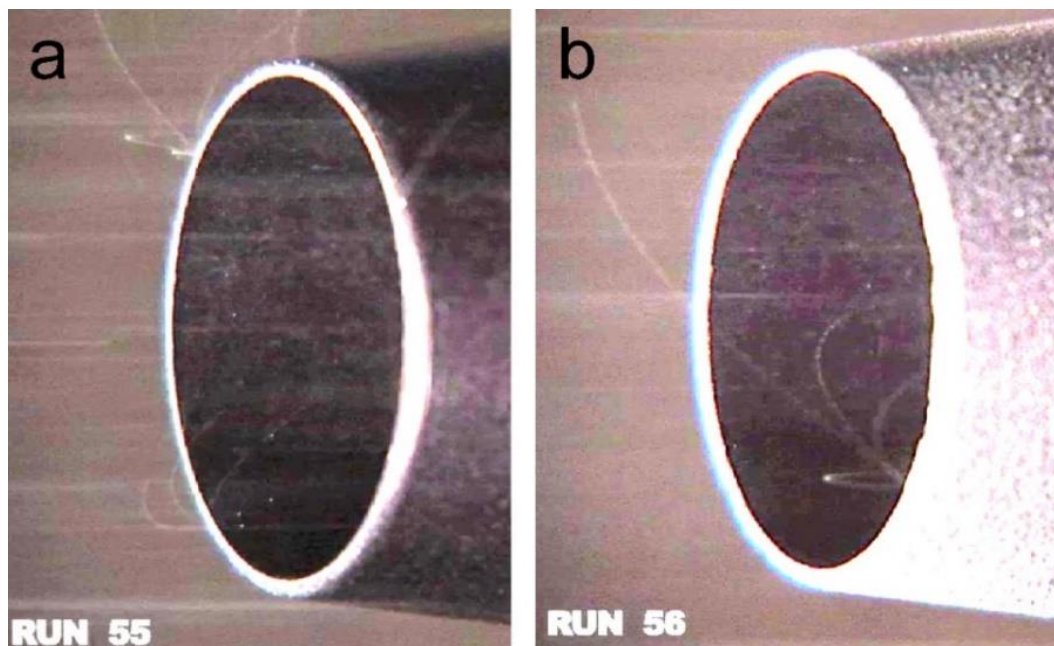


**Figure A1.** Snapshots from a high-speed video of trajectories of shattered and rebound ice particle fragments formed on impact with the CPI inlet. The measurements were conducted in the Cox and Co. wind tunnel facility (Long Island, NY, USA) in ice spray at TAS=80m/s.

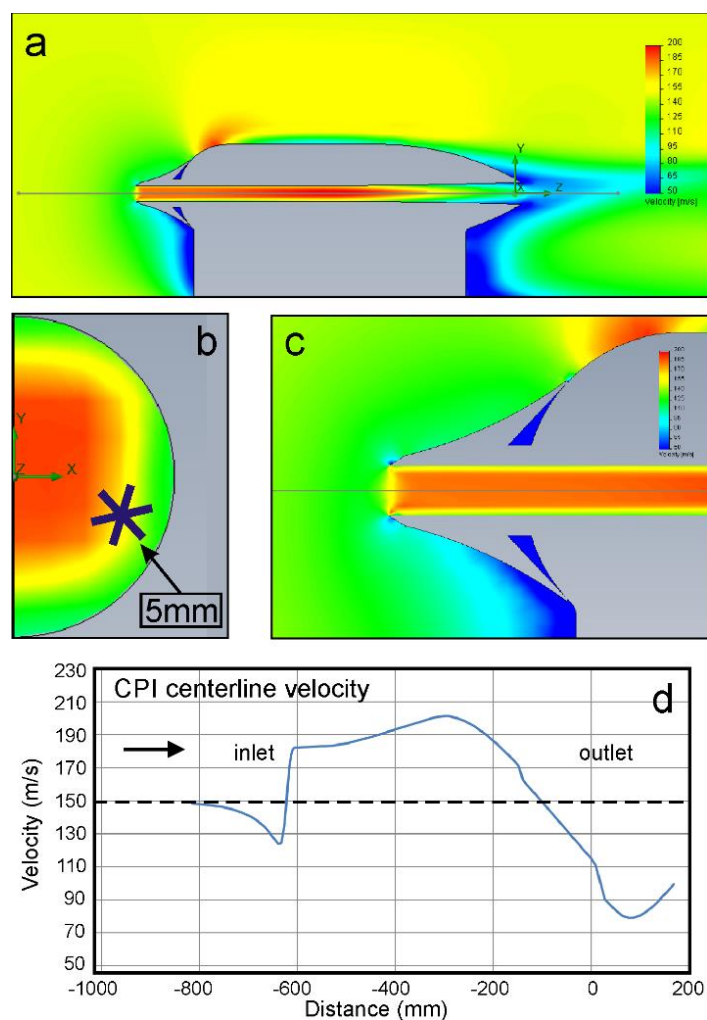


**Figure A2.** Results of the CFD analysis of flow around and through the CPI sampling tube. (a) airspeed around the CPI sensor head; (b) cross-section of speed inside the CPI inlet tube at the location of the sample volume; (c) zoomed CPI inlet area as in (a); (d) changes of the air velocity along the CPI inlet tube centerline. The simulation was performed for  $P = 450\text{mb}$ ,  $T_a = -40\text{C}$ ,  $TAS = 150\text{m/s}$

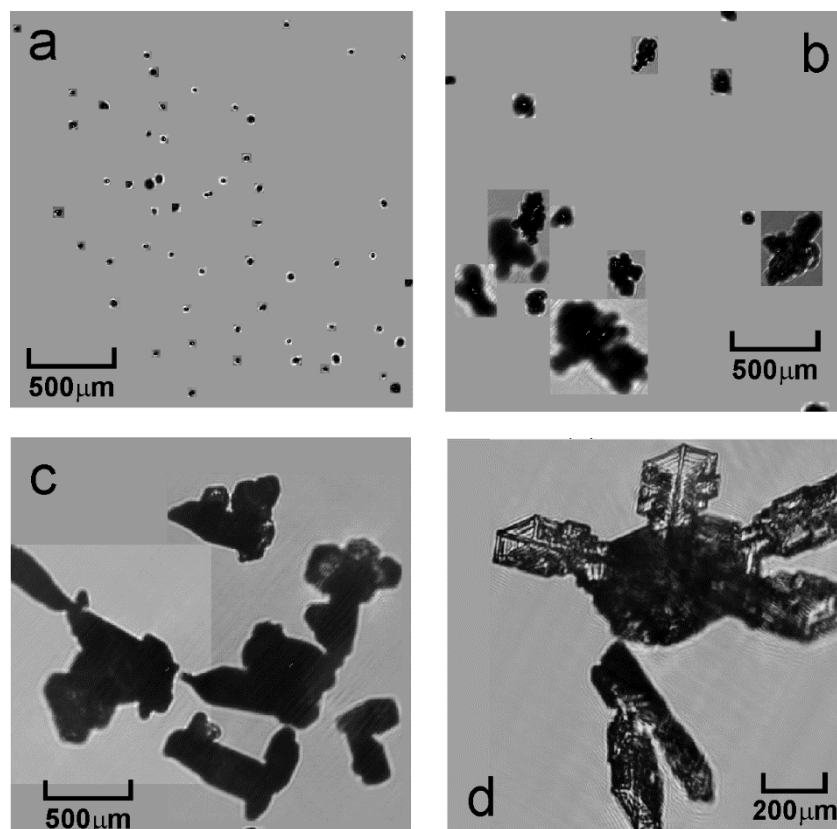


**Figure A3.** Multiple images registered in 2.3 mm × 2.3 mm CPI image frames (a,b,c). Images in (a,b) are identified as a result of shattering due to mechanical impact with the CPI inlet. Images in (c,d) are likely result from fragmentation due to aerodynamic stresses in the CPI inlet tube.

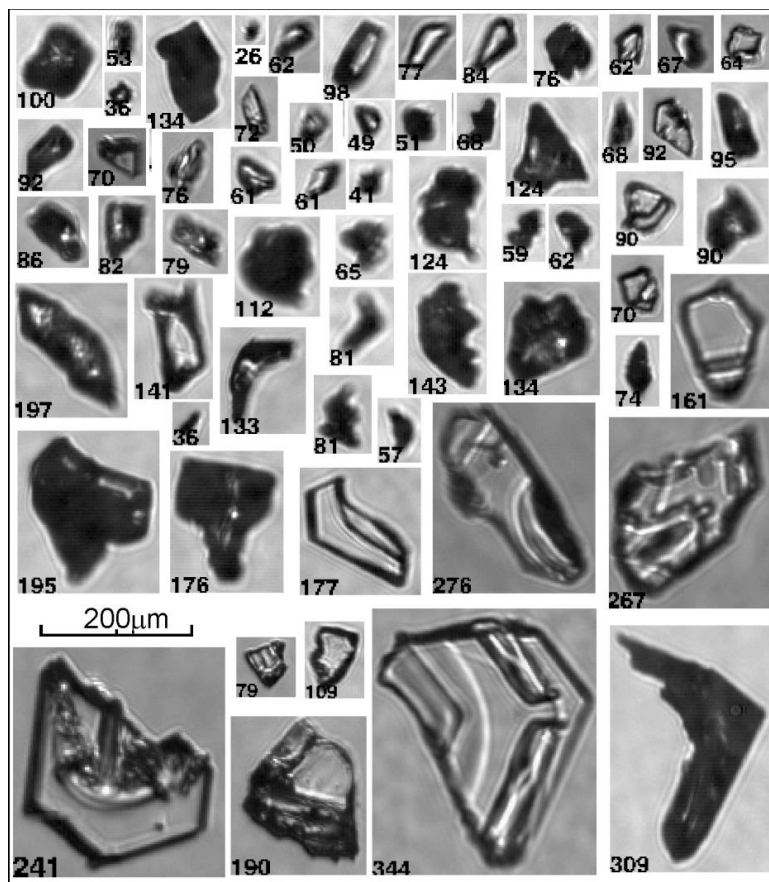


**Figure A4.** Examples of CPI images identified as shattering artifacts. Such images were excluded from analysis.